SURFACE WAVE TOMOGRAPHY OF TURKEY AND SURROUNDINGS

by

Musavver Didem Cambaz

B.Sc., Geophysical Engineering, Istanbul Technical University, 2001

M.Sc., Geophysical Engineering, Istanbul Technical University, 2003

Submitted to the Kandilli Observatory and
Earthquake Research Institute in partial fulfillment of
the requirements for the degree of
Doctor of Philosophy

Graduate Program in Geophysics Department

Boğaziçi University

2010

To the memory of Musavver Sönmez

FOREWORD

The use of seismic arrays in 1960s, dispersion studies in 1970s and the use of tomography in 1980s were the vivid subjects of seismology. Most of these subjects were developed with the progresses in other disciplines such as the advances in computer technology affecting the array processing techniques. With the beginning of 21st century the use of ambient noise as a new type of seismic source has been utilized in ultrasonic and acoustics and these improvements were adapted to seismology very quickly. The objective of this thesis is to employ some of these recent developments in seismology with the improved data quality in order to contribute to the understanding of the long standing problems on the tectonics of Turkey and surroundings. No doubt accomplishing this with a relatively new method which does not prove its reliability yet will bring questions along with the results. On the other hand solving this problem with a conventional technique of which stability is already tested and comparing the results with the method still on trial will provide more trustworthy outcome. For this reason in the frame of this thesis surface wave velocity structure of Turkey and its surroundings were obtained from the dispersion measurements of local and regional earthquakes. Long time correlations of ambient seismic noise recordings were used to determine surface wave Green's functions and use them to obtain surface wave velocity distribution in area similar way as the earthquake recordings. The results were then compared and correlated with the known geologic structures in the region. This thesis presents the surface wave velocity structure of the region with the highest resolution and largest scale that has ever been performed in the area. It is shown that the use of ambient noise correlation in this area together with the dispersion measurements of earthquakes is beneficial. The data and the results presented in this study are an initial stage of a more comprehensive work with intention to construct a detailed multi-parameter crustal earth model using several geophysical layers.

ACKNOWLEDGEMENTS

I would sincerely like to thank to my academic advisor, Prof. Dr. Hayrullah Karabulut for his support during my PhD studies. I have never lost the feeling that it has been a great privilege for me to be his student and to work with him. I would also like to thank to him especially for giving me the opportunity to work on this new and interesting subject.

I would like to express my appreciation to my co-advisor Assoc. Prof. Dr. Kerem Harmancı from Department of Electrical and Electronics Engineering of Boğaziçi University. I would like to thank to Esen Arpat for his crucial comments on the geology and tectonics of the region.

I would like to thank to Dr. Doğan Kalafat, Dr. Mehmet Yılmazer and Murat Berberoğlu of National Earthquake Monitoring Center of Boğaziçi University; for providing seismic data and information.

I would like to also thank to Mine Demircioğlu from Earthquake Engineering Department of Boğaziçi University for her fruitful help in the digitization of geologic data. I would like to thank to my colleagues; Ahu Mutlu for sharing so many things during my work at Boğaziçi University and also for turning the difficult times to fun for me with her special sense of humor, Aysegul Küsmezer from National Earthquake Monitoring Center of Boğaziçi University, for her friendship and for our ever-lasting discussions on the subject of *poles and zeros*. Thanks to the Department of Geophysics for providing a good environment for research and education

My sincere appreciation is to my spouse Caner Cambaz for being with me on my most intolerable times during this research. My special thanks are for my family for their encouragement and support through all stages of my life.

ABSTRACT

SURFACE WAVE TOMOGRAPHY OF TURKEY AND SURROUNDINGS

Seismic wave velocities can be obtained by using active or passive sources with appropriate arrays. Seismic reflection and refraction surveys using active sources are the most traditional ones. However the cost as well as inapplicability in urban areas, limits active source reflection and refraction methods in the crustal investigations. Seismic body waves and surface waves emitted from earthquakes are also widely used in seismology in order to constitute the images of the subsurface. However the insufficient path coverage between sources and stations may be the limiting factor. This amounts to the obstruction of obtaining high resolution images in crustal studies with earthquake data. In order to overcome the shortcoming of these techniques, a relatively new concept of "Passive Imaging Technique" is proposed to obtain the surface wave velocity structure of the Earth.

Generally, not only in seismology but also in other disciplines which deal with signals, accept noise as an undesired component of the signal. It is commonly believed that noise obscures data and does not contain useful information. However recent developments changed this judgment by indicating that long term correlations of 'ambient noise' can also be used as seismic source. This method promises significant improvements in the resolution and accuracy of crustal and upper mantle images. Green's functions between station pairs can be extracted from long term correlations of seismic recordings. Shear wave velocity distribution can then be obtained from the Green's functions using the conventional imaging methods.

In the frame of this thesis, for a better understanding of the character of the seismic noise, a comprehensive noise analysis has been performed for permanent and temporary broadband stations operating in Turkey and surrounding areas. Power spectral densities (PSD) were computed in the frequency range of 100 sec to 10 Hz. Probability Density Functions (PDF)

as a function of noise power, have been analyzed for the stations with available data. Noise maps have been constructed from the power spectral density estimates of selected stations in the region in order to characterize the temporal and geographical variations. Diversities in noise spectra due to different sensors, installation properties and geographical variations are discussed. Ambient seismic noise records are used to determine the group velocity variations in Turkey and surrounding regions. A database for noise correlations was constructed from the continuous recordings of 156 permanent and temporary broadband stations during 2006-2009. The cross correlations of the ambient seismic noise are calculated to determine surface wave Green's function for station pairs in the region. In order to obtain the group velocity maps from earthquakes a waveform database was formed from 285 earthquakes with magnitudes Mw>4.5 recorded by more than 270 broadband stations. Love and Rayleigh wave group velocity dispersion curves are computed and group velocity maps of Turkey and the surrounding regions have been obtained from local and regional earthquakes. Results from ambient noise were compared with the group velocity maps obtained from earthquakes. The group velocity maps were interpreted in relation to the known geological and tectonic structures in the region. The study shows the existence of significantly different crustal types in the area. Low group velocities at shorter periods (10-20 sec) are observed in local sedimentary basins, the Eastern Mediterranean and the Black Sea. The Eastern Anatolia region is also characterized by low group velocities while Pontides and Bitlis-Pötürge massif display higher group velocities. The Central Anatolia exhibits uniform velocity distribution indicating more homogenous crust. The Isparta Angle is marked by a wedge shaped-low group velocity anomaly. High velocities observed on the maps are associated with metamorphic, magmatic arcs along the orogenic belts of Pontides, Pötürge massif and crustal thinning in the Aegean region. At larger periods (40-50 sec) the Anatolian Block shows low and uniform group velocity distribution while its surroundings display higher group velocities with the exception of the eastern Mediterranean Region.

ÖZET

TÜRKİYE VE ÇEVRESİNİN YÜZEY DALGASI TOMOGRAFİSİ

Sismik dalga hızları aktif veya pasif kaynaklar kullanılarak uygun dizilimler ile belirlenebilirler. Aktif kaynak kullanılan sismik yansıma ve kırılma araştırmaları en yaygın olanlarıdır. Ancak, hem maaliyet hem de kentsel alanlardaki uygulama zorlukları kabuk incelemelerinde aktif kaynaklı yansıma ve kırılma metodlarını sınırlandırır. Depremlerden yayılan sismik cisim dalgaları ve yüzey dalgaları sismolojide yeryüzünün altındaki tabakaların görüntüsünün oluşturulması için yaygın olarak kullanılırlar. Fakat kaynak ve istasyonlar arası ışın yolunun kapsamındaki yetersizlik sınırlayıcı bir faktör olabilir. Bu deprem verisi ile kabuk çalışmalarında yüksek çözünürlüklü görüntüler elde etmenin engellenmesine neden olur. Önceki yöntemlerdeki bu eksikliklerin üstesinden gelmek için nispeten yeni bir kavram olan "Pasif Görüntüleme Tekniği" yerin yüzey dalgası hız yapısının belirlenmesi için önerilmiştir.

Sadece sismoloji değil, sinyaller ile uğraşan diğer disiplinler de gürültüyü genel olarak sinyalde istenmeyen bileşen olarak kabul eder. Genel kabul, gürültünün veriyi bozduğu ve yararlı bilgi içermediğidir. Fakat en son gelişmeler bu kabulu değiştirmiş, sismik gürültünün uzun dönemli korelasyonunun bir kaynak olarak kullanılabileceğini göstermiştir. Bu metod kabuk ve üst manto görüntülerinin çözünürlüğü ve güvenilirliğinde önemli gelişmeler vaat eder. İstasyon çiftleri arası Green fonksiyonu, sismik kayıtların uzun dönemli korelasyonundan elde edilebilir. Kesme dalgası hız dağılımı daha sonra Green fonksiyonlarından uygun görüntüleme yöntemleri kullanılarak elde edilebilir.

Bu tez kapsamında, sismik gürültü karakterinin daha iyi anlaşılabilmesi için Türkiye ve etrafında çalıştırılan geçici ve kalıcı sismik istasyonlara geniş kapsamlı gürültü analizi uygulanmıştır. Spektral güç yoğunluğu (PSD) 100 saniye ile 10 Hz aralığında hesaplanmıştır. Olasılık yoğunluğu fonksiyonları (PDF) gürültünün gücünün fonksiyonu olarak verisi uygun olan istasyonlar ile incelenmiştir. Zamana ve coğrafi dağılıma göre bölgedeki değişiklikleri görebilmek için seçilen istasyonların spektral güç yoğunluğu

kestiriminden gürültü haritaları oluşturulmuştur. Güç spektrumlarındaki farklı alıcı, kurulum özellikleri ve coğrafi farklılıklara bağlı değişiklikler tartışılmıştır. Türkiye ve etrafındaki grup hızı değişimlerini belirlemek için çevresel gürültü kayıtları kullanılmıştır. Gürültü korelasyonu için 156 genişbantlı kalıcı ve geçici istasyonun 2006-2009 süresince kayıt edilen sürekli verisinden bir veri tabanı oluşturulmuştur. Yüzey dalgası Green fonksiyonunu belirlemek için bölgedeki istasyon çiftlerindeki çevresel sismik gürültünün öz ilişkisi hesaplanmıştır. Gürültü korelasyonundan olan grup hızı haritalarının depremlerden olan grup hızı haritaları ile karşılaştırılması için 4.5'den büyük 285 depremde 270'den fazla istasyonda kayıt edilen dalgayapısı veritabanı oluşturulmuştur. Lokal ve bölgesel depremlerden Türkiye ve etrafı için Rayleigh ve Love dalgası grup hızı haritaları oluşturulmuştur. Gürültü korelasyonundan elde edilen sonuçlar depremlerden elde edilen grup hızı haritaları ile karşılaştırılmıştır. Grup hızı haritaları bölgedeki jeolojik ve tektonik gözlemler ile ilşkilendirilerek yorumlanmıştır. Bu çalışma bölgenin kabuk yapısında belirgin farklılıklar olduğunu gösterir. Yerel sedimanter basenlerde, doğu Akdeniz ve Karadeniz'de kısa periyotlarda düşük grup hızları (10-20 saniye) gözlenmiştir. Doğu Anadolu bölgesi düşük hızlar ile temsil edilirken, Pontidler ve Bitlis-Pötürge masifi daha yüksek hızlar göstermektedir. Orta Anadolu daha homojen bir kabuğu temsil eden tekdüze bir hız dağılımı gösterir. Isparta Açısı kama şeklindeki düşük grup hızı anomalisi ile işaretlenmiştir. Haritalarda gözlenen yüksek hızlar Pontidlerde orojenik kuşaklar boyunca metamorfik ve magmatik yaylar, Pötürge masifi ve Ege'de kabuksal incelme ile ilişkilendirilmiştir. Daha büyük periyotlarda (40-50 sec) Anadolu bloğu düşük ve tekdüze grup hızı dağılımı gösterirken etrafında Akdeniz Bölgesi haricinde yüksek grup hızlar gösterir.

TABLE OF CONTENTS

LIST OF FIGURES

LIST OF TABLES

LIST OF SYMBOLS/ABBREVIATIONS

AxB	Axios Basin
A-T	Anatolid-Taurid Block
CAB	Clicia Adana Basin
EAAC	East Anatolia Accretionary Complex
ETSE	Eastern Turkey Seismic Experiment
HL	National Observatory of Athens
IA	Isparta Angle
IRIS	Incorporated Research Institutions for Seismology
IZ	Istanbul Zone
KOERI	Kandilli Observatory and Earthqauke Research Institiute
KM	Kırşehir Massif
LN	Lycian Nappes
MRC	Marmara Research Center
MM	Menderes Massif
NAT	North Anatolian Trough
NOA	National Observatory of Athens
ORFEUS	Observatories and Research Facilities for European Seismology
PT	Pontides
sps	Sample per second
α	Resolution
d	Distance
r	Time
P	Power
G_a	Green's function
v(t)	Temporal window
f	Source function
Mw	Magnitude
$Ø_n(w)$	Phase
$y_j(t)$	j^{th} segment

1. INTRODUCTION

1.1. Outline

Seismic reflection and refraction surveys using active sources are traditional methods in the investigation of the earth's structure. However, the cost as well as inapplicability in urban areas, limits the use of active source methods. Seismic body waves and surface waves emitted from earthquakes are also widely used in seismology. Surface wave tomography using earthquakes has proven to be very useful in determining the structure of the crust and uppermost mantle on both regional and global scale. Their large amplitudes along long propagation paths with relatively low attenuation contributed greatly to our knowledge of the Earth's upper mantle and crustal structure. One dimensional earth models has been routinely obtained for great circle paths using the dispersive nature of surface waves while long period surface waves has been the main source of the observation for determining the tomographic image of the mantle. During the last decade with the availability of high-quality digital broadband seismic data we have seen a rapid progress in imaging the structure of crust and upper mantle with the increasing resolutions. Studies at local and regional scales are now common for regions with good coverage of stations and earthquakes. Phase and group velocity distributions obtained from surface waves correlate well with the main tectonic and geological features providing better constrains on their geometry and relation to the regional tectonics.

However insufficient path coverage of seismically inactive regions is a limiting factor resulting in the obstruction of high resolution images. In order to overcome the shortcomings of conventional techniques an alternative, called Passive Imaging Technique, has been proposed (Weaver and Lobkis, 2001; Derode *et al.,* 2003; Snieder, 2004; Larose *et al.*, 2004). The method was first tested in ultrasonic and acoustics (Weaver and Lobkis, 2001), later on applied in a number of disciplines.

According to this new technique surface wave Green's function can be extracted between two stations by long term correlations of ambient seismic noise. Noise is conventionally described as disturbance in the signal which does not represent part of a

message from a specified source (Sheriff, 1991). Such definition supposes that noise obscures the signal and does not contain useful information. However the new branch of physics called “mesoscopic physics” is challenging this assumption. The theory indicates that a residual coherence is preserved from the superposition of linear waves which can be utilized by long term correlation of ambient noise. Rather than waiting for earthquakes, information related to propagation paths is recovered from ambient seismic noise that is constantly produced by fluctuations in the Earth’s atmosphere and oceans. The new method promises significant improvements in the resolution and accuracy of crustal and upper mantle images. Nowadays surface wave tomography based on cross-correlations of ambient seismic noise has been applied successfully at local and regional scales (Shapiro and Campillo, 2004; Campillo and Paul, 2003; Bensen *et al.,* 2008; Ritzwoller, 2008; Stehly *et al.,* 2008; Li *et al.*, 2010).

In the first chapter, a review of the geologic and tectonic setting of the study area is presented. Results of the previous geologic studies reviewed and maps of tectonic and geologic units are presented. Previous geophysical studies performed in the area are also reviewed.

An analysis is performed in this study in order to understand the instrumental, temporal and spatial characteristics of seismic noise. Chapter 2 covers the power spectral density method used for the analysis of seismic noise. Diurnal, seasonal, instrumental and spatial variations of noise are presented.

Chapter 3 presents the cross-correlation of ambient seismic noise using recordings of both permanent and temporary seismic stations in Turkey. The long term cross correlations of the ambient noise are calculated to determine Green’s function for station pairs. Group velocities are computed from the estimated Green’s function and group velocity maps are obtained.

Chapter 4 covers a surface wave tomography study using regional earthquakes. A waveform catalog is formed by selecting 285 earthquakes in the region between 1997 and 2009 with magnitudes Mw > 4.5. Dispersion curves of the signals in between 10-50 sec are

obtained by using the Multiple Filter Analysis. Group velocity variations are computed and mapped for the selected period ranges.

In Chapter 5, the features of group velocity maps are discussed in relation to geology and tectonics of the region.

1.2. Geology and Tectonic Settings

Turkey is located in the east-west trending segment of the Alpine-Himalayan orogenic belt on the boundary between Gondwana in the south and Laurasia in the north. Within this belt different continental and oceanic branches related to the opening and closure of the Paleozoic and Mesozoic oceanic basins can be found. These basins are named with a common term as Tethys Ocean (Göncüoğlu *et al.,* 2000). Although the geometry and evolution of the Tethys Ocean is still in debate, there is a concensus regarding the presence of Paleo-Tethys on the south and Neo-Tethys on the north both rifted from the Gondwana margin (Stampfli, 2000). The present tectonic regime in the region follows closure and destruction of the Neo-Tethyan oceans (Figure 1.1).

The northern Neotethys is located between the Sakarya continent in the north and the Anatolide-Tauride Platform in the south. The southern Neotethys which separated Arabian Platform in the south from Anatolide-Tauride Platform in the north is located along the Southeast Anatolian Suture. Two major E-W trending ophiolite belts indicate the closure and destruction of Neotethys (Stampfli, 2000).

Various continental blocks that make up present-day tectonics of Turkey is mainly divided into six major lithospheric fragments including the Strandja, the Istanbul and the Sakarya zones, the Antolide-Tauride Block, the Kırşehir Massif and the Arabian Platform (Şengör and Yılmaz, 1981; Şengör *et al.,* 1982; Okay, 1989; Okay *et al.,* 1994).

The Strandja, the Istanbul and the Sakarya zones show similar geologic patterns with the Laurasia are referred as the Pontides. The Izmir-Ankara-Erzincan suture separates these units with the Kırşehir Massif and the Anatolide-Tauride block. The Anatolide-Tauride

Block in the south shows similar Paleozoic stratigraphy with the Arabian Platform and also with the northern margin of Gondwana (Okay and Tüysüz, 1999).

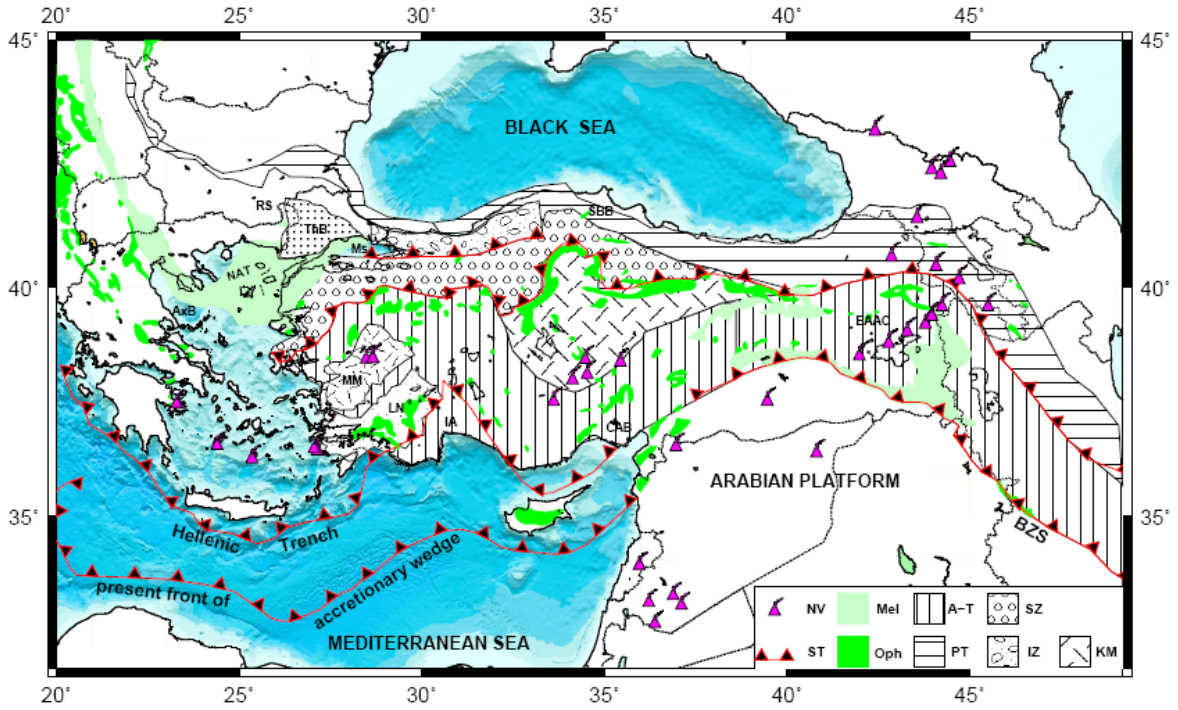

Figure 1.1. Tectonic setting of Turkey; AxB, Axios Basin; A-T, Anatolid-Tauride Block; CAB, Clicia-Adana Basin; EAAC, East Anatolian Accretionary Complex; IA, Isparta Angle; IZ, Istanbul Zone; KM, Kırşehir Massif; LN, Lycian Nappes; MM, Menderes Massif; NAT, North Aegean Trough; PT, Pontides; RS, Rhodope-Strandja Basin; SBB, Sinop-Boyabat Basin; SZ, Sakarya Zone; ThB, Thrace Basin. Green and light green units represent the ophiolites and ophiolitic mélanges, respectively. Bathymetry of the region derived from ETOPO5. Purple volcano signs show neogene and quaternary volcanism. Red triangles show the sutures and earlier subduction zones. (Modified from Stampfli, http://www-sst.unil.ch/research/plate_tecto/present_day.htm; Okay and Tüysüz 1999; Robertson 2000; Tatar *et al*., 2000; Yılmaz *et al*., 1998.

The Istanbul zone is characterized by a thick Ordovician to Carboniferous, sedimentary sequence which rests unconformably on a Precambrian metamorphic basement. It is bordered by the Strandja massif in the west, which has late Jurassic deformation and metamorphism, separated in the south along the Intra-Pontide suture from the Sakarya zone. The Sakarya zone contains no in situ Paleozoic sedimentary rocks and

underwent strong deformation and metamorphism in the late Triassic and then again in the Eocene to Miocene interval (Şengör and Yılmaz, 1981). The east-west oriented Intra-Pontide suture, marked by slivers of serpentinite, blueschist, basic volcanic rock, and Upper Cretaceous to middle Paleocene pelagic limestone is the remnant of the Mesozoic Intra-Pontide Ocean (Şengör and Yılmaz, 1981).

The Arabian Platform consists of marine, sedimentary succession accumulated from early Cambrian to middle Miocene time. The ophiolite of the Arabian platform forms a giant nappe accumulation (Yılmaz, 1993). The Bitlis Massif forming an E-W trending mountain range in southeast Anatolia is a metamorphic complex. Two tectonic units; an old, high grade metamorphic core and a metamorphic cover representing a platform sequence constitute this massif (Yılmaz, 1993). Bitlis Massif and its ophiolitic cover is fragmented by the rifting of the Maden Basin. For this reason, the various ophiolite fragments were transported into the basin. Wide spread volcanic activity accompanied the sedimentation in this region (Yılmaz, 1993).

The Anatolide-Tauride Block forms the main part of the southern Turkey. This unit shows a similar Paleozoic stratigraphy to the Arabian platform and also with Gondwana. There is a massive ophiolite and accretionary complex accumulation over this block. The Antolide-Tauride block can be described in three regional metamorphic complexes; The Tavşanlı zone, the Afyon zone and the Menderes Massif. The Bornova Flysch Zone in the Anatolide-Tauride block exists between the Izmir-Ankara-Erzincan suture and the Menderes Massif (Okay and Tüysüz, 1999).

In the central Anatolia, the Kırşehir Massif consists of metamorphic and voluminous granitic rocks. These metamorphic rocks of the Kırşehir Massif with isotopic ages from Cretaceous constitute a coherent metasedimentary sequence of granulite, gneiss, micashist, metaquarzite, marble and calc-silicate rocks and they are folded and multiply deformed rocks (Seymen, 1984; Okay and Tüysüz, 1999). The accretionary complex and the metamorphic rocks which are intruded by granitic rocks cover large areas in the Kırşehir Massif.

The Black Sea basin is composed of two deep basins (Figure 1.2): the western Black Sea basin, which is underlain by oceanic to suboceanic crust, contains a sedimentary cover of up to 19 km thick. The eastern Black Sea basin which is underlain by thinned continental crust has 12 km thickness of sediments (Nikishin, *et al*., 2003). These basins are separated by the Andrusov Ridge that is formed from continental crust and overlain by 5-6 km thickness of sedimentary cover (Robinson, 1997).

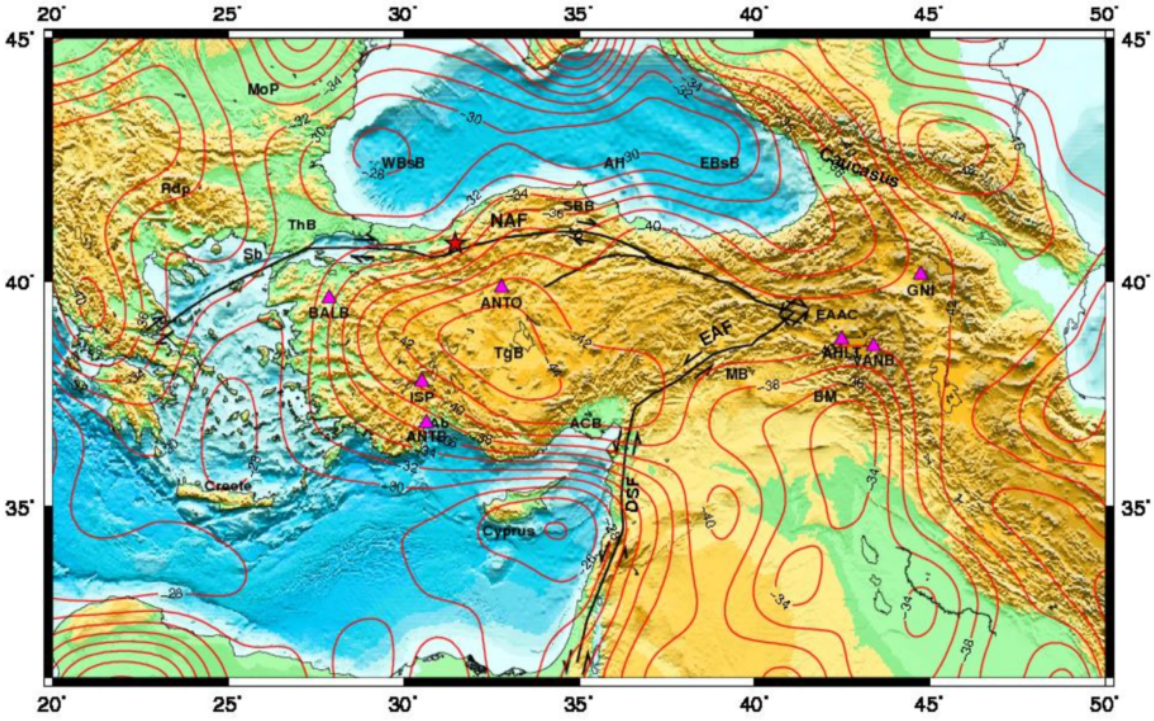

Figure 1.2. Topography and crustal thickness of Turkey and surroundings (Mooney *et al.,* 1998) ; Abreviations: AR, Andrusov Ridge; AxB, Axion Basin; CAB, Clicia-Adana Basin; EAAC, East Anatolian Accretionary Complex; EAF, East Anatolian Fault; MoP, Moesian Platform; NAF, North Anatolian Fault; SBB, Sinop-Boyabat Basin; ThB, Thrace Basin; TgB, Tuz Golu Basin; WBsB, Western Black Sea Basin; EBsB, Eastern Black Sea Basin; Sb, Saros Bay. The red star shows the location of an aftershock of 12 November Düzce earthquake (Mw=5.0). Bathymetry and Topography of the region derived from ETOPO5 and GTOPO30.

Anatolia is surrounded by seismically active boundaries and interactions with a variety of crustal types and tectonic styles. As a result of continuous intense deformation

the region contains diverse structures, such as suture zones, metamorphic complexes and young orogenesis. High topography in the Eastern Anatolia as a result of collision of Arabian plate with Eurasia, relatively low topography in the Western Anatolia with extension due to the subduction indicates significant variations on the crustal structures. Eastern Anatolia has a high topography, more than half of the region has an elevation of about 1.5 km (Yılmaz *et al.*, 1987). Figure 1.3 shows the map of Turkey with the topographic elevations more than 1.5 km in the region.

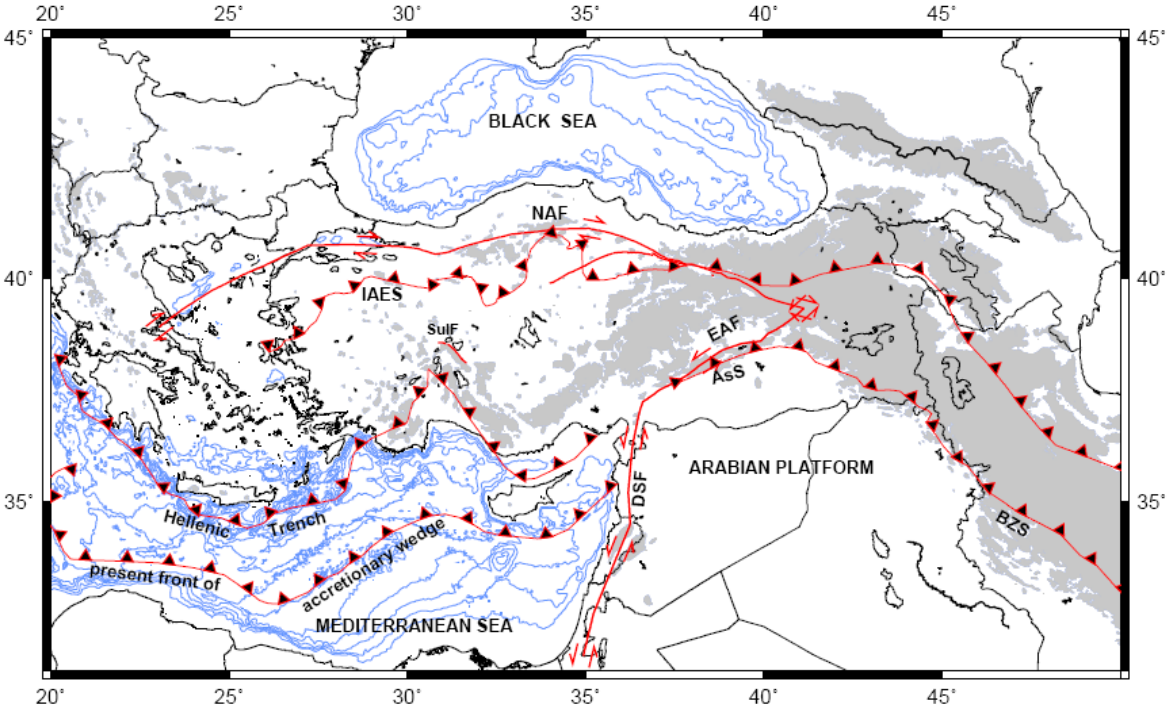

Figure 1.3. Faulting and topography map of Turkey and surroundings. AsS, Assyrian Suture; BZS, Bitlis-Zagros Suture; EAF, East Anatolian Fault; DSF, Dead Sea Fault; IAES, Izmir-Ankara-Erzincan Suture; NAF, North Anatolian Fault; SulF, Sultandağ Fault. Gray shaded area shows the topography higher than 1.5 km.

Three major structures dominate the active tectonics of Turkey; the Hellenic-Cyprus trench, dextral North Anatolian Fault and sinistral East Anatolian Fault (Figure 1.3). The Anatolian plate is being extruded along these intra-continental strike-slip fault zones between the converging Eurasian and Arabian plates. The western part of the Anatolian Plate is dominated by E-W trending horst and graben structures (Stampfli, 2000). The Central Anatolia forms a broad transitional tectonic zone between the extensional tectonic

regime of the Western Anatolia and the strike slip tectonic regime of the Eastern Anatolia (Koçyiğit *et al*., 2000). The central Anatolia is also a continental back-arc of the North dipping Hellenic-Cyprus subduction zone. Most of the geological structures of Central Anatolia and the Taurides, including Isparta angle, have been sourced from the tectonic and magmatic events related to this active convergent plate boundary (Glover and Robertson, 1998; Koçyiğit *et al*., 2000).

1.3. Previous Studies

Turkey and the surrounding areas have been the target of many geophysical studies due to its active tectonics and the high rate of seismicity. Continuous regional deformation along the seismically active boundaries contains diverse structures such as suture zones, metamorphic complexes and young orogens (Stampfli, 2000). Significant variations exist on the tectonic styles and crustal structures. Until recently, investigations on the crustal thickness and seismic velocities from the surface waves and receiver functions used the sparse distribution of the stations in the region. Mindevalli and Mitchell (1989) analyzed group wave velocity data by using the regional earthquakes. They have found the average crustal thickness as 40 km and the upper mantle shear velocity as 4.2 km/s by using the recordings of ANTO station. Using receiver function analysis Saunders *et al*., (1998) found that the crust is approximately 30 km thick in the western Turkey whereas it increases up to 34 km at the eastern part of it. Zor *et al*., (2003) performed receiver function studies in the eastern Turkey by using the 29 broadband seismic station of PASSCAL network recorded during the Eastern Turkey Seismic Experiment (ETSE) (Sandvol *et al*., 2003). They found an average crustal thickness of 45 km in the eastern Turkey. Al-Lazki *et al*., (2003) inverted Pn phase travel time residuals observed low Pn velocities beneath the eastern Anatolia. Gök *et al*., (2003) mapped the Sn propagation efficiencies in the Anatolian and Iranian Plateau. Maggi and Priestly (2005) studied the Turkish – Iranian plateau using the surface waveform tomography and obtained a low shear wave velocity anomaly in the uppermost mantle beneath the plateau. During the Western Anatolia Seismic Recording Experiment (WASRE) Zhu and others installed five broadband and 45 short-period temporary seismic stations throughout the Menderes Massif of western Turkey, distributed partly as a dense, 100-km-long, N-S linear array and partly as a regional network in order to study crust-upper mantle structure and seismicity. They have combined teleseismic

waveform data from these stations with data from several permanent seismic stations and determined crustal thickness variations in the Aegean region from the receiver function analysis. They indicated a general trend of westward crustal thinning from 36 km in central Anatolia to 28–30 km in the central Menderes Massif to 25 km beneath the Aegean Sea (Zhu *et al*., 2006). Some other works have also been performed in the region at greater scale in order to estimate group and phase wave velocity variations. Curtis *et al*., (1998) studied fundamental mode surface wave in Eurasia and Indonesia and estimated phase velocities in between 20-170 sec. They have correlated the phase velocity variations with tectonic structures. Ritzwoller and Levshin (1998) performed a surface wave tomography in Eurasia including some parts of Africa and the Middle East and studied the dispersion characteristics of broadband fundamental mode surface waves in the period range of 20-200s for Rayleigh waves and 20-125 sec for Love waves. Pasyanos *et al*., (2001) performed a similar work in Middle East and North Africa from surface wave group velocity dispersion. They have computed the Rayleigh and Love wave velocities for periods from 10-60 seconds. They have obtained short period structure which is well correlated with large sedimentary features and long period Rayleigh wave inversion which is sensitive to fast velocities that correlate with the relatively thick Zagros Mts. and Turkish-Iranian Plateau. Another surface wave dispersion study was performed by Pasyanos (2005) across Eurasia and North Africa. In their study, path density increased by improving the spatial resolution and expanding the period range. The significance of their work was its being the first surface wave dispersion study performing the group wave velocity dispersion at various periods. By using the conjugate gradient method with a variable smoothness parameter in the inversion procedure, they have obtained higher resolution models in the period range from 7-100 seconds. Karagianni *et al*., (2005) derived a 3-D tomographic image of the shear-wave velocity structure of the crust–uppermost mantle in the Aegean region by using the group velocities of the Rayleigh wave fundamental mode. They have used a database consists of 185 regional earthquakes recorded at broad-band stations that were installed for a period of six months in the Aegean area within the framework of a large-scale experiment. They have inverted 80 local dispersion curves by using a non-linear inversion approach, deriving the corresponding 1-D shear velocity models. They have obtained an approximately 20–22 km thin crust in most of the central Aegean sea and in the remaining Aegean sea area they have observed a crustal thickness less than 28–30 km. DiLuccio and Pasyanos (2007) used group velocity

maps for Rayleigh and Love waves to determine 1-D crust and upper-mantle structure at a regular series of points in the Eastern Mediterranean region. They produced a 3-D lithospheric model containing maps of sediment and crustal thickness. Sodoudi *et al*., (2006) computed P and S receiver functions from 65 permanent and temporary broadband stations in the Aegean region to image Aegean and African Moho. Yelkenci (2006) investigated the crustal structure in Central Anatolia by using receiver function analysis. Gök *et al*., (2007) obtained lithospheric structure in the Eastern Turkey using the receiver functions and surface wave group velocities. Another study was performed in order to develop the 3-D upper mantle P wave tomographic model for Eastern Turkey by using teleseismic phase readings (Zor, 2008).

Variation of the crustal thickness in the region where has been studied by many researchers (Mindevalli and Mitchell, 1989; Saunders *et al*., 1998; Zor *et al*., 2003; Zhu *et al*., 2006; Gök *et al*., 2007). A general consensus is on the variation of the crustal thickness in region exists with a direct proportion with the variation of topography. A crustal thinning observed from 36 km in central Anatolia to 28-30 km in Menderes Massif and to 25 km beneath the Aegean Sea by Zhu *et al*., (2006). Average crustal thickness has been observed as 36 km in the Arabian plate, 44 km in the Anatolian Block and 48 km in the Anatolian Plateau by Gök *et al*., (2007).

2. SEISMIC NOISE ANALYSIS

2.1. Introduction

Seismic stations are never at rest during their routine daily recordings and they constantly contain small movements of the earth's crust (Lay and Wallace, 1995). Noise is conventionally described as disturbance in the signal which does not represent part of a message from a specified source (Sherrif R. E., 1991) and signals always contain noise as an undesired interference with the valuable information. Ambient seismic noise is mainly made up of surface waves with varying properties in different period bands (Friedrich *et al*., 1998; Ekström, 2001; Stehly *et al*., 2006). The analysis shows that noise is temporally and spatially variable and strongly frequency dependent (Lay and Wallace, 1995; Pedersen *et al.,* 2007).

Seismic noise has been studied comprehensively from the beginning of instrumental seismology. Relationships of seismic noise and sea waves, storms and atmospheric variations have been investigated by many researchers. Bertelli in the 19th century emphasized a correlation between the long period signal recorded by a pendulum and disturbed air pressure, and he suspected the influence of coastal sea waves (Bertelli, 1872; Stutzman *et al*., 2000; Bonnefoy-Claudet, 2006). But the major review concerning seismic noise has been first carried out by Gutenberg with a comprehensive work into the nature and the origin of microseisms (Gutenberg, 1911). Gutenberg has studied the microseisms characterized by a regular nearly sinusoidal motion with periods in general between 4-10 seconds (Gutenberg, 1931; 1958). His observations show that neither the air pressure, nor its change or storm can be the cause of microseisms. His results show that no possible disturbance near the surface of the ocean can be propagated through the water to the bottom, but that the energy of the waves transformed by the surf to the coast is large enough to cause the measurements. According to this theory Gutenberg claimed that the primary and the secondary microseisms are believed to be related to the interaction of sea waves with the coast. Later on Bernard (1938) and Longuet-Higgins (1950) showed the relation between microseism periods and oceanic swells. Bernard (1938; 1941a; 1941b)

observed that the microseism peak period is half of the period of the oceanic waves (Stutzman *et al.,* 2000; Bonnefoy-Claudet, 2006). Longuet – Higgins (1950) explained microseism that they are generated by pressure variations on the sea bed due to ocean waves raised by the wind and stated that the primary microseism has periods similar to the main swell at 10-20 sec and the secondary microseism originates from the nonlinear interaction between direct and reflected swell at 5-10 sec pressure variations. The necessary condition for the generation of microseisms on the present hypothesis is the interference of groups of waves of the same wavelength traveling in opposite directions.

Between the 1950 and 1970 technical improvements in instrumentation allowed significant advances in the understanding of the noise phenomena. Brune and Oliver (1959) published the curves of high and low seismic background displacement based on a world wide survey of station noise and since that time the subject has been a part of the research. Later on, with the establishment of World Wide Standard Seismograph Network (WWSSN) in the 1960's studies on noise levels of long period seismographs have began by Peterson and Orsini (1976) over the period range from 0.1 to 1000 sec. Soon after, these works were extended to longer periods by Agner and Berger (1978) and to shorter period with low noise spectra from Texas by Li (1981). Peterson (1993) performed an intensive report on the observations and modeling of seismic background noise. His first objective was to present a catalog of seismic background noise spectra obtained from a worldwide network of seismograph stations. The latter aim was to refine and document models of seismic background noise that have been in use for several years (Peterson, 1993). Now it has been more than a decade since the last comprehensive model of ambient Earth noise is published by him and his work was the first comprehensive global study from a variety of networks. The Peterson noise curves and the representation of New High Noise Model (NHNM) and New Low Noise Model (NLNM) have standardized the way of representing seismic noise.

Since 1970 the number of works dealing with seismic noise has accelerated impressively and the majority of these works are focused on the applicability of seismic noise to some specific case studies. Analyzing the seismic noise for microzonation and the use of noise background vibration in array techniques were popular subjects in 1980's and

1990's. Applications were mainly dedicated to geotechnical engineering and site studies (Bonnefoy-Claudet, 2006). Current applications of seismic noise focus on the estimation of Green's functions for a crustal structure. With the tremendous increase in the use of noise on this new method the analysis of noise influence of the seismic noise has been studied by many researchers (Stehly *et al*., 2006; Campillo, 2006; Pedersen *et al*., 2007). In Turkey, seismic noise level was studied previously by using seven broadband stations in order to investigate the daily and seasonal variations in the region (Köseoğlu, 2001).

With the recent progress in signal processing techniques besides being an unwanted signal, seismic noise become an efficient and creditable way of exploration in seismology. The most recent developments exhibit that the subsurface information of Earth is recovered with the processing of ambient seismic noise as an inexpensive and robust source. Several methods based on ambient seismic noise records are widely used in seismology for determining the velocity structure of Earth either in engineering studies or in the studies of crust and mantle. This implementation of noise brings the significance of understanding the variations of ambient seismic noise in the region for interpreting the results in a trustworthy manner. Knowledge of seismic noise spectrum is important in understanding the origin of microseisms and also for interpretation of the results of various ambient seismic noise studies held in the region. Since the noise varies widely as a function of period, time, geography a precise evaluation of location, time and period can be obtained by an extensive seismic noise analysis from the measurements of seismic stations. The objective of this study is to analyze both of the temporal and spatial characteristics of ambient seismic noise in Turkey. For this purpose power spectral densities of the broadband seismic stations were computed in the frequency range of 100 sec – 10 Hz. Diversities in noise spectra were investigated in terms of different installation properties, diurnal, seasonal and geographic variations. The PSD calculated from one year of data was stacked and statistical properties such as median, mode, average, minimum, maximum, and the 90^{th} percentile have been obtained for each station and component.

2.2. Seismic Noise Characterization

The sources of the seismic noise can be either from the instrumentation or from ambient Earth vibrations. Noise levels due to instrumentation are well below the seismic

background noise so they do not dominate the recording on seismometers (Havskov and Öttemöller, 2008). Ambient seismic noise defines ambient vibrations of the ground caused by sources such as tides, water waves striking the coast, turbulent wind, effects of wind on trees or buildings, traffic or human based noises (Boonefoy-Claudet, 2006). When the power spectral density curves of noise calculated for the stations it can be seen that the noise has a characteristic variations with respect to period or frequency.

Ambient seismic noise basically has two different origins named as cultural and natural representing the microtremors and microseisms, respectively. The origins of microtremors are mainly cultural from the actions of human beings. The other sources of microtremors are rain, traffic, wind, industrial noise in the urban areas. Cultural noise is mainly seen as high frequency noise surface waves greater than 1.0 Hz and they attenuate within several kilometers in distance and depth. So the cultural noise generally has significantly lower noise levels in boreholes and deep tunnels. Cultural noise shows strong diurnal variations and it has characteristic frequencies depending on the distribution of the noise source (McNamara and Buland, 2004). Wind, water and the geologic noise constitute the other sources of microtremors.

The spectral boundary between microseisms and microtremors is accepted as 1.0 Hz in most of the studies, but this limit can be shifted to a lower frequency (Seo, 1997). Microseisms are commonly used for the continuous oscillations of the ground. The main causes of microseisms are the atmospheric disturbances, oceanic storms etc, but the nature of these seismic sources is still not completely understood (Holcomb, 1989). Ocean generated microseisms are a constant source of energy and ambient seismic noise is dominated by two peaks of microseism at 7.0 sec and 14 sec period (Friedrich *et al*., 1998). A peak, which is known as microseismic peak or double frequency peak, takes place around 7.0 sec. A relationship between this peak and oceanic waves is associated with storms in various studies (Gutenberg, 1931; Ramirez, 1940). A further progress was occurred with the explanation of Longuet-Higgins (1950) on the theory of the establishment of this microseism that ocean waves of equal period traveling in opposite directions generate standing waves of half the period. The noise peak observed around 14 sec, which is called as single frequency peak, has smaller amplitude than the double frequency peak. Haubrich *et al*., (1963) demonstrated a close relationship between

microseisms and ocean waves at the beaches. At single frequency peak (14 sec), microseisms can only be generated in coastal regions in shallow water. Microseisms are generated directly through gravity waves of the ocean at this period. The height of the water on the ocean at a fixed point varies with the motion of the wave. Water wave energy is directly converted to seismic energy through vertical pressure variations that have the same periods as the water waves (Friedrich *et al*., 1998).

2.3. Description of Stations

Analysis of seismic noise in the frame of this study started in 2005 by using 39 broadband stations recording in the region. In 2005 the National Earthquake Monitoring Center (NEMC) of Kandilli Observatory Earthquake and Research Institute (KOERI), was operating 29 broadband stations and the rest of the stations was operated by Marmara Research Center (MRC), IRIS/USGS, and GEOFON. KOERI has continuously increased the number of broadband stations in 2006 and 2007. The number of broadband stations exceeded 100 in 2008. For a better understanding of the noise variations in the region we have enlarged the database with the recent stations of KOERI. We have increased the number of stations to 120 whereas the 77 of these stations are operated by KOERI and seven of them are operated by MRC. Data from a temporary network operated in between the 1999-2001 with 29 broadband stations during the Eastern Turkey Seismic Experiment (ETSE) is included in the analysis. ANTO and GNI stations operated by IRIS and ISP, MALT, CSS, APE stations operated by GEOFON were also added with CHOS station of Aristotle University of Thessaloniki. Figure 2.1 shows the locations of the stations operating in 2007 in the region, which is used in this study. Green triangles indicate the ETSE stations operated during 1999-2001. Red triangles show all other stations recording in the region operated by various networks such as KOERI, MRC, GEOFON and IRIS during 2005-2007.

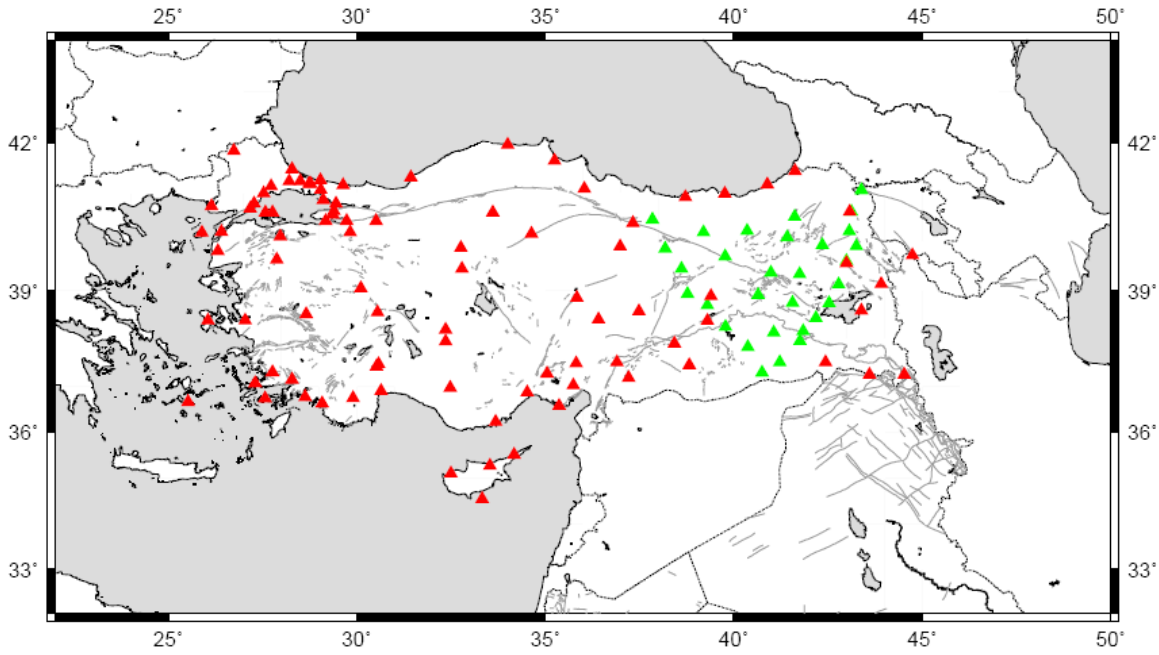

Figure 2.1. Permanent and temporary seismic stations used in the noise analysis. Red triangles are the broadband stations from different networks recording during 2005-2007. Green triangles are ETSE stations operated during 1999-2001.

The broadband stations used in this study have different types of instrumentation. GEOFON stations and GNI were equipped with Streckeisen STS-1 (360 sec) and STS-2 (120 sec) seismometers with a Quanterra datalogger, which allow the recording of all relevant seismic signals from high frequency local events to the earth tides with sufficient dynamic range. ANTO station is equipped with KS3-6000 seismometer with a Quanterra digitizer. CHOS station is equipped with CMG-3ESP (100s-50Hz) seismometer. All of these stations from ORFEUS network recorded continuously with 20 sps. The broadband stations of ETSE project were equipped with STS-1 seismometers and REFTEK 72 A recorders with the exception of EZRM station (Sandvol *et al.,* 2003). A Guralp CMG 3-T seismometer was used at EZRM with 24 bit digitizer recorded continuously at 40 sps. KOERI and TUBITAK networks have been using different seismometer types. Guralp CMG 3T (300 sec and 120 sec), CMG 40T (30 sec), CMG 6T (30 sec), CMG 3ESP (30 sec and 60 sec) types of seismometers are recording mainly at 50 sps. Relevant information on the equipment of the KOERI network can be found on the web page of NEMC at *http://www.koeri.boun.edu.tr/sismo/default.htm.*

2.4. Power Spectral Density Method

Power Spectral Density (PSD) estimation which describes the distribution of power with frequency is a standard method for quantifying seismic background noise. The spectral density estimation can be performed by using a parametric or nonparametric (classical spectral estimation) approach. Parametric PSD estimation tries to fit a model to the signal by minimizing a given cost function such as Burg's Entropy Method, Yule Walker method, etc. On the other hand, non-parametric methods do not make any assumptions on the data or model and use the data directly. The Periodogram, Modified Periodogram, Bartlett's Method and Welch's method are the common non-parametric PSD estimation methods (Marple, 1987; Kay, 1988; Stoica and Moses, 1997). In the frame of this thesis Welch's spectral estimation method from the nonparametric spectral estimation techniques were used to estimate the distribution of seismic noise power.

The periodogram method relies on the definition of the PSD however, the periodogram method provides high resolution for sufficiently long data lengths, but it is a poor spectral estimator due to the high variance that does not decrease with increasing data length (Stoica and Moses, 1997). The high variance of the periodogram motivates the development of modified methods that have lower variance at a cost of reduced resolution. The latter methods; Bartlett's method and Welch's spectral estimation method were developed in order to decrease the variance by recommending various solutions such as applying window or dividing the data into segments or overlapping the divided segments etc.

Welch's spectral estimation method was modified from the Bartlett's method. Welch applied a data window to the data in each segment prior to the computation of the segment periodogram and he permitted these data segments to overlap. Let the Equation 2.1 denote the *jth* data segment,

$$y_j(t) = y((j-1)K + t)$$
$$t = 1,..., M \qquad (2.1)$$
$$j = 1,..., S$$

The sequences do not overlap if *K=M. If K=M/2* data segments overlap by 50 per cent between successive segments. The windowed periodogram corresponding to $y_j(t)$ computed as

$$\hat{\emptyset}_J(\omega) = \frac{1}{MP}\left|\sum_{t=1}^{M} v(t)\, y_j(t) e^{-i\omega t}\right|^2 \qquad (2.2)$$

Where P defines the 'power' of the temporal window {*v*(t)}

$$P = \frac{1}{M}\sum_{j=1}^{L}\left|v(t)\right|^2 \qquad (2.3)$$

The Welch spectral estimation is determined by averaging the windowed periodograms:

$$\hat{\emptyset}_w(\omega) = \frac{1}{S}\sum_{j=1}^{S}\hat{\phi}_J \qquad (2.4)$$

In Welch method the use of different truncation windows reduce the effect of side-lobes and the estimation bias, on the contrary decrease the resolution slightly. Besides with letting the overlapping he increased the number of data segments that are averaged for a given data record length in order to decrease the PSD estimate variance. Further detail on the theory of spectral estimation techniques can be found at Stoica and Moses (1997).

Before beginning to the process of the data for power spectral estimation one hour long data segments have been formed from continuous time series for each station and each component. Data down sampled to 20 sps for all stations and components in order to obtain a unique sampling rate from different networks. Instrument responses, mean and long period trends have been removed before the computation of the power spectral density curves. In the data processing procedure neither the body and surface waves from the earthquakes, nor the system transients and instrumental glitches removed from the data. The power spectral density estimate for each hour recording has been computed by using the Welch spectral estimation method. In order to improve the Fast Fourier Transform (FFT) speed ratio, by reducing the number of operations, the number of samples in each of the 13 time series segments is truncated to the next lowest power of two. Each segment is truncated with a window that is the same length as the segment. After all, segments were averaged to provide a PSD for each one-hour time series. Description of data processing procedure can be found in McNamara and Buland (2004) and McNamara and Boaz (2005). The steps in data processing of power spectral density method are summarized in Figure 2.2 with an example of estimated power spectral density curves. The power spectral density curves plotted for each station and each component as a function of period (sec) to decibel (dB) with respect to acceleration $(m/s^2)^2/Hz$ (McNamara and Buland, 2004). Raw frequency distributions were constructed by gathering individual power spectral densities by binning periods in 1\8 octave intervals and binning the power in 1.0 dB intervals. The lowest and the highest noise models of Peterson (1993), has been also plotted in order to compare the noise levels. For a wealthy seismic noise characterization, statistical properties such as minimum, median, mode, average, maximum and the 90^{th} percentile were also calculated and plotted.

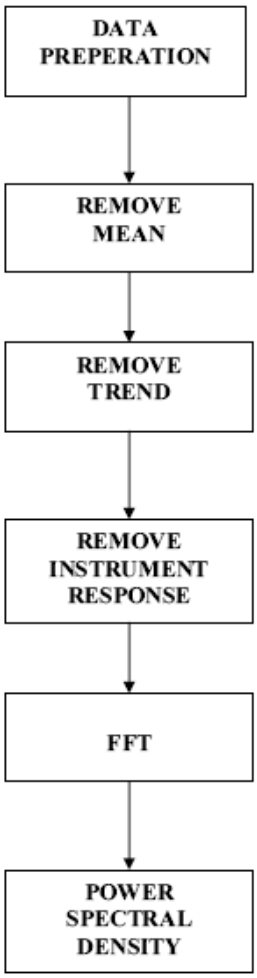

Figure 2.2. The steps of data processing for the seismic noise analysis.

Power spectral density curves represent the variation of seismic noise for each hour data segment. In order to estimate the true variation of seismic noise probability density functions (PDFs) from the PSDs processed. Raw frequency distribution are taken in 1/8 octave intervals. Figure 2.3 shows the PDF computed from vertical component at station CSS constructed using the PSDs recorded during the year in 2005. The probability of occurrence of a given power at a particular period was plotted with a color bar. High and low noise models were also plotted with the PDF for direct comparison. The minimum and maximum noise levels have generally very low probability estimates so they do not represent common station noise levels. The mode and 90^{th} percentile may affected by system transients (McNamara and Buland, 2004).

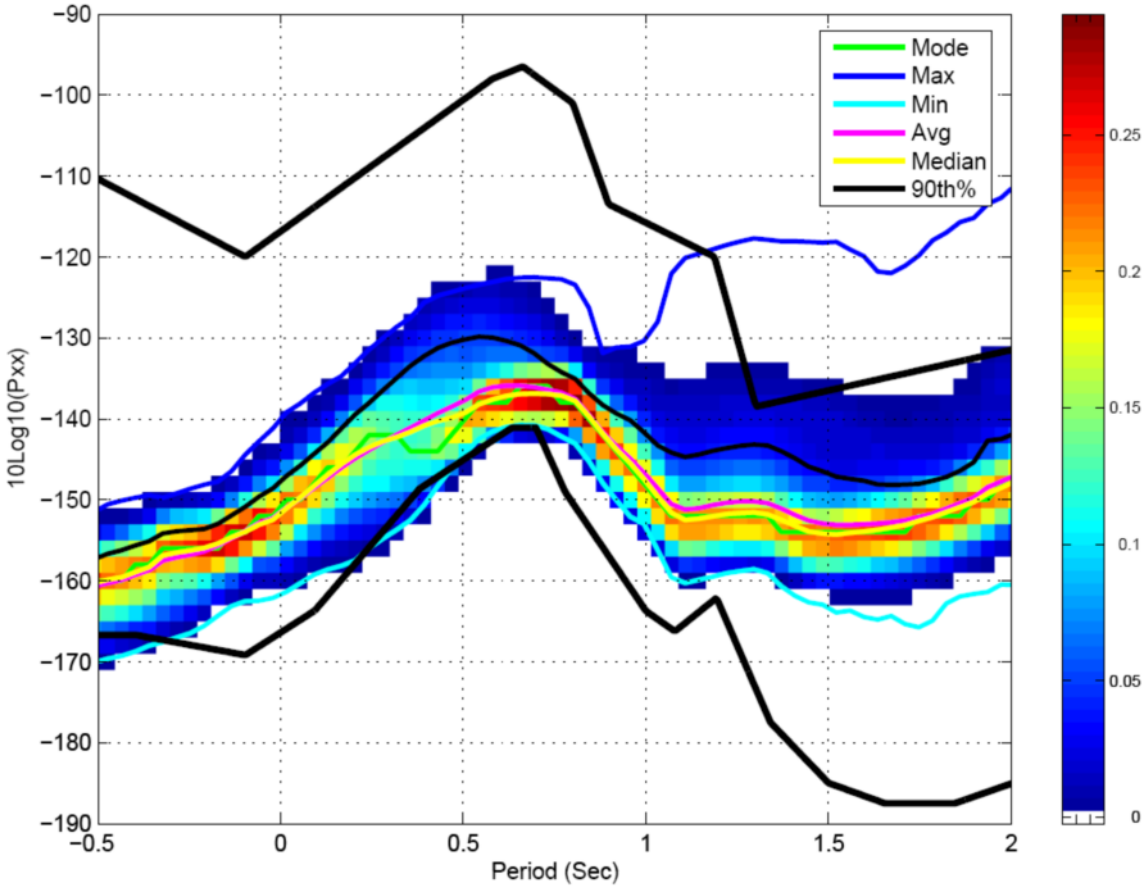

Figure 2.3. Probability Density Function of the vertical component of CSS station constructed from 1554 PSDs during the period of January 2005 to January 2006. The horizontal axis is logarithmic.

2.5. Instrumental Variations of Seismic Noise

The aim of seismic noise analysis is to investigate the temporal and geographical variations of the natural sources of seismic noise. However, seismic noise level not only changes temporally and geographically but also changes according to the noise variations induced by sensor or sensor installation. In order to see the effect of sensor types and installation properties we have compared different types of instrumentation. Stations with different instrumentation were compared for their recording performances. Figure 2.4 shows the PDF of the selected stations with different recording ranges and seismometer types. The stations (MRMX, YLVX) include sensors with 30 sec, (ADVT, AGRB) 120 sec and (ANTO, VANB) 300 sec.

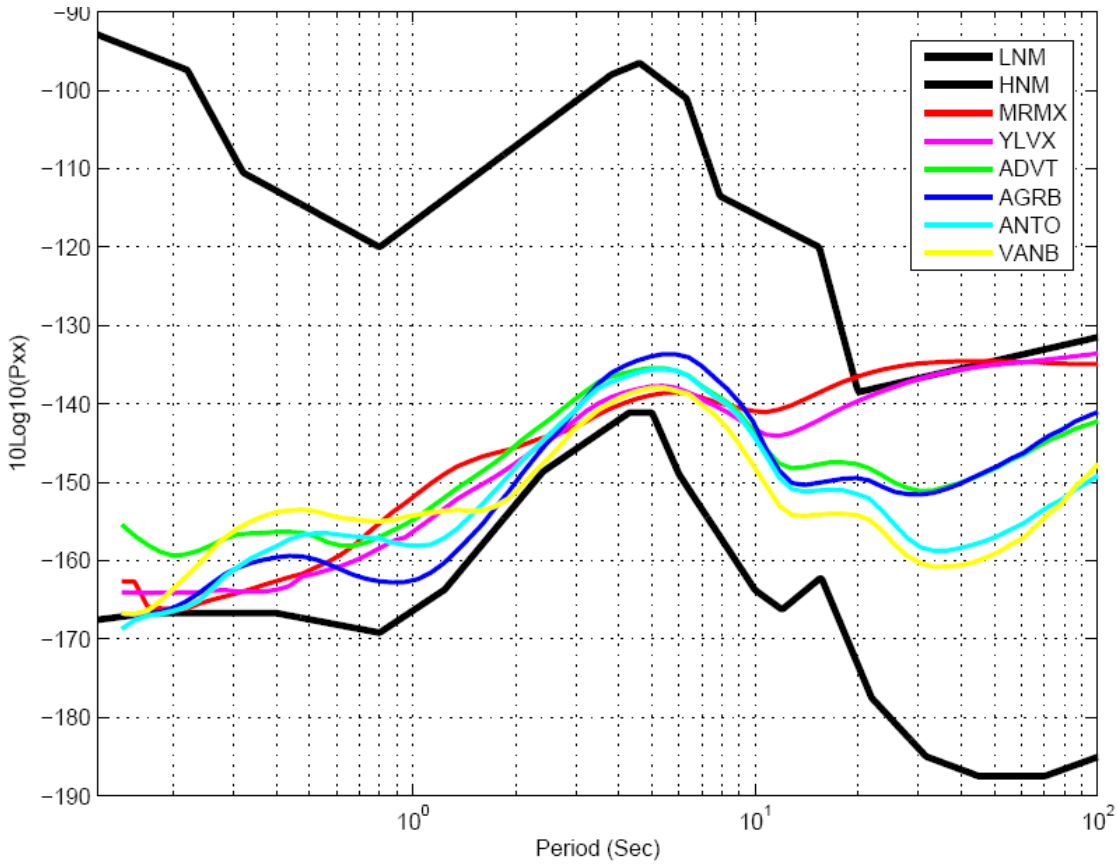

Figure 2.4. Average power spectral density curves of MRMX, YLVX, ADVT, AGRB, ANTO and VANB with low and high noise models.

We observe spectral peaks at approximately 7.0 and 14 sec as in the LNM and HNM. When the average power spectral density curves are compared, stations operating with the same instrument type show similar noise levels especially at the longer periods. CMG 40T seismometers of MRMX and YLVX exceed HNM at periods higher than 20 sec. ADVT and AGRB (120 sec) stations show approximately equivalent variations at longer periods with ANTO and VANB stations. At shorter periods the average PSD values have similar behavior and close to LNM.

2.6. Temporal Variations of Seismic Noise

In order to see the temporal variations of seismic noise we investigate the diurnal and seasonal variations of seismic noise separately. One year of data was stacked for the analysis. In order to discriminate the diurnal variations day time computations are

performed in the time period from 10:00 to 18:00 and night time computations included in the time period from 22:00 to 06:00. Seasonal variations of seismic noise were computed by averaging power spectral density over quarters of the year. Each quarter of the year was computed by the accumulation of three months. December, January, February cumulated as winter, March April May as spring, June, July, August as summer and September, October and November cumulated as fall.

2.6.1. Diurnal Variations of Seismic Noise

Diurnal variations of seismic noise are plotted by computing power spectral density over periods of eight hours of local time. The results for VANB station from KOERI network is shown on Figure 2.5. The figure at the top represents the day time hours (10:00 -18:00) for three components whereas the bottom one represents the night time hours (00:00 – 08:00). Seismic noise levels at day time and night time hours show similar variations especially at periods longer than 1. sec. The noise level at longer periods is typically higher on the horizontal components than on the vertical component. At periods shorter than 1.0 sec seismic noise levels between day time and night time hours differ up to 10 dB and has a higher value at day time hours. Average seismic noise level (pink curve) of VANB station has approximately a value of -165 dB for daytime hours at 10 Hz; whereas the average seismic noise level of night time hours for the same data set is well below -170 dB for all three components. Higher seismic noise levels during the day time hours and lower seismic noise levels at night time hours are the result of temperature variations, atmospheric and cultural activity. Temporal variations of seismic noise have been studied by Stutzmann *et al*., (2000). According to their study, diurnal variations occur mostly due to the human activity in daytime. The stations located in suburbs have higher noise levels than the stations outside the populated areas and in general seismic noise is higher during the day than night.

Figure 2.6 shows the diurnal variations of seismic noise at ANTO station for three components. ANTO seismic station has been installed in 1992 at Ankara by IRIS/USGS. Elevation of the station was 883 m and the sensor is located at 195 m depth. There is not much difference between the day time and night time seismic noise levels. Even at the shorter periods of the power spectral density curve, where the cultural noise variations can

be observed more exhaustively, the noise levels are not significantly different. This is a result of the installation depth of the ANTO station.

The effect of wind speed to borehole stations at higher frequencies was studied by Withers *et al*., (1996). They have studied high-frequency (> 1.0 Hz) seismic noise characteristics as a function of wind speed and shallow depth by measuring the wind speed at stations installed to different depths and observed a strong correlation between Seismic Background Noise (SBN) and wind speed. According to their study SBN was contaminated by wind speed and this can be reduced by increasing the depth of the station location. The lower noise levels of ANTO station at higher frequencies are observed as expected when compared with the stations at surface.

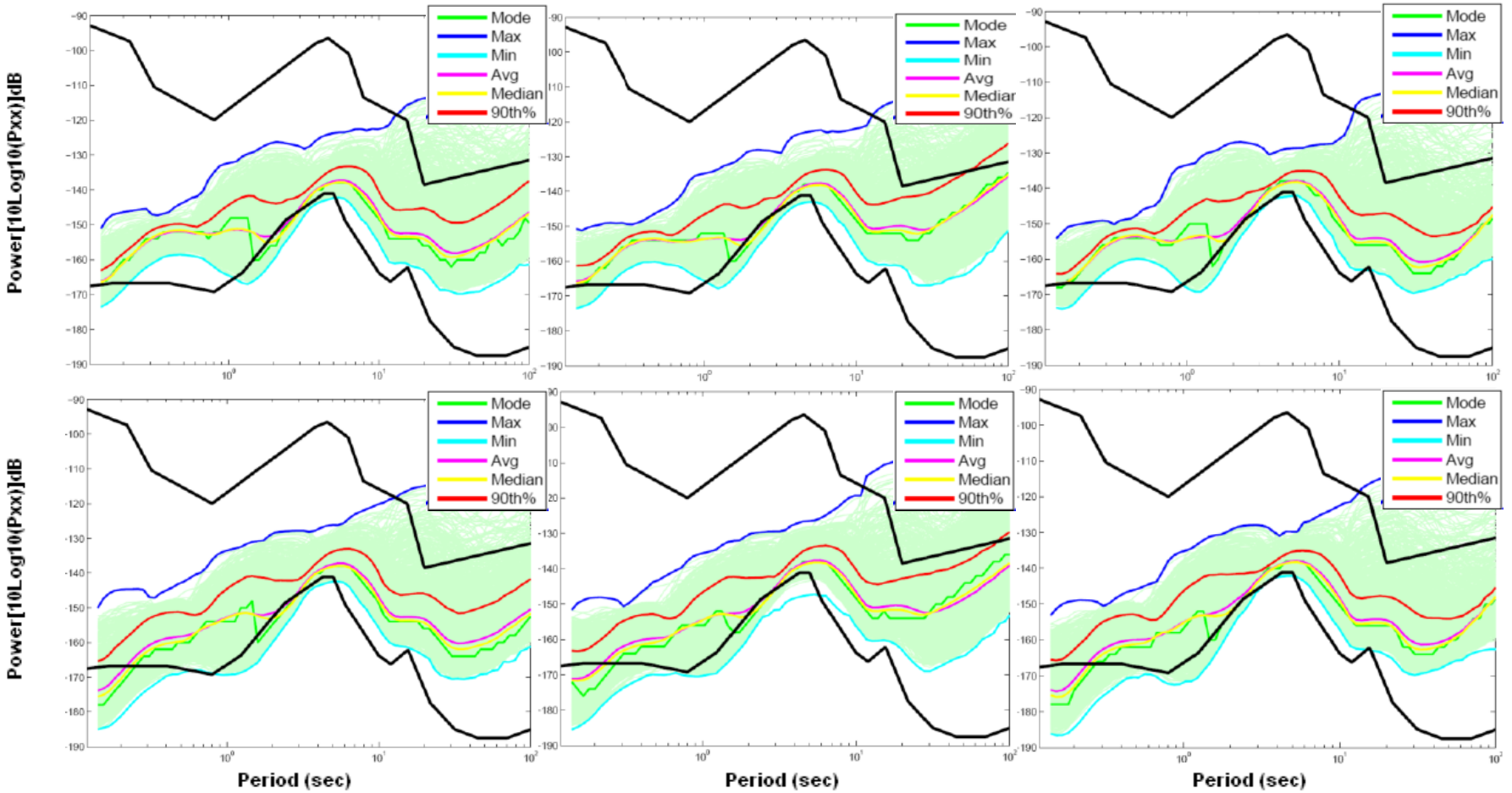

Figure 2.5. Power spectral densities of VANB station, for day time (10:00 to 18:00 at the top) and night time (22:00 to 08:00 at the bottom) hours, for BHE, BHN, BHZ component from left to right, respectively. Green curves indicate individual PSD function for each hour. Thick black lines show high and low noise levels of Peterson. Different colors indicate the statistical variations such as Mode, Maximum, Minimum, Average, Median and 90th percentile.

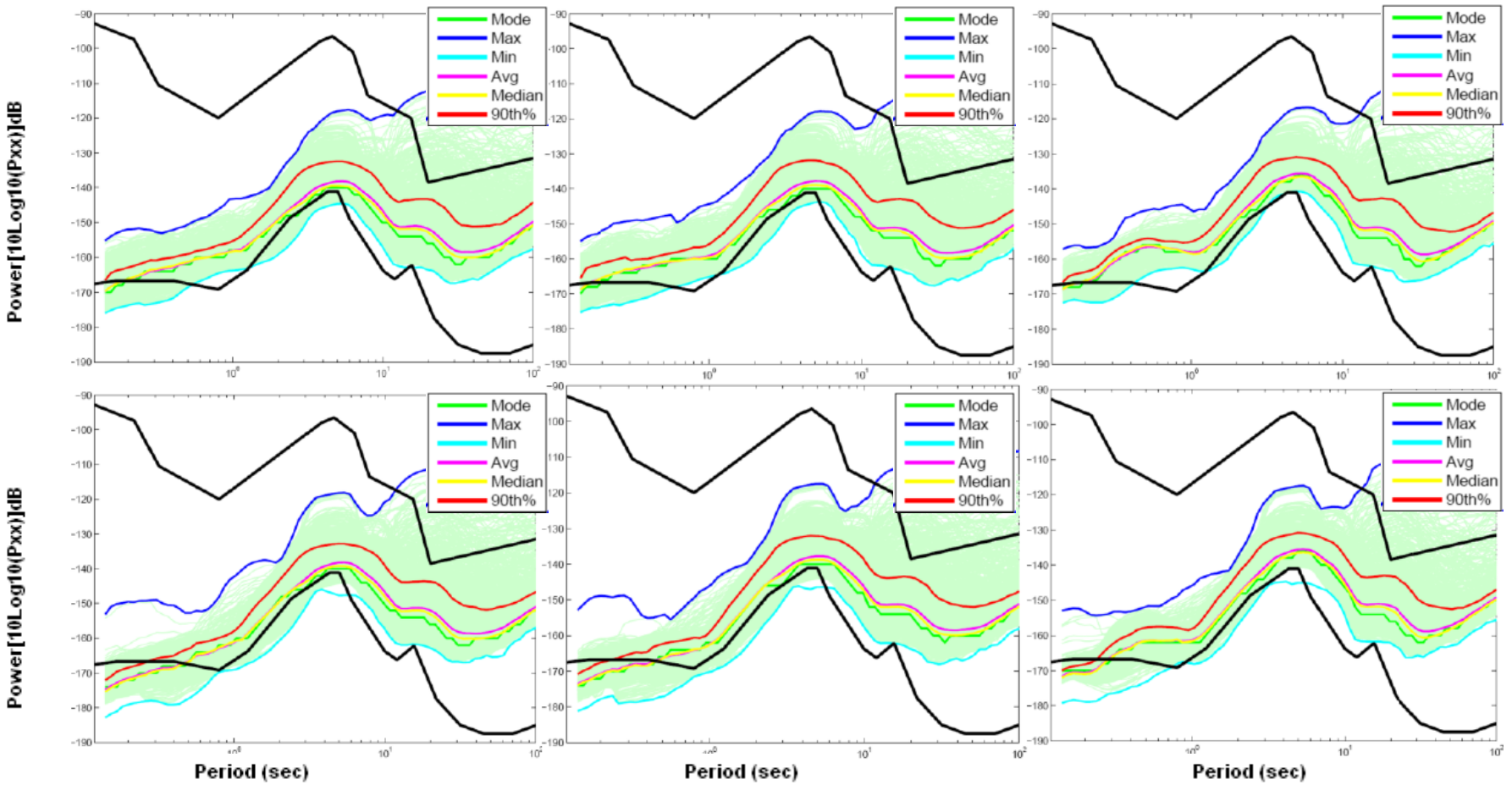

Figure 2.6. Power spectral densities of ANTO station, for day time (10:00 to 18:00 at the top) and night time (22:00 to 08:00 at the bottom) hours, for BHE, BHN, BHZ component from left to right, respectively. Green curves indicate individual PSD function for each hour. Thick black lines show high and low noise levels of Peterson. Different colors indicate the statistical variations such as Mode, Maximum, Minimum, Average, Median and 90th percentile.

2.6.2. Seasonal Variations of Seismic Noise

Seasonal variations of seismic noise were investigated for APE station by averaging power spectral densities over quarters for the year. The APE station is located in Apirathos, Greece, operated by National Seismic Network of Greek within the GEOFON network. Seasonal variations of seismic noise for the vertical component were plotted on Figure 2.7. Figures show four different quarters of the year computed by the accumulation of three months. When the amplitudes of the noise levels are compared especially at the dominant period of the microseismic peak around 7.0 sec the highest noise levels are observed during winter and the lowest noise levels were observed during summer. The amplitude of the seismic noise levels during spring and fall are between the noise levels of summer and winter.

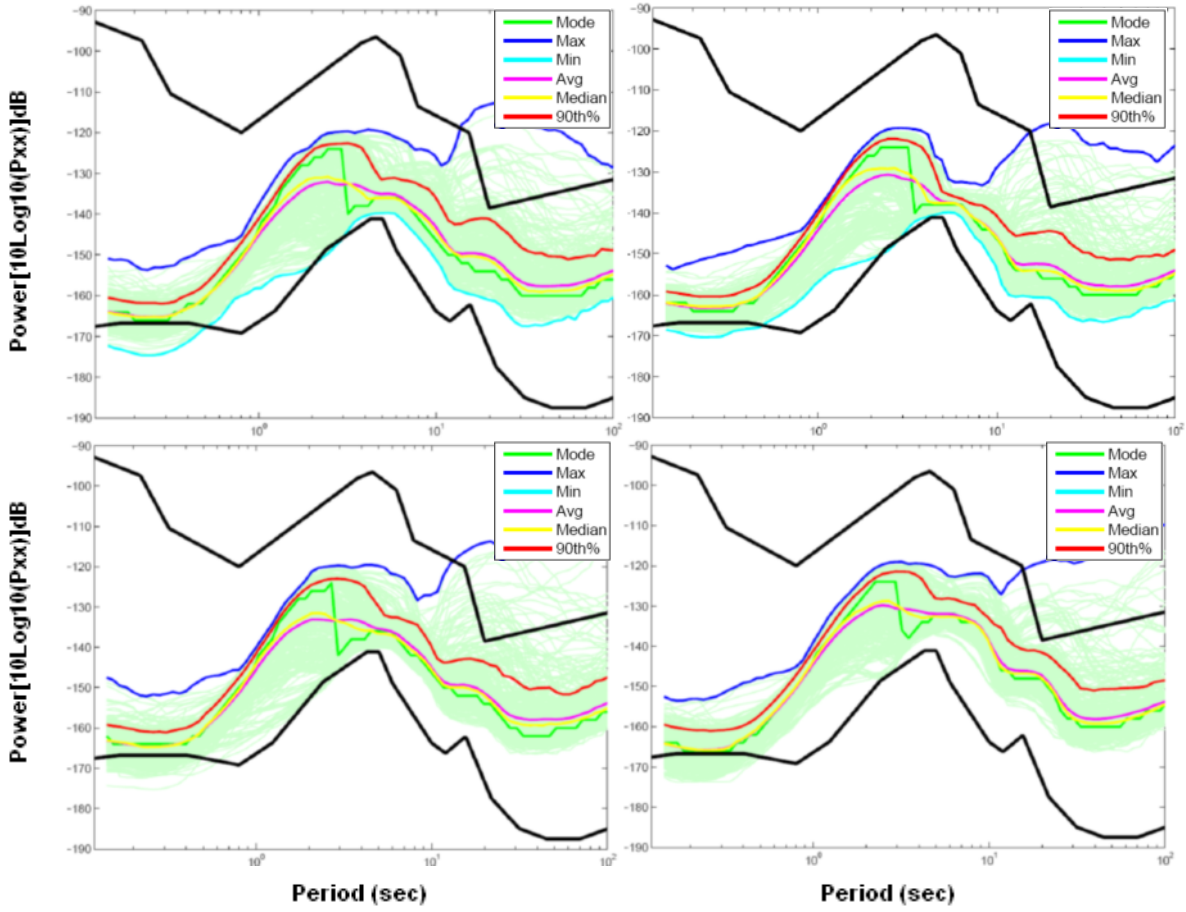

Figure 2.7. Seasonal variations (spring, summer, fall, winter) of seismic noise level for vertical component of APE station.

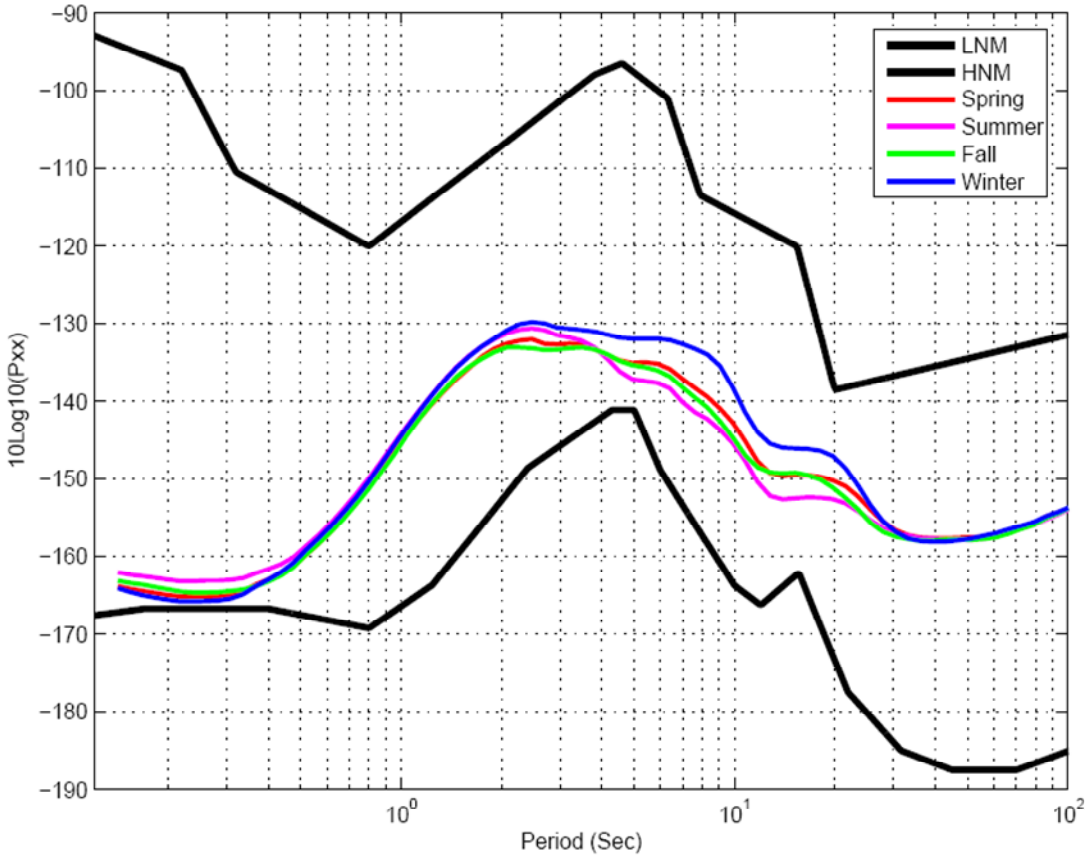

Figure 2.8. Average variations of seismic noise level of vertical component of APE station for four seasons.

Figure 2.8 shows the average power spectral density variations of the vertical component APE station for four seasons. The highest noise level is observed during winter and the lowest noise level is observed during summer.

According to the earlier studies on the variation of seismic noise there is a close correlation with the number of the storms and the seismic noise levels at especially around the dominant periods of the microseismic peak (Stutzmann *et al*., 2000; McNamara and Buland, 2004; McNamara and Boaz, 2005). In their research dominant peak period in fall and winter is shifted toward longer periods. In spring and summer the amplitude level is lower with a maximum at shorter periods and these variations are explained with the number and energy of the storms observed during that season.

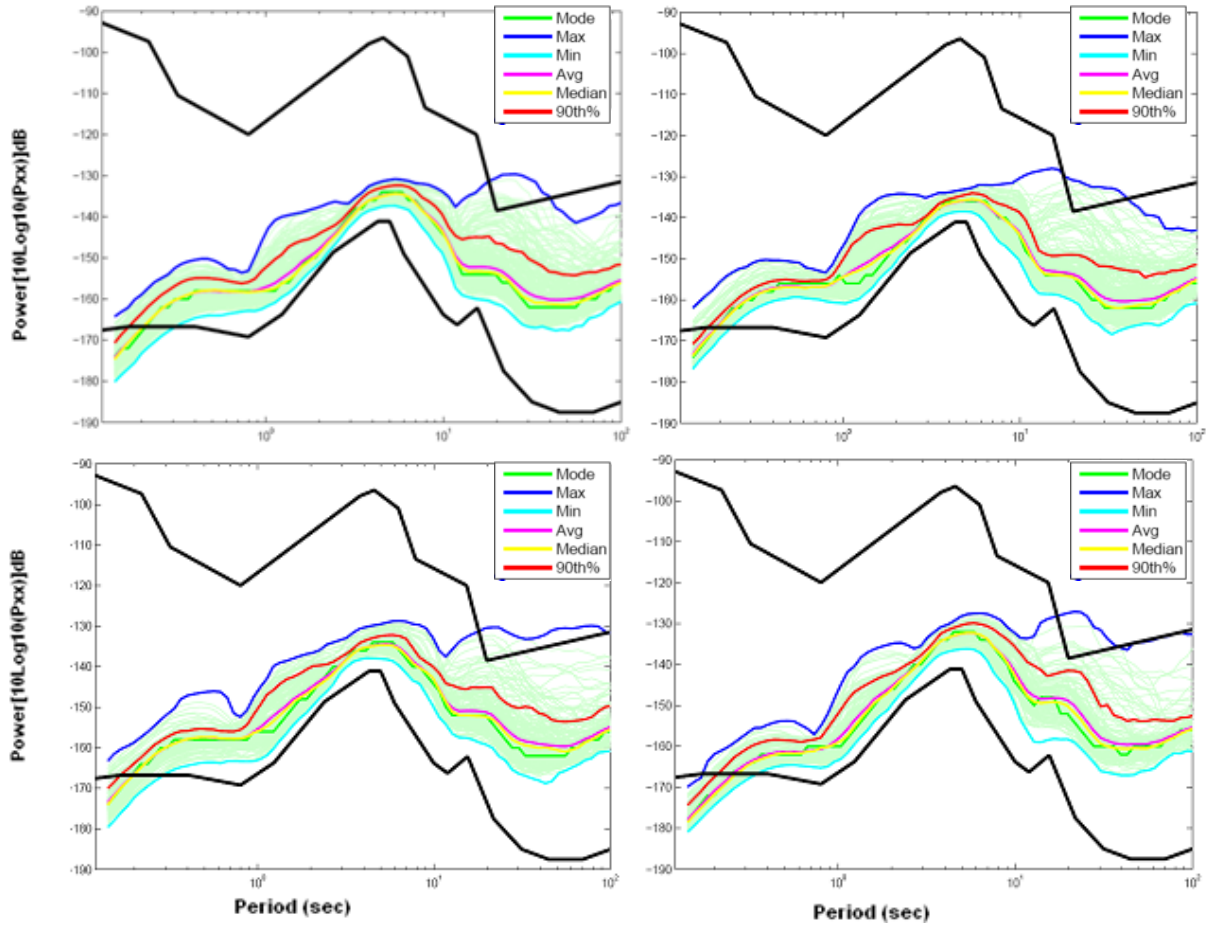

Figure 2.9. Seasonal variations (spring, summer, fall, winter) of seismic noise for vertical component of GNI station.

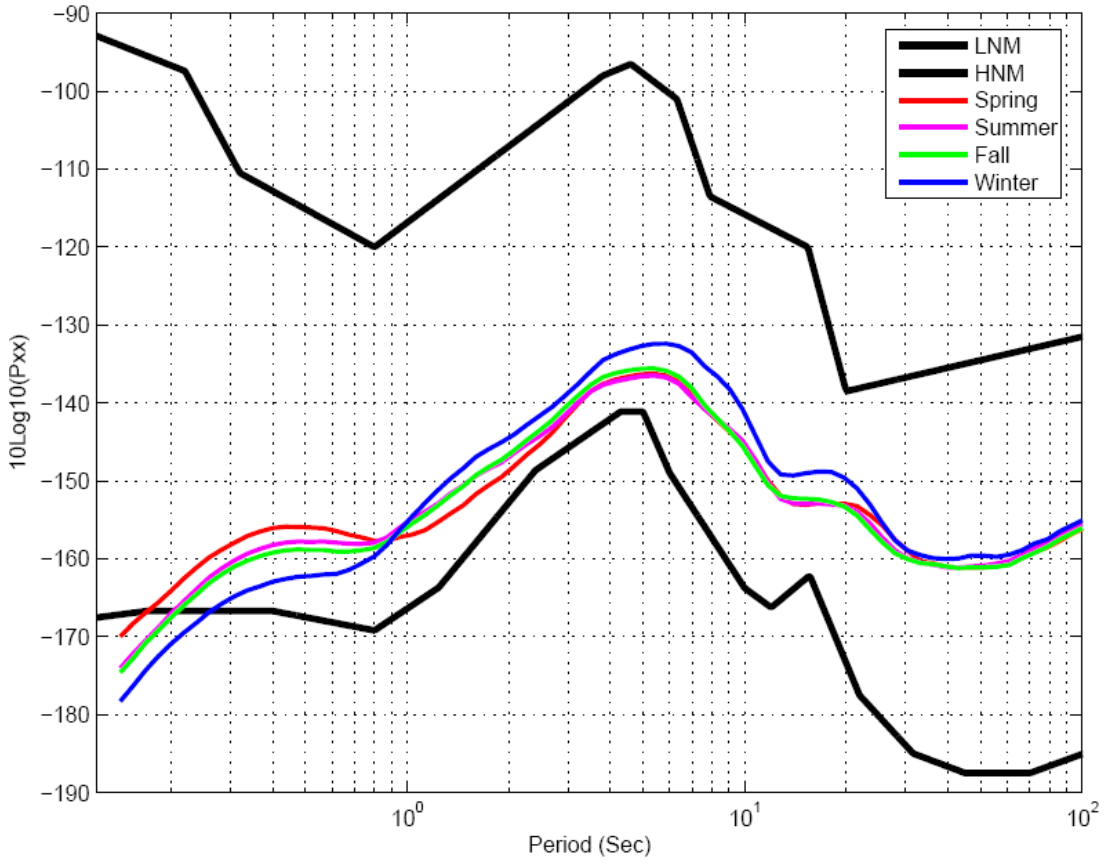

Figure 2.10. Average variations of seismic noise level of the vertical component of GNI station for four seasons.

GNI station of IRIS/USGS was installed in February in1994 at Armenia. The station is located in a vault inside a mountain with approximately 60 meters of overburden. The seasonal seismic noise variations of station GNI is presented in Figure 2.9. The power spectral density curves are generally in between the highest and lowest noise levels of Peterson. Cultural noise which is generally significant at periods lower than 1.0 sec is low due to the special location of the station. Accumulation of different seasons show relatively higher noise levels during winter and lower noise levels during summer. Figure 2.10 shows the average power spectral density variations for the vertical component of GNI station for four seasons. There is a few decibel of difference between the noise levels of summer and winter. At winter GNI station has the highest noise level at the single and double frequency peak with a 2.0-3.0 dB range of difference than the spring, summer and fall noise levels.

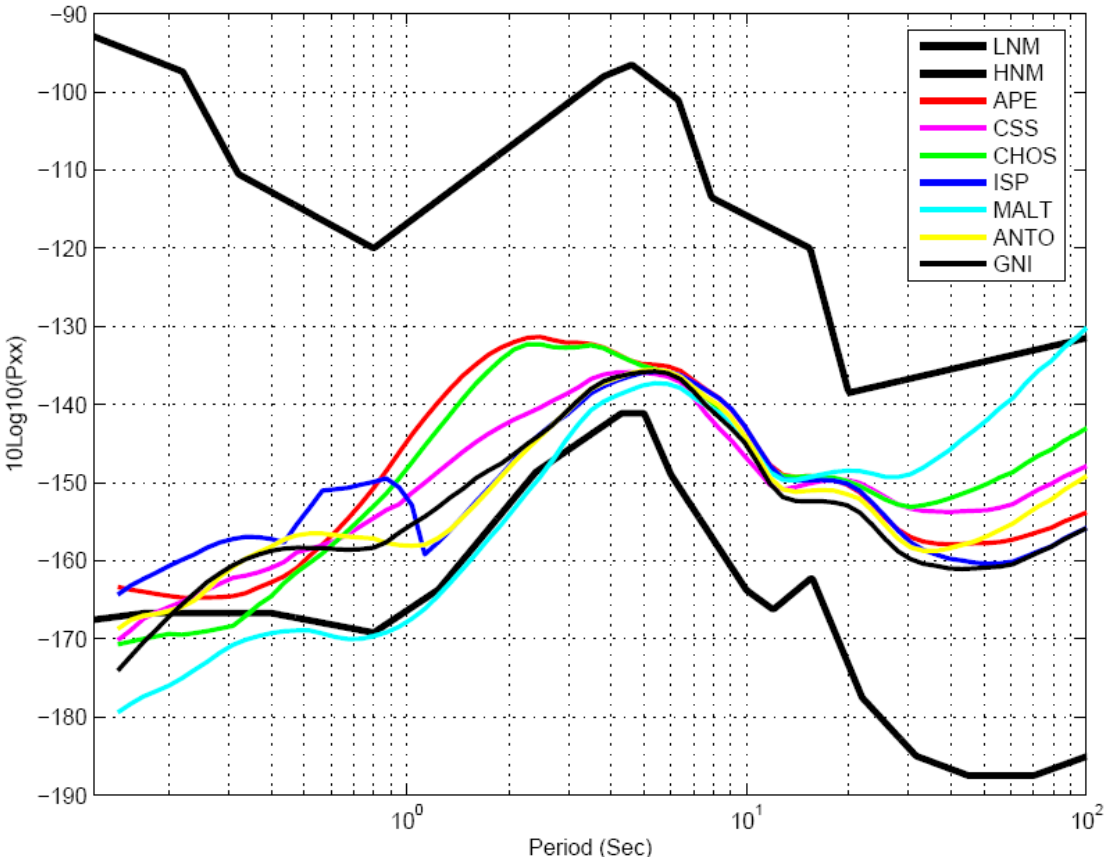

Figure 2.11. Average power spectral density curves of the vertical component of APE, CSS, CHOS, ISP, MALT, ANTO and GNI stations.

Figure 2.11 represents the average power spectral density curves of different types of stations (APE, CSS, CHOS, ISP, MALT, ANTO and GNI) for one year of data from different networks. APE station with CHOS station has the highest noise levels at 2.0-4.0 sec periods with -132 dB level. The CSS station has a noise level of approximately -140 dB at the same periods. The highest noise level for ISP and MALT stations takes place at 6.0 sec and have lower values (-145 dB) than APE and CHOS. The differences in noise levels for the stations at island and land at this microseismic period band may be correlated to the generation of oceanic waves.

2.7. Spatial Variations of Seismic Noise

Spatial variations of seismic noise are computed using the average spectral density variations for the stations at selected periods. In order to create maps for the geographical variations of noise a kriging algorithm is used to determine values at a regular grid from sparsely sampled stations. The seismic stations with instruments of 120 and 360 sec periods are selected to compute the maps for the spatial variations.

Figure 2.12 shows the maps of the spatial variations of average seismic noise levels at 1.0 sec period during day time hours for three components. At this period cultural noise dominates the signal and the coastal areas of Turkey have significantly higher noise than the continental parts. Lowest noise level at 1.0 sec period range is observed in the Eastern Anatolia with a noise level of approximately -165 dB. At this period rain, traffic, gusts of wind, industrial and human noise in the urban areas affect the seismic noise level. This can be correlated with the population and the human activity. At microseism periods (Figure 2.13) average day time seismic noise levels do not show strong variations. Seismic noise levels are varying between the -128 to -148 dB ranges in all three components. At longer periods (Figure 2.14) average day time seismic noise level show more uniform distribution between the -130 to -160 dB ranges.

Average night time (Figure 2.15 – Figure 2.17) seismic noise level variations show similar results with day time variations. The only difference is that the seismic noise levels at night time hours is lower than the day time noise levels at 1.0 sec period.

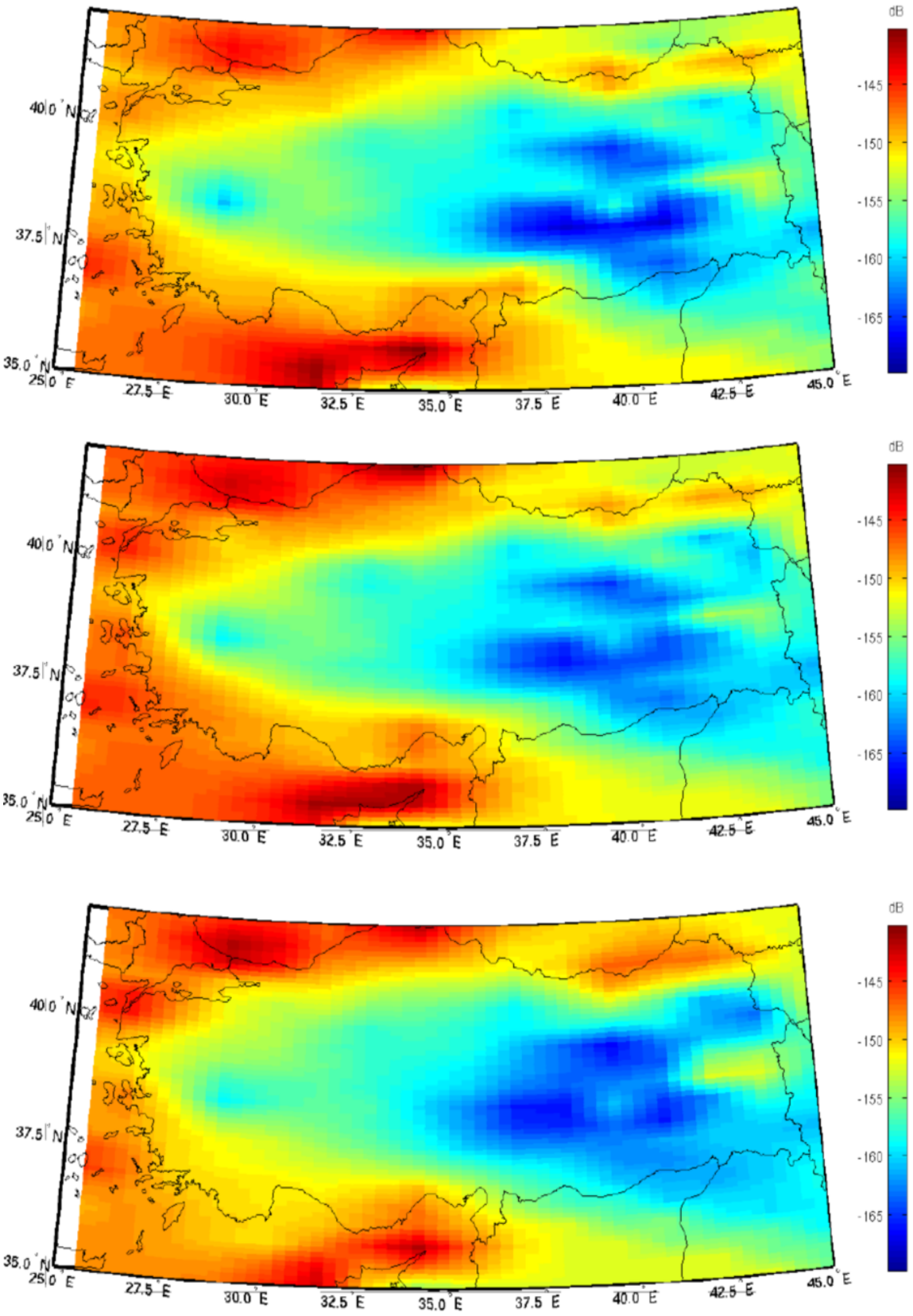

Figure 2.12. Spatial variations of seismic noise at BHE, BHN, BHZ components for 1.0 sec period range at day time hours.

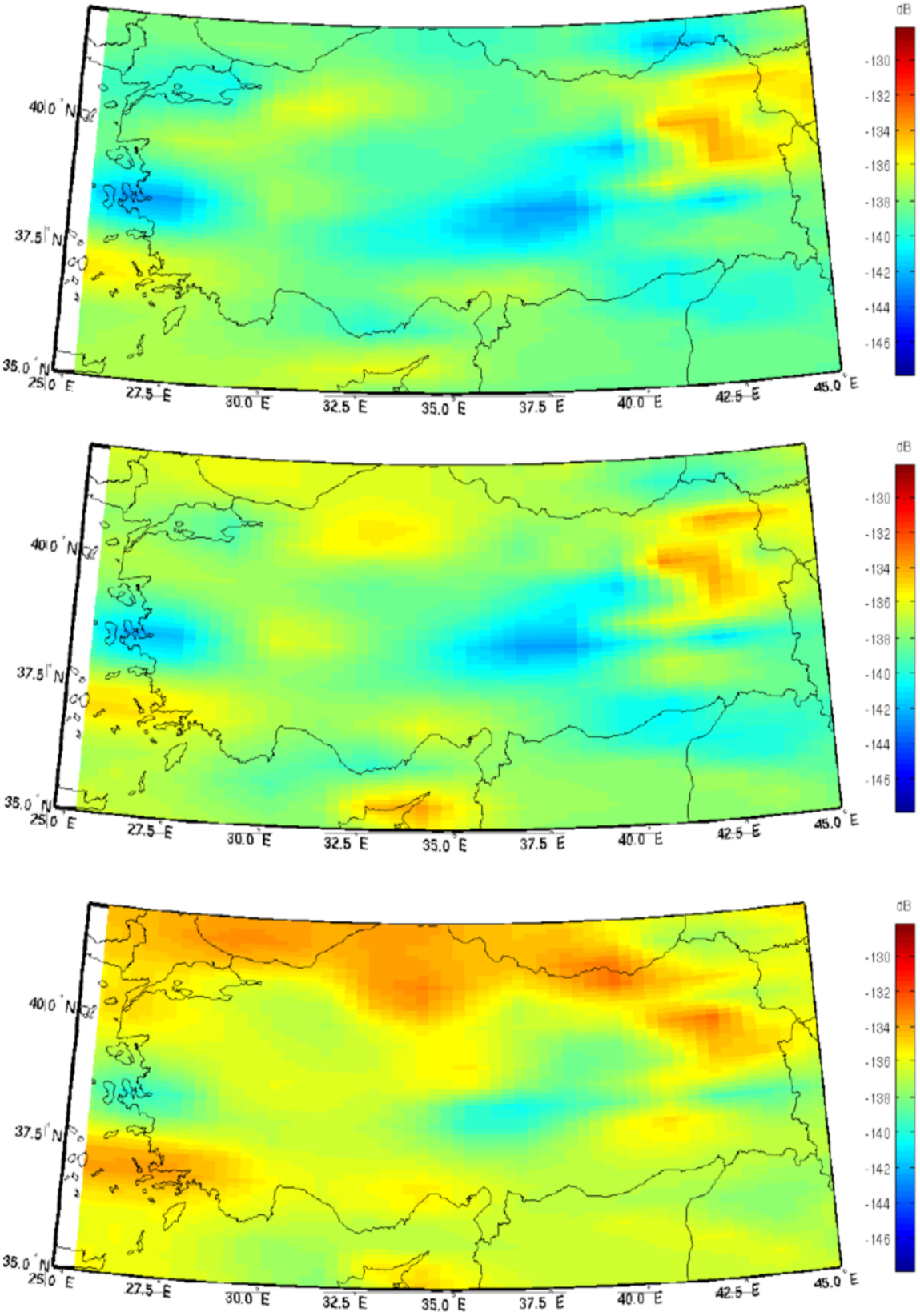

Figure 2.13. Spatial variations of seismic noise at BHE, BHN, BHZ components for 4.0 sec period range at day time hours.

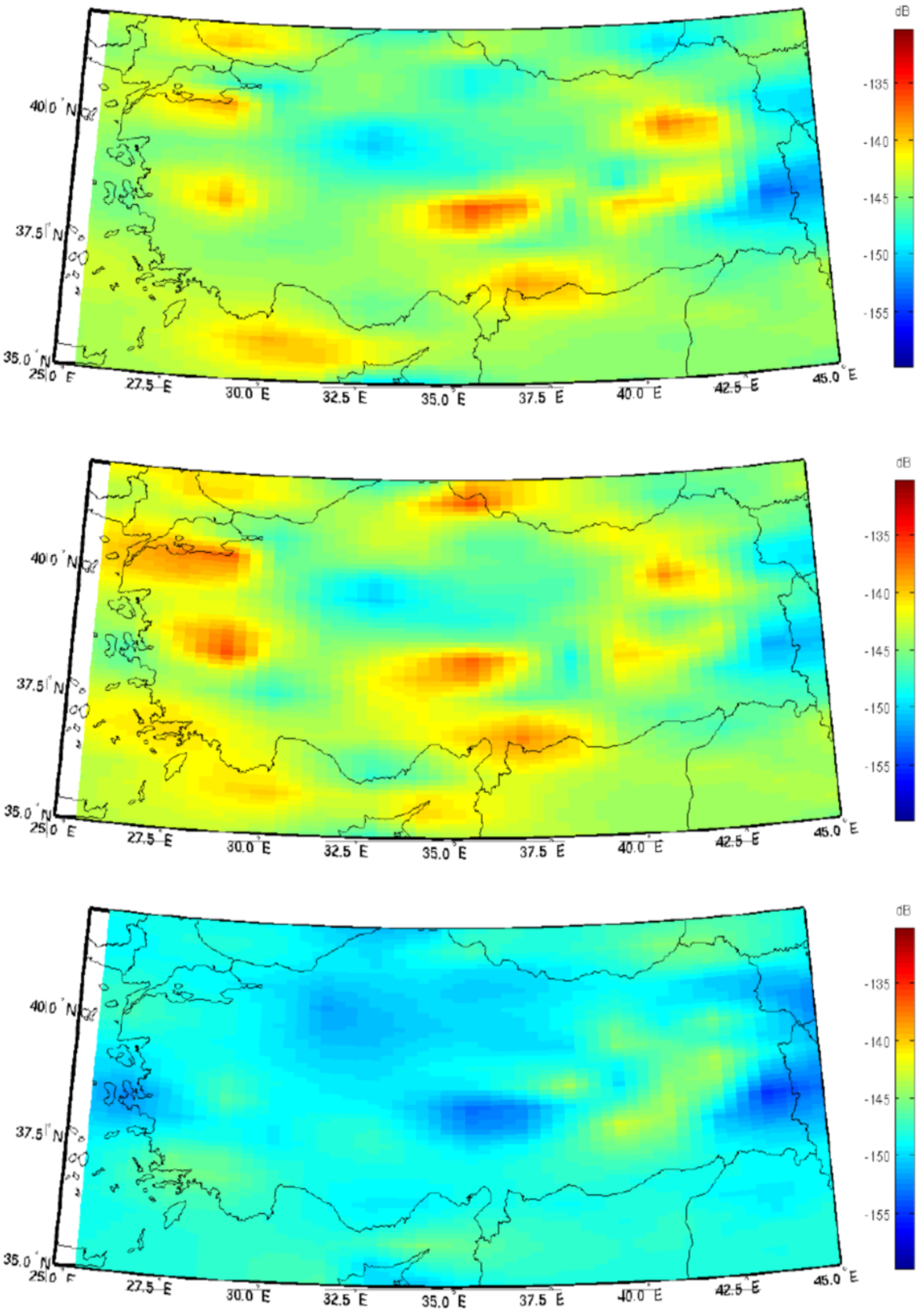

Figure 2.14. Spatial variations of seismic noise at BHE, BHN, BHZ components for 15 sec period range at day time hours.

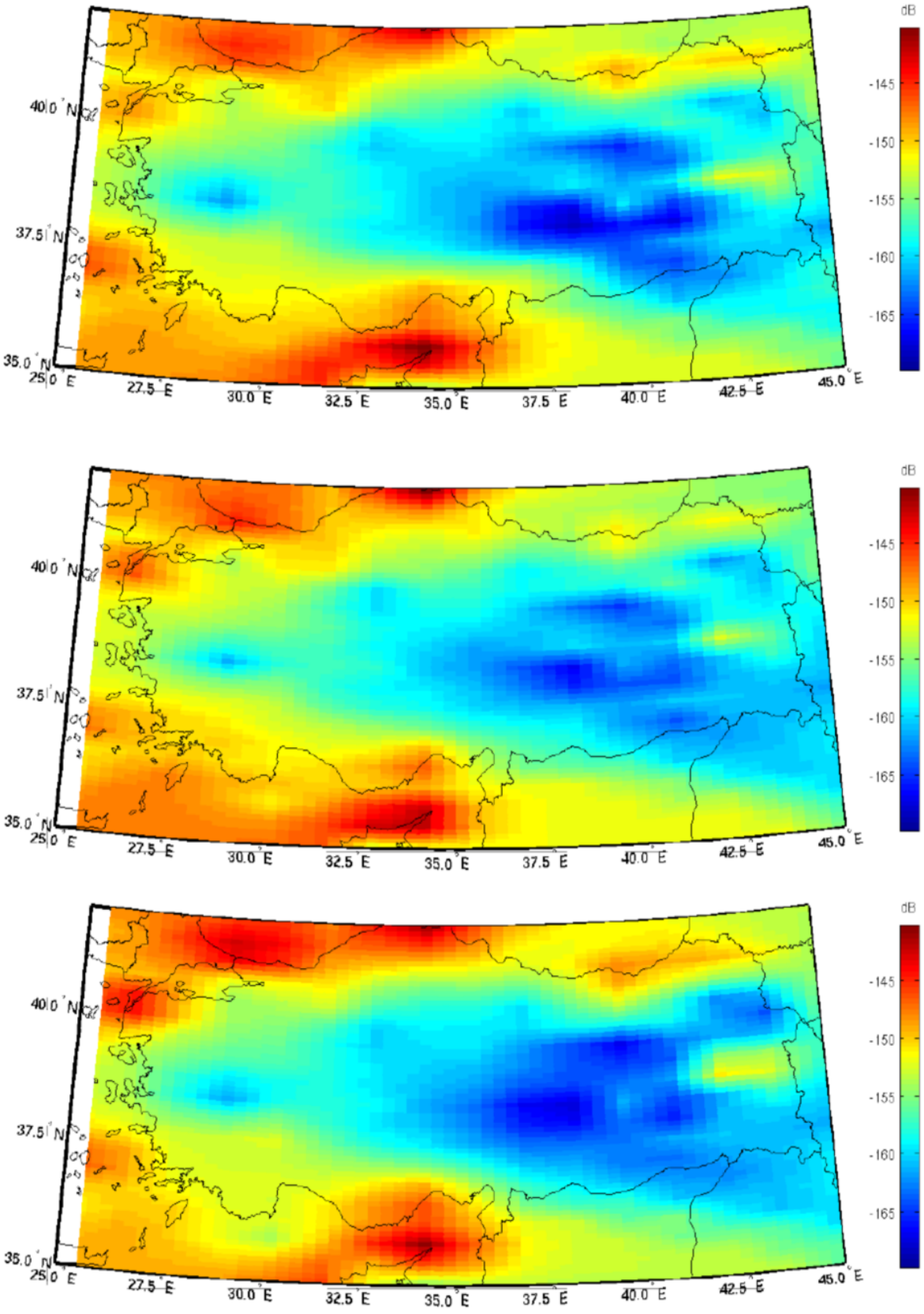

Figure 2.15. Spatial variations of seismic noise at BHE, BHN, BHZ components for 1.0 sec period range at night time hours.

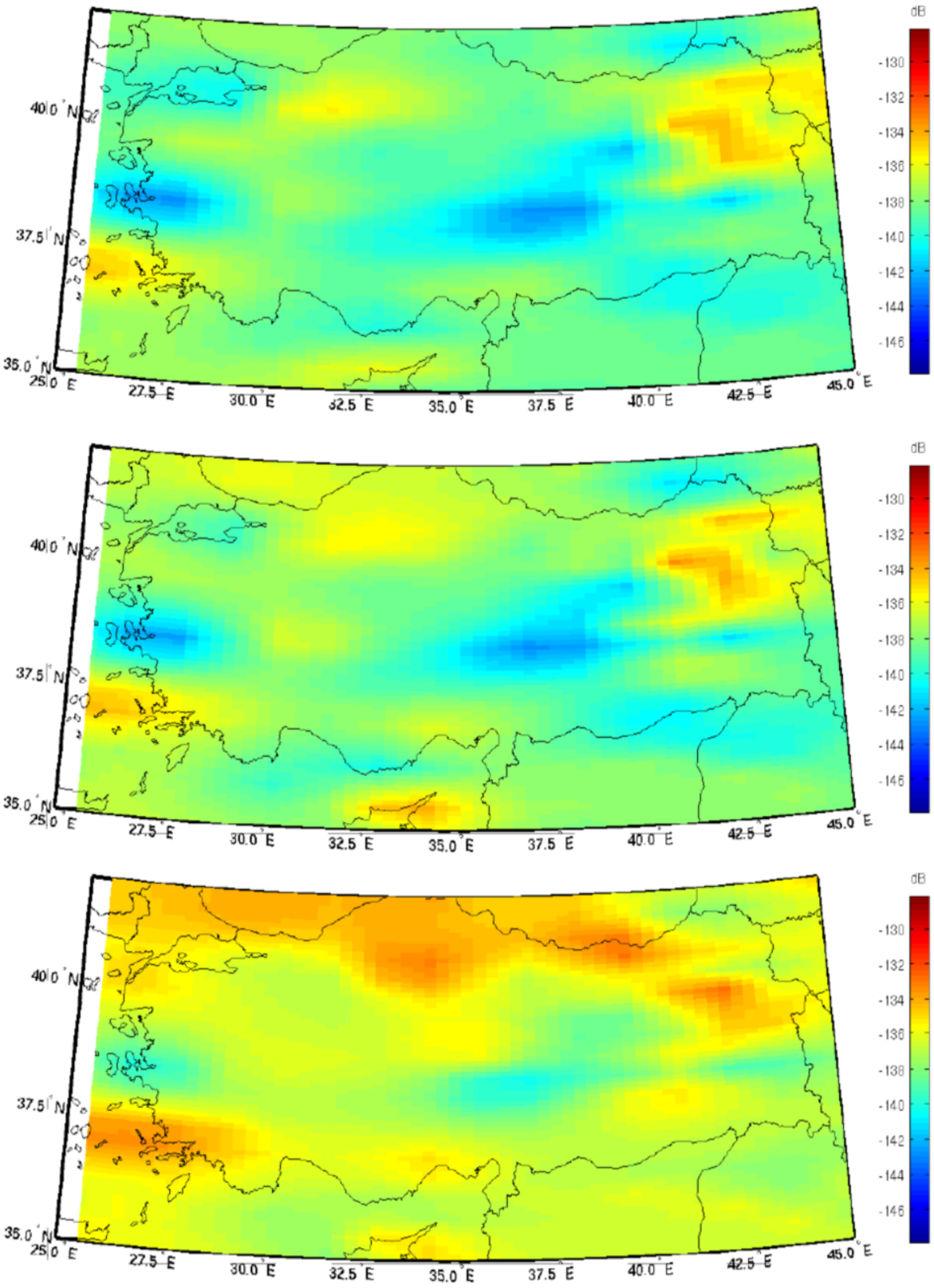

Figure 2.16. Spatial variations of seismic noise at BHE, BHN, BHZ components for 4.0 sec period range at night time hours.

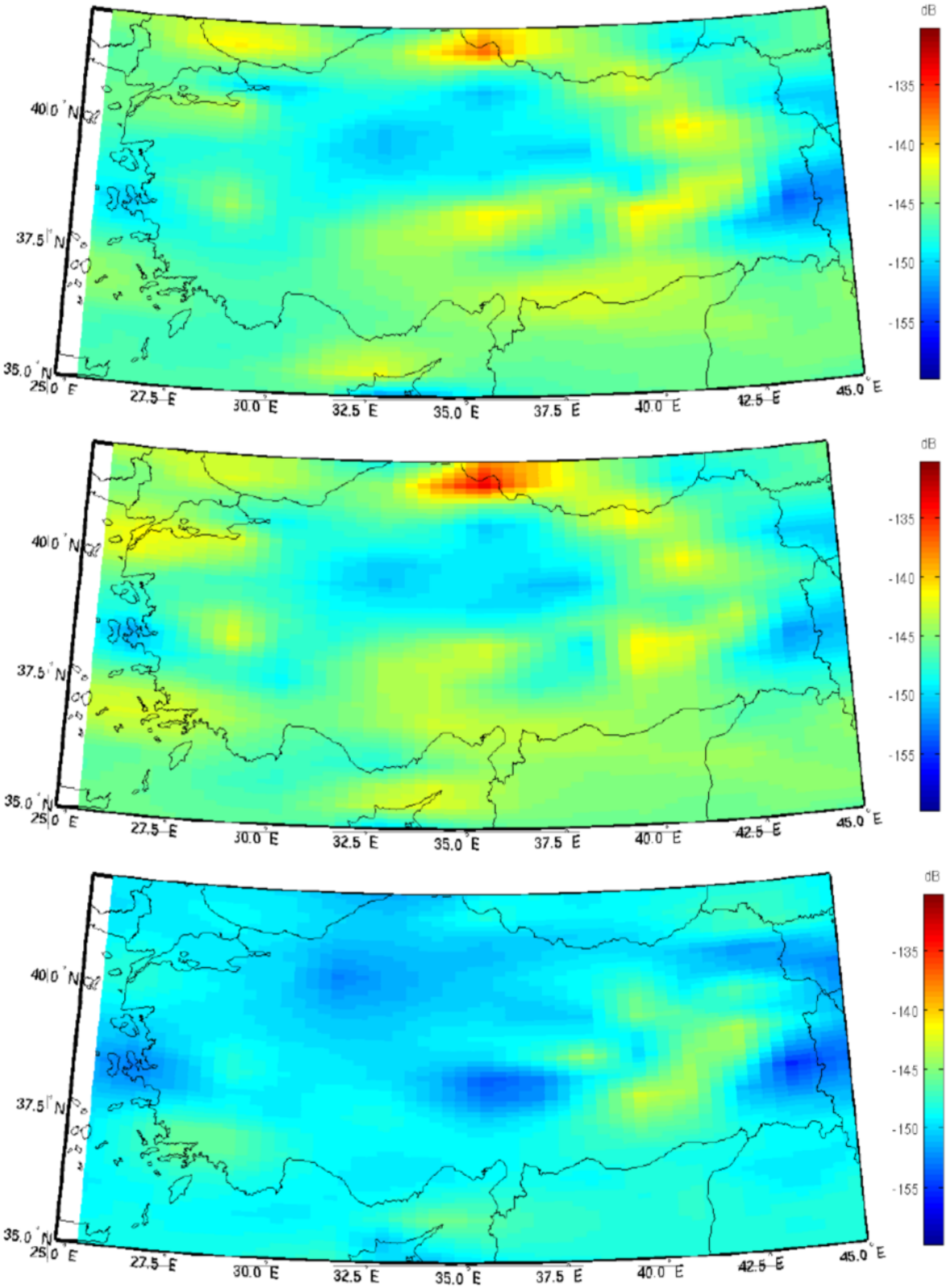

Figure 2.17. Spatial variations of seismic noise at BHE, BHN, BHZ components for 15 sec period range at night time hours.

2.8. Discussions

Diurnal, seasonal, instrumental and spatial variations of seismic noise are studied in the frequency band of 0.01 - 10 Hz by using the power spectral density method for the broadband stations in the region. Majority of the broadband stations are recording between globally accepted noise levels of Peterson. Broadband stations with 120 sec and 300 sec instruments have better noise characteristics than stations with 40 sec instruments.

Diurnal variations exhibit differences in noise level especially at the higher frequencies during the day time and night time hours. The correlations of cultural noise at shorter periods with the human activity especially at the urban areas are observed. We observe higher day time noise levels than the night time noise levels at period ranges shorter than 1.0 sec. ANTO station as an exception and does not exhibit a significant change in noise levels during day time and night time hours.

Seasonal noise levels show variations mainly at periods corresponding to the double frequency peak level and exhibit higher values during winter and lower values during summer. When we compare seismic noise levels at double frequency peak for different stations on different geographic locations, stations located at islands (APE, CSS) indicate the higher noise levels. In general coastal (APE, CSS, CHOS) stations have higher noise levels than the continental stations (ISP, MALT, ANTO, GNI) at 2.0-4.0 sec period ranges.

Spatial variations of seismic noise have been computed by using the average spectral density variations for the selected period ranges. At 1.0 sec period range seismic noise level is sensitive to cultural noise. Seismic noise levels are higher at the coastal areas and relatively lower at the continental sites. This spatial variation of seismic noise is in good correlation with the cultural noise levels typically higher in the regions with high population where the industrial and cultural noise is expected to be higher in the western and coastal parts.

At four second period map of spatial variations do not show strong variations. Highest noise levels are around -130 dB and the lowest noise levels are around -140 dB at this period range. At longer periods seismic noise level variations due to geography

decreases. At 15 sec map of spatial variations seismic noise levels vary only few per cent around -150 dB.

3. AMBIENT SEISMIC NOISE CORRELATION

3.1. Introduction

Surface waves contain a great deal of information about the structure of the Earth's crust and upper mantle. They dominate over body waves at teleseismic differences and can be extracted easily from seismic records. The main advantage of using surface waves is that velocity can be measured at a number of different frequencies. Most of the studies in seismology, energetic sources such as earthquakes and explosions are needed in order to determine the Earth structure. But the high cost of explosions and infrequent and inhomogeneous distributions of earthquakes brings some limitations to these studies. However recent laboratory experiments and theoretical studies on correlation of long time sequences of seismic noise show that Earth structure can be imaged without the need of these sources. The main idea is the principle that the Green's functions between two stations can be obtained by cross-correlations of random wavefields recorded by these stations. In order to prove that the Green's functions can be estimated from the stack of cross-correlations of noise records, different mathematical approaches were developed (Weaver and Lobkis, 2001; Snieder, 2004; Wapenaar, 2004, 2006; Gouedard *et al.,* 2008) and various assumptions were made about noise characteristics and the properties of the medium (Yao *et al.*, 2009). The applicability of the method with these different approaches was tested by laboratory experiments as well as both synthetic and real data. Now the method is used not only in seismology but also in other disciplines with exciting results.

It was commonly believed that the diffuse wave fields reveal no information about the medium that they propagate. But with the recent progresses in ultrasonic it was shown that the noise correlation function gives the waveform that would be obtained in a direct pulse/echo measurement (Weaver and Lobkis, 2001). In order to demonstrate this assertion Weaver and Lobkis (2001) performed a number of experiments on extracting Green's function between two points from the field-to-field correlation of a diffuse ultrasonic field. According to their experiments the time derivative of the autocorrelation of the thermal noise in an ultrasonic receiver circuit will be identical to the directly obtained pulse-echo signal waveform. Weaver and Lobkis (2001) interpreted their results by using the

equipartitioning of modes. After that Lobkis and Weaver (2001) generalized the results to the case that randomization of the noise sources is not produced by the distribution of sources but it can be provided by multiple scattering in a heterogeneous medium, either (Gouedard *et al.,* 2008).

Derode *et al*., (2003) prepared a laboratory experiment for extracting Green's function from the correlation based on time reversal invariance and presented numerical simulations in open and closed multiple scattering media to support the argument. They have examined if the Green's function can still be recovered from the correlations of an ultrasonic wavefield in an open scattering medium. To do this, they presented experiments both in a closed cavity with perfectly reflecting (Dirichlet) boundary conditions or in an open medium with absorbing boundary conditions. They showed that recovering the Green's function was possible not only in a closed cavity but also in an open multiple scattering medium.

Campillo and Paul (2003) which computed the correlations of seismic coda from 101 distant earthquakes and extracted the Green's function from these correlations supported the idea presented by Derode *et al*. (2003). The work of Campillo and Paul (2003) was also important in proving the applicability of the technique not only in the extremely controlled and favorable conditions of the laboratory but also with real data obtained from the recordings of earthquakes. The use of correlation technique is becoming more common not only in seismic exploration (Wapenaar *et al*., 2004) but also in the other application fields such as heliosesimology (Rickett and Claerbout, 2000), marine acoustics (Roux *et al*., 2003), and ultrasonic with either an active source or thermal noise (Weaver and Lobkis, 2001, 2003; Roux and Fink, 2003). Latter studies continued on the further development of the technique on the use of correlation (Larose *et al*., 2004; Shapiro and Campillo, 2004; Snieder, 2004; Gouedard *et al*., 2008) and the data processing (Bensen *et al*., 2007) procedures. Nowadays the cross-correlation technique is widely used in the seismic tomography studies (Shapiro *et al*., 2005; Larose *et al.,* 2006; Lin *et al*., 2007; Yang *et al*., 2007; Moschetti *et al*., 2007; Yang and Ritzwoller, 2008; Bensen *et al.,* 2008; Ritzwoller, 2008; Stehly *et al.,* 2008; Li *et al.*, 2010).

The objective of this part of the work is to employ this relatively new technique in order to utilize the seismic data with improved quality and increased quantity for the understanding of the regional tectonics of Turkey. However, accomplishing this with a relatively new method will not prove its reliability. Therefore solving this problem with a 'conventional' technique of which stability is already tested and comparing the results with the correlation method might be valuable. In this chapter the method, application and results of ambient seismic noise correlation are presented. Long time correlations of ambient seismic noise recordings are used to estimate surface wave Green's functions and utilized to obtain surface wave velocity distribution. A continuous waveform database has been formed by using the permanent and temporary broadband stations operating in the region. The cross-correlations of the ambient seismic noise between each station pair have been calculated to determine the Green's function of those station pairs. Group wave velocity maps were obtained from the calculated Green's functions using multiple filter analysis. Computed group wave velocity maps are presented for selected periods.

3.2. Data

In the investigation of this passive imaging technique temporary and permanent broadband stations of KOERI, TUBITAK-MRC, ETSE, have been used. Supplementary data from IRIS and ORFEUS depository were obtained for the permanent stations operated in the region by various networks. Before performing the ambient seismic noise correlation study a comprehensive noise analysis was performed on the properties of seismic noise (Chapter 2). A larger database was used for the cross-correlation of ambient seismic noise records.

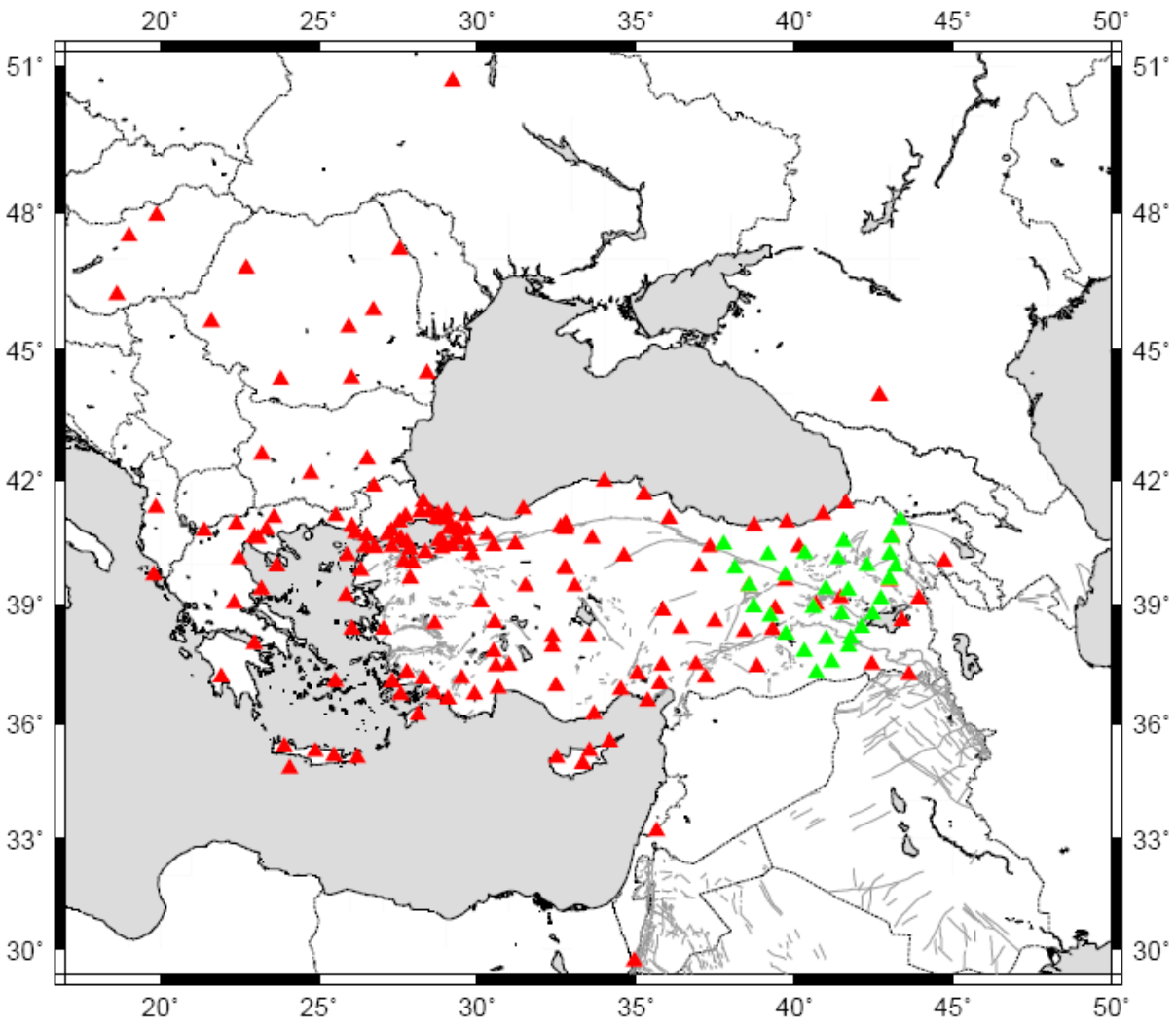

Figure 3.1. Station distribution used for correlation analysis. Triangles show stations used for this study. Red triangles indicate the stations recorded during 2006-2009 operated by various networks. Green triangles indicate the stations recorded during the ETSE project in between 1999-2001.

Figure 3.1 shows the locations of the seismic stations operating in the region, which is used in this study. Data from these stations have been collected and 24 hour long data segments with one sample per second have been formed for each station. Data from these stations were also used in the analysis with other broadband stations operating in the region during the same time period. Detailed information on the network and stations used for the ambient seismic noise correlation was presented in the second chapter.

3.3. Theory

Fully diffuse wave fields are composed of waves with random amplitudes and phases but propagate in all possible directions. This property of diffuse wave fields allows us to obtain information about any possible path that can be extracted by computing cross-correlations between pairs of receivers (Weaver and Lobkis, 2001; Lobkis and Weaver, 2001; Campillo and Paul, 2003; Shapiro and Campillo, 2004). The theoretical background in extracting the Green's function between two stations can be described by modal representation of diffuse wavefields, elastodynamic representation theorems and stationary phase arguments (Weaver and Lobkis, 2001; Snieder, 2004; Wapenaar, 2004, 2006; Roux *et al.,* 2005; Paul *et al.,* 2005; Yao, et al., 2009). These different approaches make different assumptions about noise (source) characteristics and (stochastic) properties of the medium (Yao *et al.*, 2009). Gouedard et al., (2008) discussed the theoretical conditions required to extract the Green's functions between two receivers from the cross-correlations of noise records.

One of those approaches is based on equipartitioning of the Earth's modes (Weaver and Lobkis, 2001). In this case the normal modes of the system are uncorrelated and all carry the same amount of energy (equipartitioning). This technique can be exhibited without any assumption about the noise sources location or their activation time. Only assumption is that there is equipartition at the boundaries of the boundaries of the region of interest (Gouedard *et al.*, 2008). However, in contrary of extracting Green's function with equipartitioning, Snieder (2004) suggested that Green's functions can be extracted from scalar waves in a homogeneous medium having embedded scaterers. The main assumption is that the scatterers are acting as secondary sources of singly and multiply scattered waves (Snieder, 2004).

Here we follow the derivation proposed by Gouedard *et al.,* (2008). The main idea is when averaged over long time series seismic noise can be accepted as a seismic noise field. In such a case, Green's function can be estimated from cross correlations between two receivers Gouedard *et al.,* (2008).

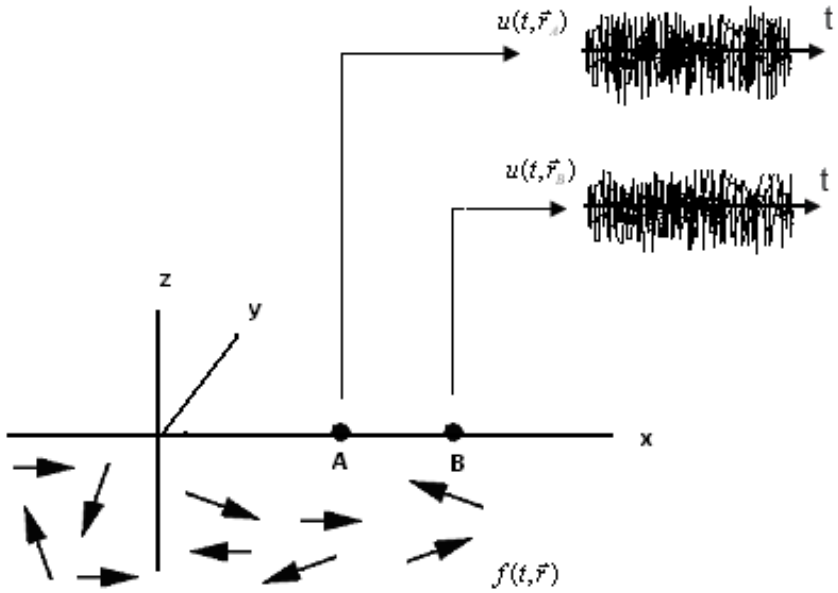

Figure 3.2. Definition of the geometric variables.

Displacement fields $u(t,\vec{r}_A)$ and $u(t,\vec{r}_B)$ recorded at two receivers at locations A and B in a medium with a random noise field $f(t,\vec{r})$, is presented in Figure 3.2. The time domain cross-correlation between the two receiver locations can be defined as;

$$C(\tau,\vec{r}_A,\vec{r}_B) = \lim_{T\to+\infty}\frac{1}{T}\int_0^T u(t,\vec{r}_A)\overline{u(t+\tau,\vec{r}_B)}dt \qquad (3.1)$$

In Equation 3.1 the bar denotes the conjugate. The displacement can be written by using the Green's function G_a and the source function f such as;

$$u(t,\vec{r}) = \int_0^\infty dt' \int_X G_a(t',\vec{r},\vec{r}_s) f(t-t',\vec{r}_s)d\vec{r}_s \qquad (3.2)$$

It is assumed that f is a white noise distributed everywhere in the medium X, acting at any time t.

$$C(\tau,\vec{r}_A,\vec{r}_B) = \lim_{T\to+\infty}\frac{1}{T}\int_0^T dt\int_0^\infty ds\int_X d\vec{r}_s G_a(s,\vec{r}_A,\vec{r}_s) f(t-s,\vec{r}_s)$$
$$x\int_0^\infty ds'\int_X d\vec{r}_s'\overline{G_a(s',\vec{r}_B,\vec{r}_s') f(t+\tau-s',\vec{r}_s')} \quad (3.3)$$

In the frequency domain, white noise contains all the frequencies with a random phase and in the time domain, this is a random wavefield such that the position and activation time of each source are uncorrelated (Gouedard *et al.,* 2008). In this case, the limit T can be replaced by an ensemble average;

$$\lim_{T\to+\infty}\frac{1}{T}\int_0^T f(t-s,\vec{r}_s) f(t+\tau-s',\vec{r}_s')dt$$
$$= \mathrm{E}\left[f(t-s,\vec{r}_s) f(t+\tau-s',\vec{r}_s')\right] \quad (3.4)$$
$$= \sigma^2\delta(\tau+s-s')\delta(\vec{r}_s-\vec{r}_s')$$

$$C(\tau,\vec{r}_A,\vec{r}_B) = \sigma^2\int_0^\infty ds\int_X d\vec{r}_s G_a(s,\vec{r}_A,\vec{r}_s)\overline{G_a(s+\tau,\vec{r}_B,\vec{r}_s)} \quad (3.5)$$

Equation 3.5 can be obtained where σ yields the variance of the white noise (Gouedard *et al.,* 2008). By using the expressions of the Green's function in an attenuating medium with an elliptic differential operator Green's functions of the positive and negative lags can be obtained as;

$$\frac{d}{d\tau}C(\tau,\vec{r}_A,\vec{r}_B) = \frac{-\sigma^2}{4a}(G_a(\tau,\vec{r}_A,\vec{r}_s) - G_a(-\tau,\vec{r}_A,\vec{r}_s)) \quad (3.6)$$

This equation means that the time derivative of the cross-correlation computed between the wavefields recorded at A and B gives the Green's function of the medium (Gouedard *et al.,* 2008).

3.4. Computation of Green's Function

Data processing procedure for the computation of Green's function consists of a number of steps. A continuous waveform database is created for the analysis prior to cross-correlation. A detailed description of the data processing procedure for the ambient seismic noise correlation was presented by Bensen *et al*., (2007). Four stages of data processing procedure were applied to the data (Figure 3.3). First stage shows the steps involved in preparing single-station data before the cross-correlation. Second stage outlines the cross-correlation procedure and stacking. Third stage includes dispersion measurement and the last one is the error analysis and the data selection process (Bensen *et al*., 2007).

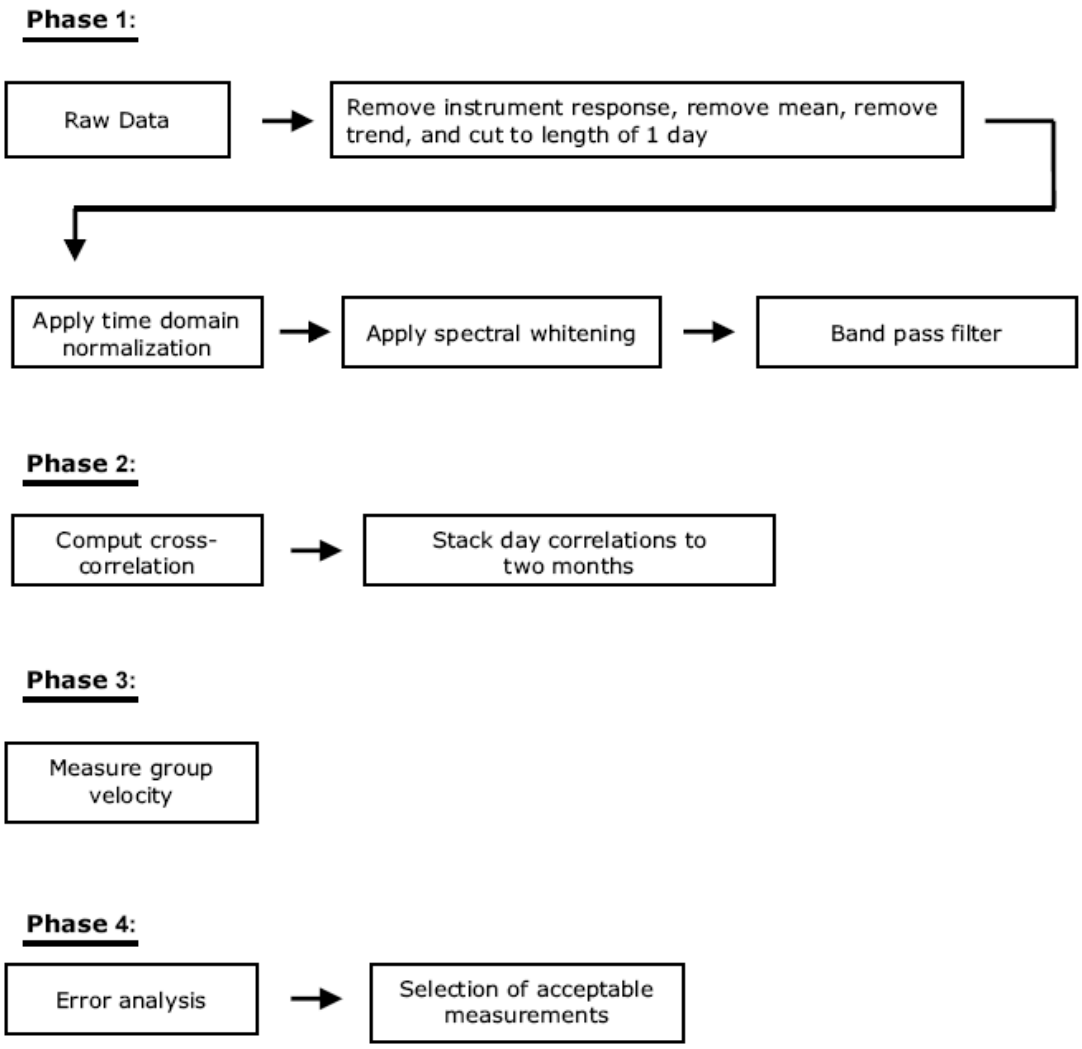

Figure 3.3. Schematic representation of the data process. (Modified after Bensen *et al*., 2007).

Data processing procedure applied in this study is similar to the one described in the work of Bensen *et al*., (2007). Data from all the stations in the region are sampled to one sample per second prior to data processing. Then 24 hour long data segments are created for each station from the continuous data recordings of broadband seismic stations. Mean, trend, and instrument response are removed in this stage. Earthquakes and other disturbing effects such as instrumental irregularities are removed by applying temporal normalization in this stage. Additionally, spectral whitening was applied in order to remove the effects of microseism at double frequency (~7 sec) and single frequency (~14 sec) periods. Cross-correlations and stacking are performed daily in the frequency domain.

For accurate representation of Green's function a medium of homogenous and random distribution of noise sources is needed. However the noise distribution inside the earth is neither homogenous nor random. But the distribution of noise sources can be homogenized when long time sequences are used. It was introduced previously during the theoretical background of the technique that in a multiply scattering medium the convergence of cross-correlations to the Green's functions is also effective together with a sufficient number of averaging processes (Campillo, 2006). Hence, after this single station process completed, cross-correlations are computed and stacked for each station pairs by using approximately three years of data. This correlation process amounts to a number of $n(n-1)/2$ station pairs where n is the number of stations. In this study more than 12000 time-series are obtained from the cross-correlations of 156 broadband stations recorded during 2006-2009. Approximately 750 time series obtained from the cross correlations of ETSE stations and other broadband stations operated during 1999-2001. Two months stacks of cross-correlations of each station pair are computed and compared in order to see if there are any seasonal variations of the estimated Green's functions. The resulting cross-correlations are two-sided time-functions with both positive and negative correlation lags. In this study the correlations lags are stored from -1000 to 1000 sec which depend on the speed of the waves and the maximum inter-station distance.

Figure 3.4 shows the cross-correlations between AGRB and GADA stations. The distance between two stations is 1462 km and the group wave velocity computed from both positive and negative lag is 3.2 km/s. Each trace shows the two months stacks of correlations and the trace at the top shows the final stack for 24 months. Two months of

stacks indicate that there is not significant deviation from the final stacked time series. It is recognized easily that the final stacked correlation has much higher S/N ratio than two months stacks. The resulting waveforms represent waves traveling in opposite directions between the stations. The positive and negative correlation lags which are also referred as causal and acausal, respectively, would be identical if the sources of ambient noise are distributed homogeneously in azimuth (Bensen *et al.,* 2007). However, considerable asymmetry can also be observed.

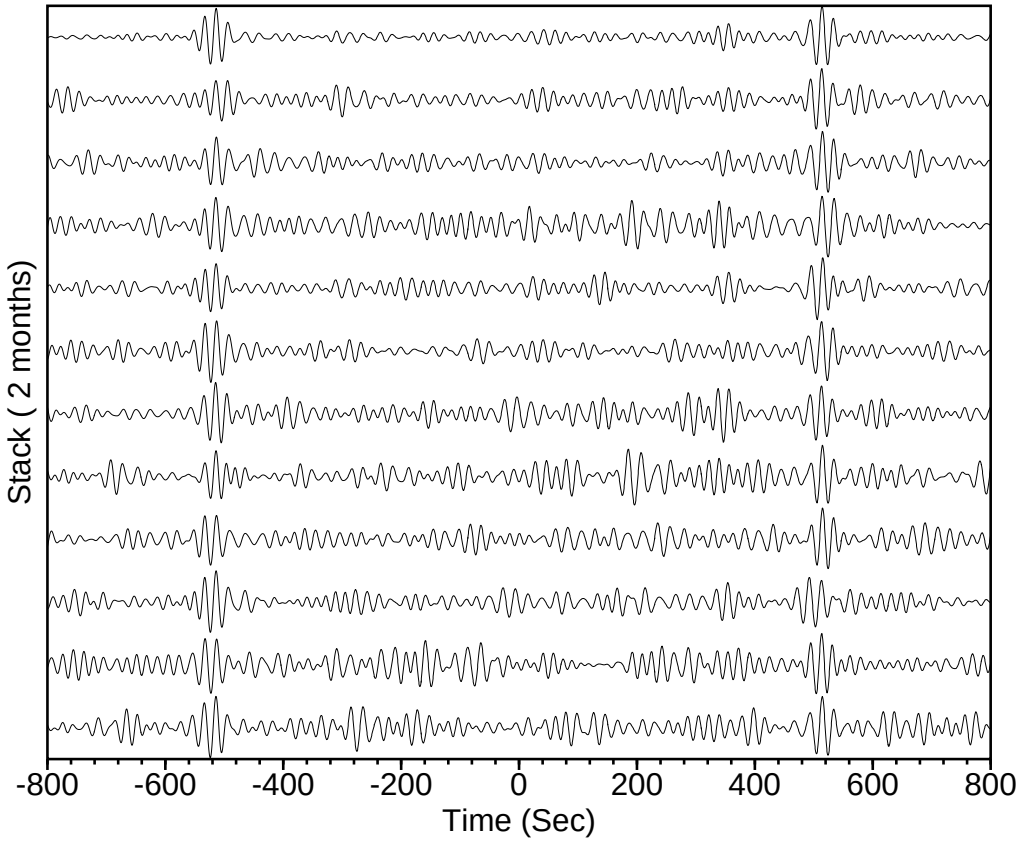

Figure 3.4. Cross-correlations for the vertical components of AGRB and GADA stations with interstation distance of 1462 km and filtered in the 18-22 sec period band. The traces are normalized with their maximum values.

Figure 3.5 shows another example of long term cross-correlations between the stations AGRB and KRTS. The inter-station distance is 745 km. There is significant asymmetry between the positive and negative lags and a clear time shift on the positive lags stating at 6^{th} 2-months stack. In order to investigate the existence of this time asymmetry between the cross-correlation lags arrival times of a teleseismic event was

shown in Figure 3.6. Time asymmetry on the correlation pairs appears after the 6th 2-months stacks. A teleseismic event was selected in the same period with two stations near KRTS. Records show that first arrivals appear almost at the same time for the stations CEYH and MERS. But, there is an almost 40 sec of time shift at KRTS station when compared with MERS and CEYH stations. Similar time shifts can be observed at the traces in Figure 3.5. We eliminate these traces from the final stack of correlations.

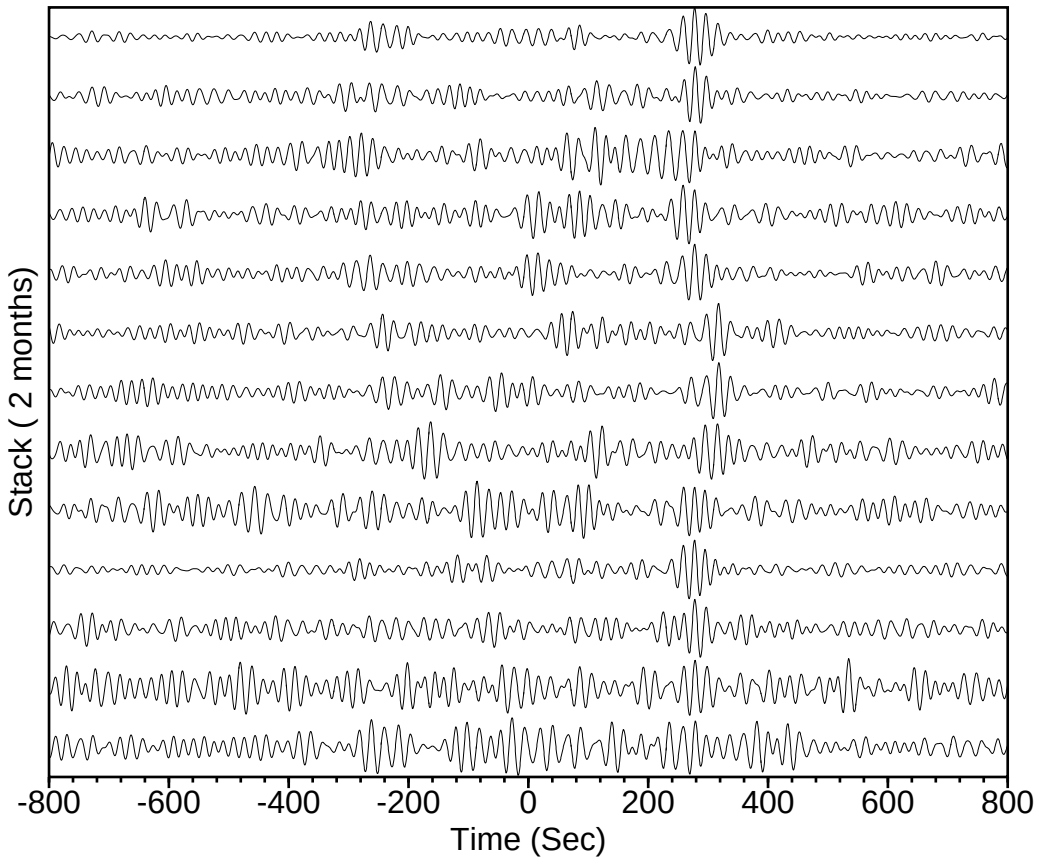

Figure 3.5. Cross-correlations for the vertical components of AGRB and KRTS stations with interstation distances of 745 km filtered in the 18-22 sec period band. The traces are normalized with their maximum values.

The final example is shown in Figure 3.7 between AGRB and SHUT with an inter-station distance of 1081 km. There is no coherency between final stack and 2-months stacks. Therefore the Green's function is not representative for the path. Since the stations used in this study is located in the same geographical area it is not expected to have significant variations in the noise filed. Therefore the failure for computing a representative Green's function is likely the result of poor station quality.

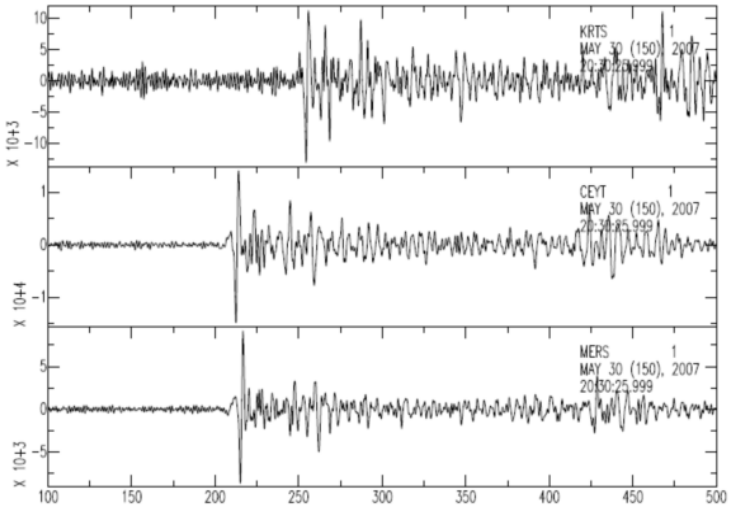

Figure 3.6. A teleseismic earthquake recorded at KRTS (top), CEYT (middle), MERS (bottom) stations. A time shift of 40 sec is apparent between KRST and other stations.

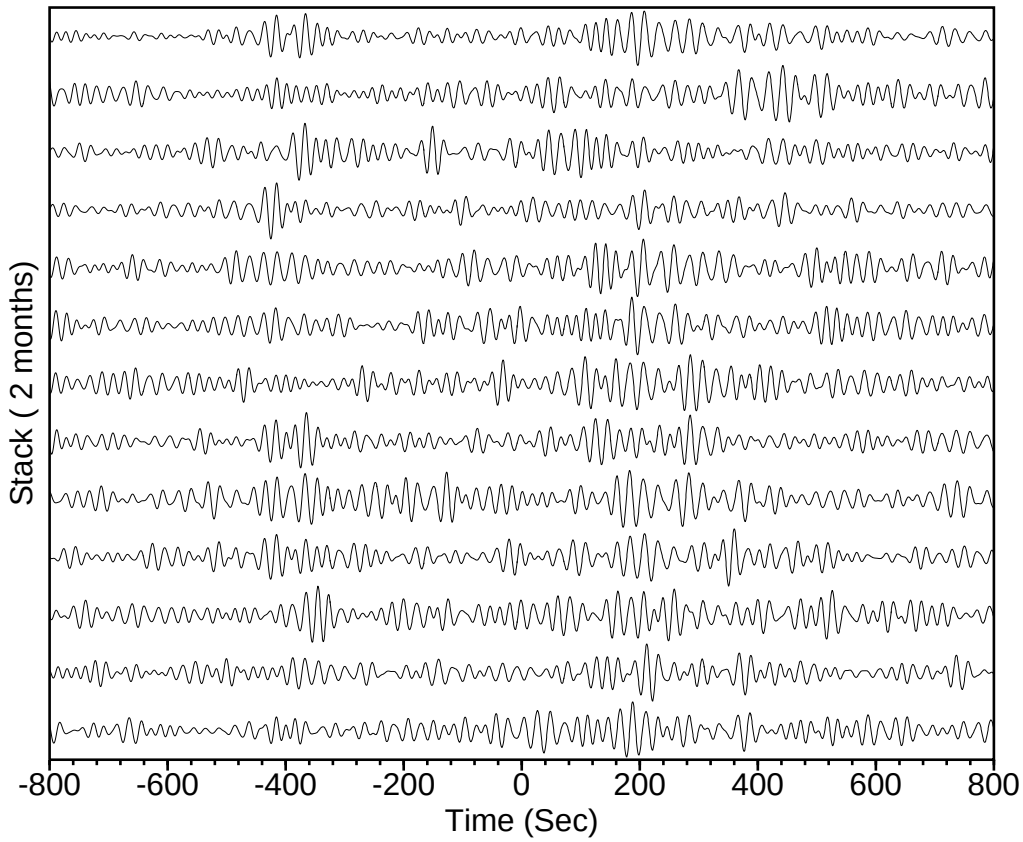

Figure 3.7. Cross-correlations for the vertical components of AGRB and SHUT stations with interstation distances of 1081 km filtered in the 18-22 sec period band. The tracesare normalized with their maximum values.

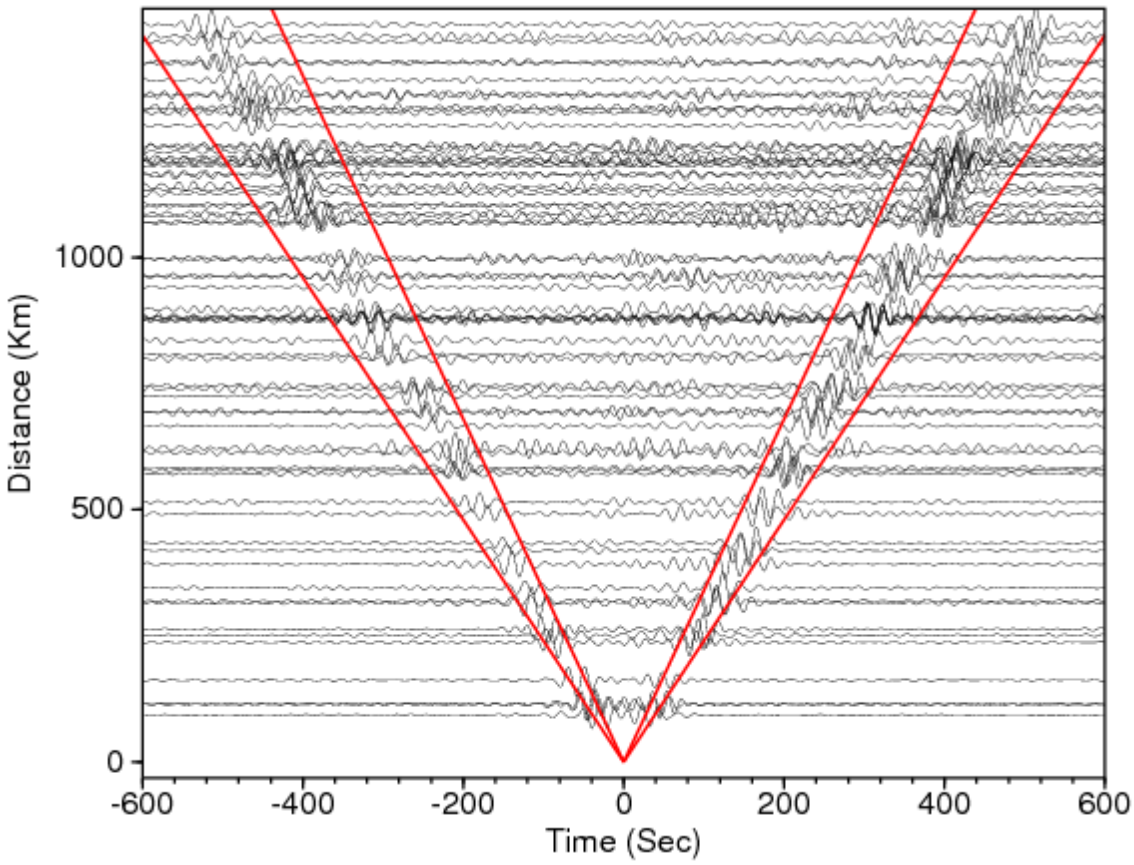

Figure 3.8. A record section centered at station AGRB for vertical component. Cross correlations are ordered by station distances. Both positive ('causal') and negative ('acausal') lags are shown. Two sided Green's functions filtered between 18 and 22 seconds periods. Red curves indicate the minimum velocity (2.4 km/s) and the maximum velocities (3.4 km/s) at positive and negative lags.

Figure 3.8 shows the results of two year stacks of cross correlations between the vertical components recordings of AGRB station with the other vertical components recordings of the broadband stations. The resulting waveforms correspond to the estimated Green's functions of Rayleigh waves. Cross correlations are computed at 20 sec period (18-22 sec bandwidth). In each of those cross-correlations, positive (causal) and negative (acausal) components show the Rayleigh wave signals coming from the two opposite directions. There is an obvious symmetry between positive and negative lag indicating a uniform distribution of noise. The group wave velocity envelopes 2.4 km/s and 3.4 km/s also shown on the figure indicate the expected value of Rayleigh wave velocity for 20 sec period.

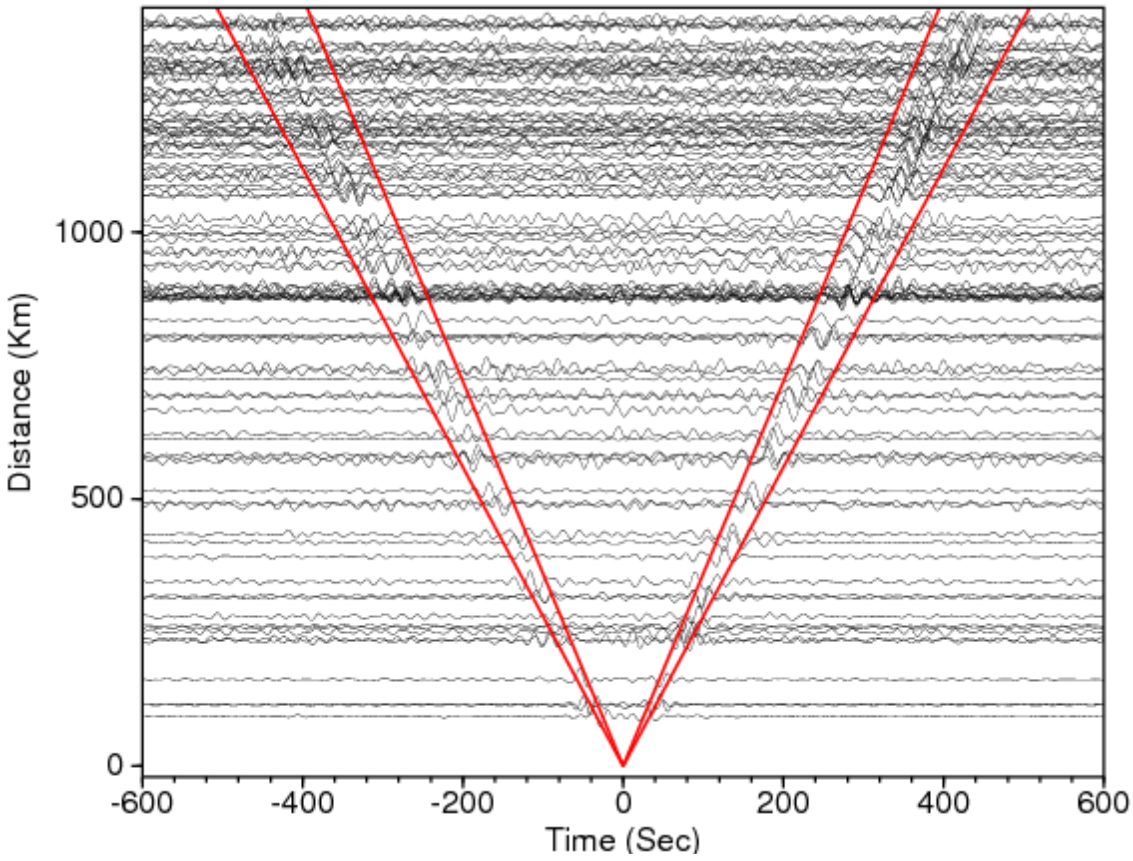

Figure 3.9. A record section centered at station AGRB for transverse component. Cross correlations are ordered by station distances. Both positive ('causal') and negative ('acausal') lags are shown. Two sided Green's functions filtered between 18 and 22 seconds periods. Red curves indicate the minimum (2.8 km/s) and the maximum (3.6 km/s) velocities at positive and negative lags.

Figure 3.9 shows the cross correlations for the transverse component recordings for the same station geometry. The resulting waveforms correspond to the estimated Green's functions of Love waves. Both positive and negative components well developed between group wave velocities of 2.8 km/s and the 3.6 km/s. Although the same amount of data were used for vertical and transverse component it is obvious that vertical components containing Rayleigh waves have better S/N ratio. This is an indication that Rayleigh waves are dominant in ambient seismic noise.

After the cross-correlations are computed and stacked, an analysis is performed for the selection of well-estimated Green's functions. The selection is based on;

1) The number of two month stacks is greater than three which indicate that there should be at least six months of data used for the computation.
2) There are not significant perturbations on the two months stacks within the group wave velocity window of signal when compared to final stack.
3) The Signal/Noise ratio is computed and the values greater than 10 are accepted. The signal is assumed as the maximum amplitude within the signal window (between times corresponding to minimum and maximum group wave velocities) and noise is computed from the absolute mean value of the window outside the signal window.
4) The signals for positive and negative delays on the final stack have similar waveform shapes and group wave velocities. The group wave velocities are estimated from the maximum of the envelope of the signals within the pre-specified group wave velocity window. If the difference between the group wave velocities of two sides is less than five per cent the velocity estimate is accepted for the path.
5) The paths with inter-station distances greater than three wavelengths ($\Delta > 3\lambda$) are accepted. The Green's functions smaller than these values are ignored.

Group wave velocity as a function of period can also be obtained by applying any frequency–time analysis technique (Dziewonski *et al., 1969*). In this study, in order to compute group wave velocities, envelopes of the signal were calculated and group wave velocities are simply estimated from the maximum value of the envelope of the signal and distance.

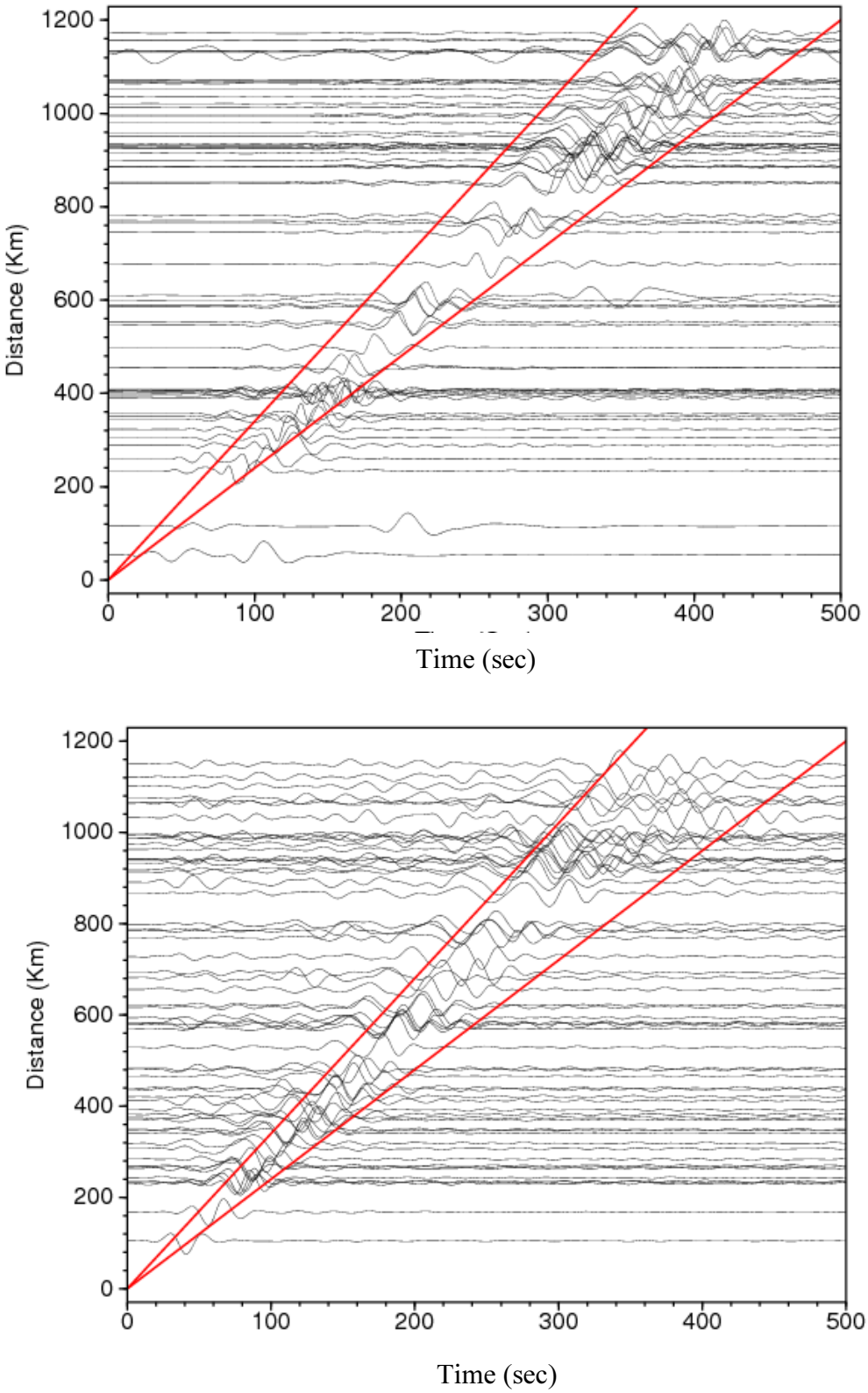

Figure 3.10. Top: The event gather of the earthquake band-pass filtered between 30-60 sec periods. Bottom: The estimated Green's functions from the long term correlations of PTK station with the other broadband stations. Red curves indicate the times corresponding to velocity of 2.4 km/s and 3.4 km/s.

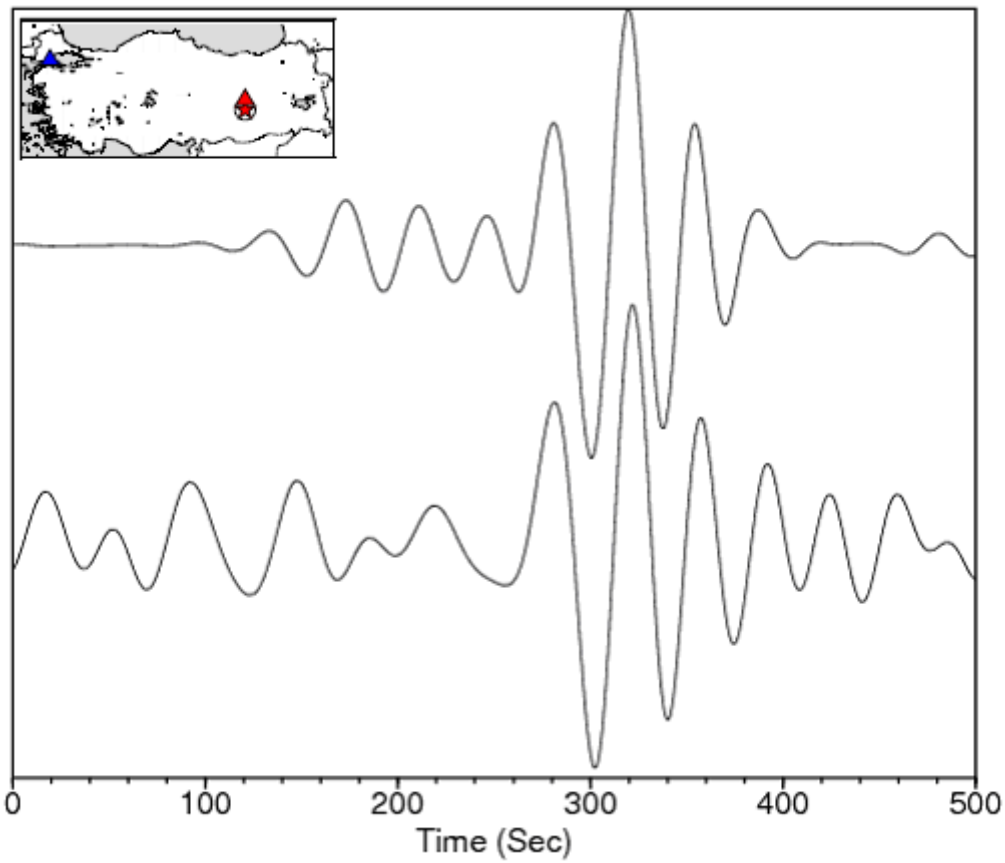

Figure 3.11. Comparison of the observed waveforms from the earthquake and the estimated Green's functions from the cross-correlation of PTK and RKY stations. The inner figure shows the locations of the earthquake (red star), RKY station (blue triangle) and the PTK station (red triangle).

For the reliability of the estimated Green's functions obtained from cross-correlations the final test is performed by comparing them to the recordings of an earthquake. The waveforms of surface waves emitted directly from an earthquake and the waveforms obtained from the cross-correlations are compared in Figure 3.10. The selected earthquake occurred near PTK station (February 21, 2007, Mw=5.7, lat=38.32, lon=39.28, depth = 10 km). Figure 3.10 shows the vertical component waveforms of this earthquake recorded by 80 broadband stations (top), and shows the waveforms emerged from cross-correlations of ambient seismic noise records with the vertical component recordings of PTK station (bottom), together. The Rayleigh waves can be observed in both time sections within the specified group wave velocity window.

Figure 3.11 shows the earthquake recording at a selected station, RKY, for comparison with the estimated Green's function between RKY and PTK. The earthquake data is band-pass filtered between the 30-60 sec periods as the correlations are computed. The inset figure shows the locations of the RKY and PTK stations with the location of the earthquake. The waveform at the bottom represents the cross-correlation of the RKY station with the PTK station which is located at a close distance to the earthquake. This similarity of the waveforms confirms that the cross-correlations approximates well to the Green's functions of Rayleigh waves.

3.5. Tomography

A variable smoothing technique has been performed to generate group wave velocity maps (Pasyanos, 2005). The study region is divided into equal-area cells and the following system of equations is obtained.

$$t = \boldsymbol{D}\, s \tag{3.7}$$

$$\lambda\, \mathbf{L}\, s = 0 \tag{3.8}$$

where, t is a vector of surface wave group arrival times, D is a matrix containing the distances traveled in each cell, and *s* is a vector of group wave velocity slowness. Equation 3.8 imposes the smoothness constraint on the model parameters by constructing the two dimensional Laplacian operator L of the slowness. The damping factor λ controls the trade off between fitting the travel times and smoothing the model. The inversion does not strongly depend on the initial velocity model. However a fine grid could create regions with low or no ray coverage. Pasyanos (2005) proposed a variable smoothing operator to improve the resolution when the ray density is higher. In this study a variable smoothing operator was performed with a multi-step process for the inversion. A larger grid size was adopted at the first step with a constant initial model resulting in a low resolution solution. The grid size was halved in the second step with the initial model obtained in the previous step.

3.6. Checkerboard Tests

The resolution of the data set is also a function of the path density, azimuthal distribution and average path length of rays. The path distribution depends on the nature of the data set and related to resolution when the azimuthally coverage is relatively uniform. A number of tests using both real and synthetic data are performed to select the optimum cell size and smoothing parameters for tomography. Figure 3.12 and 3.13 shows the ray path coverage for the vertical and transverse component Green's functions, respectively. Figure 3.14 shows checkerboard tests for the vertical component to determine the effect of path coverage on the solution. The results only indicate if the path coverage is sufficient but will not give information on the irresolution (Vdovin *et al*., 1999). The initial checkerboard models contain alternating velocity values of 3.0 and 3.5 km/s for low and high velocity regions with four degree and two degree patterns. A grid size of four degrees was used at the beginning then the image computed with two degree grid size. Both the magnitudes and the shape of the rectangular patterns were recovered in the majority of Turkey for four degree and two degree and patterns (Figure 3.13). The results are consistent with the path densities shown in Figure 3.12. The resolution degrades for two degree and one degree patterns outside of Turkey with poor ray coverage, especially in the eastern Anatolia. In the Arabian plateau and outside of Turkey the smearing of the patterns also indicates the insufficient ray coverage. Structures smaller than two degree, cannot be resolved in the areas with low ray coverage. Such areas are located along the Black Sea coast, Hellenic arc and Mediterranean coast. However the long wavelength features (>2 degree) can still be recovered in majority of the domain with the exception of the northern part of the Black Sea.

The resolution of Love waves is poor compared to Rayleigh waves (Figure 3.15). The number of paths for Love waves is approximately half of Rayleigh waves (~2500 for Rayleigh waves and 1300 for Love waves). As a result the patterns in the majority of the area are not constrained well. We only present the results of 20 sec for Love waves and the inversion is performed with one degree grid size.

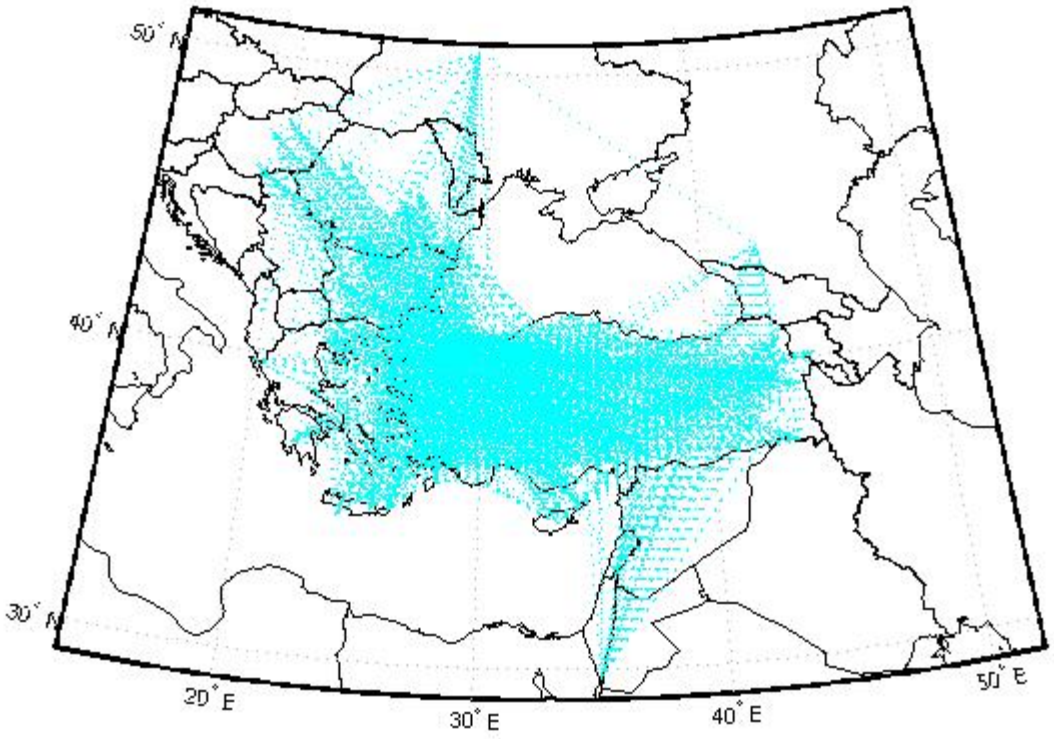

Figure 3.12. Ray paths for 15 sec period Rayleigh wave group velocity measurements from cross correlations.

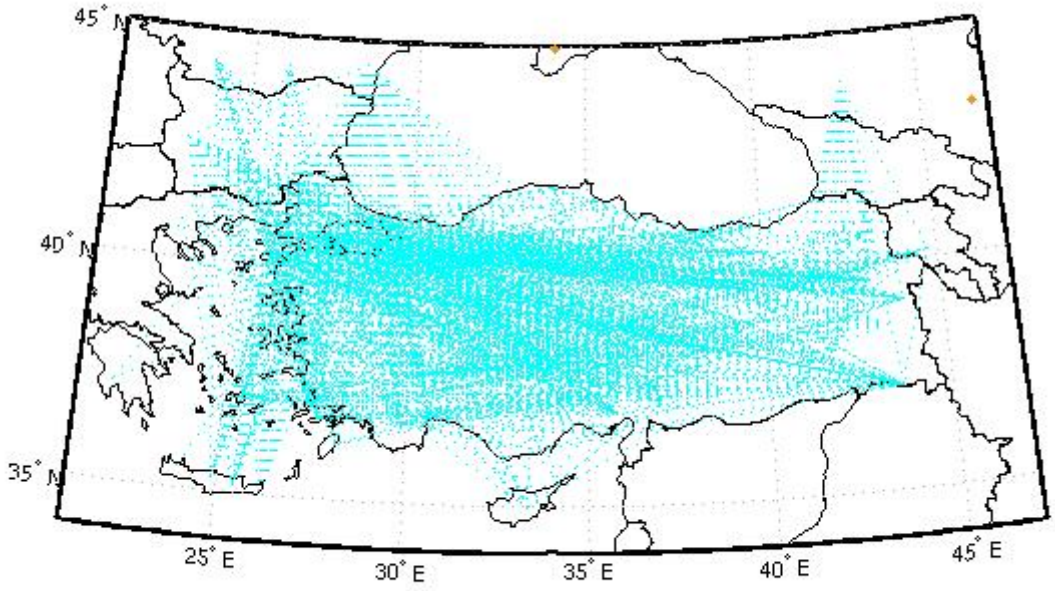

Figure 3.13. Ray paths for 20 sec period Love wave group velocity measurements from cross correlations.

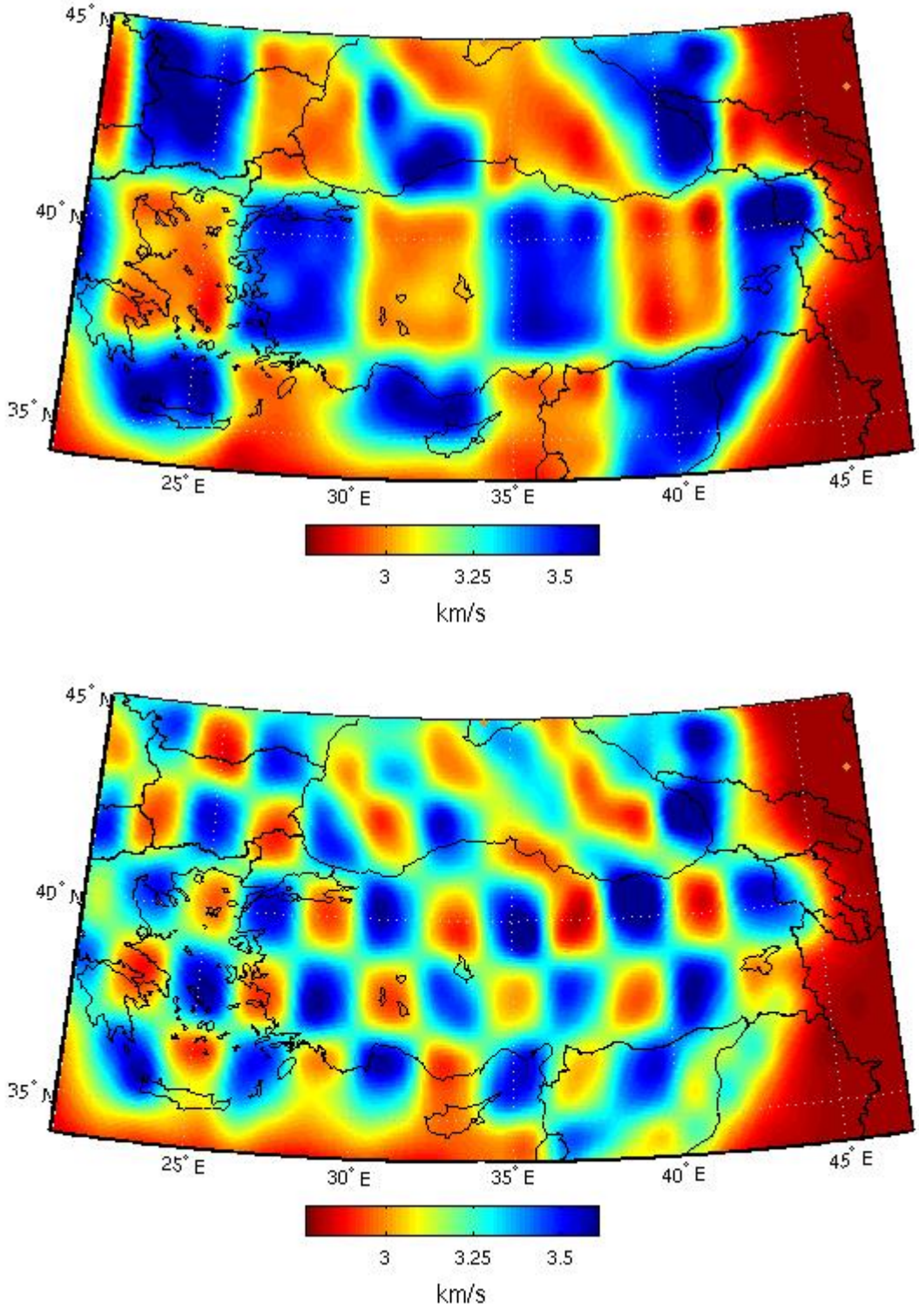

Figure 3.14. Checkerboard resolution tests using the path coverage of 15 sec Rayleigh waves. Two types of input patterns with four by four degree (top) and two by two degree (bottom) are tested.

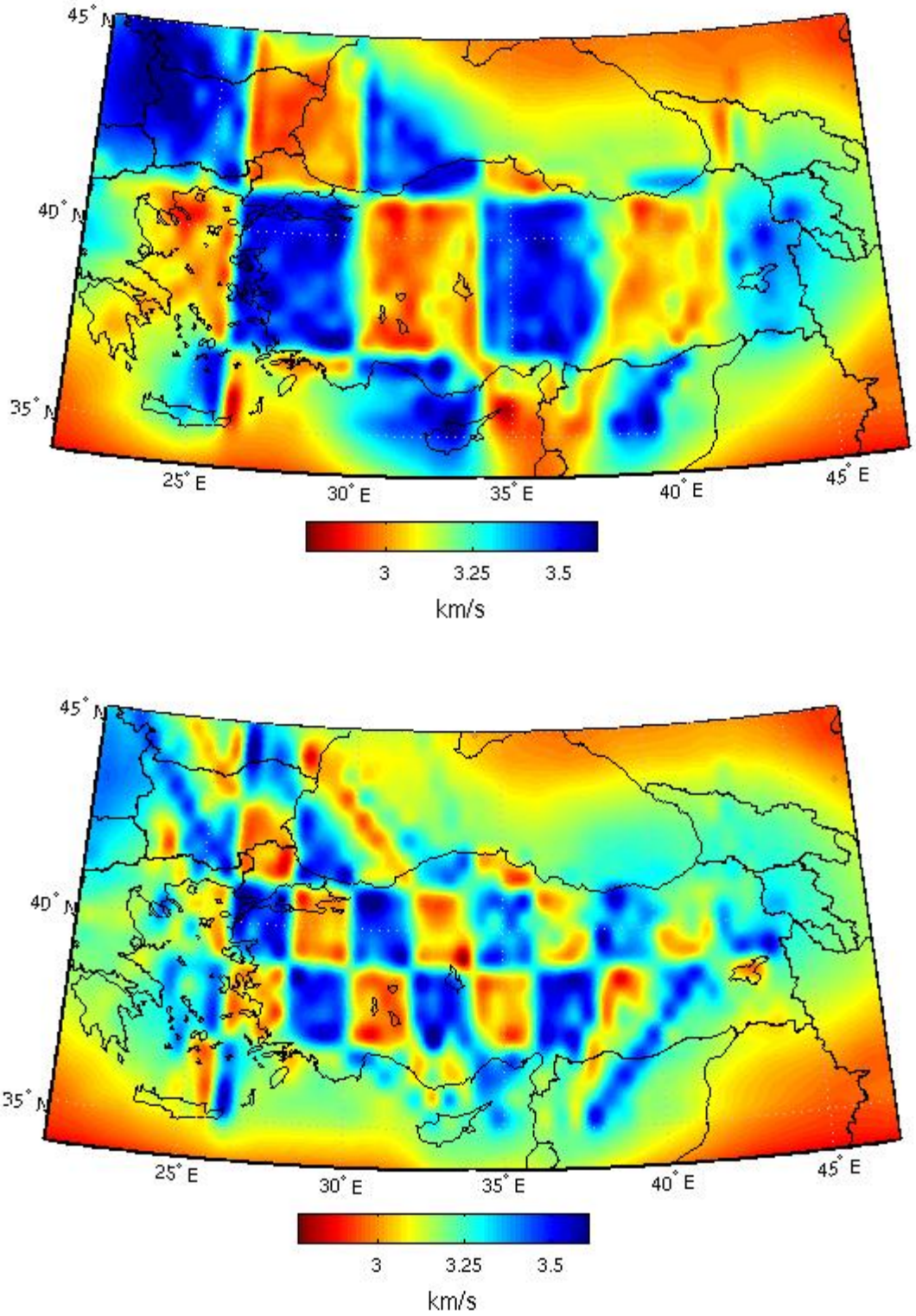

Figure 3.15. Checkerboard resolution tests using the path coverage of 20 sec Love waves with four by four degree (top) and two by two degree input and output (bottom).

3.7. Group Velocity Maps and Discussions

Group velocity maps are computed in few steps. At the first step the smooth group wave velocity maps obtained at each period to identify and discard group wave velocity measurements with travel time residuals larger than 20 sec. Then the final group wave velocity maps computed in three steps as explained during the checkerboard tests. The group wave velocity maps estimated with two degree grid interval and then the resulting maps used as the input model to compute maps with one degree grid spacing. The final maps are computed with 0.5 degree grid interval.

Using the tomographic inversion method, both Rayleigh and Love wave group velocity maps are computed. Group wave velocity maps are produced for several smoothing parameters, λ = 50, 100, 200. Smoothing parameter with a value of 200 was preferred in this study, which gives relatively smooth maps with small solution errors. After the selection criteria approximately 2500 paths were used to invert group velocity maps for Rayleigh waves and less than 1300 paths were used to invert group velocity maps for Love waves. Rayleigh wave group velocity maps are computed for 15, 20 and 25 sec periods. However only at 20 sec period Love wave group velocity map was computed. The path coverage at other periods was insufficient for reliable tomographic images

Figure 3.16 shows the Rayleigh wave group velocities at 15 sec period. Waves with 15 sec period sample crust up to a depth of 10 km in thickness. Group wave velocities at this period range are sensitive to upper crust and it is mainly influenced by local sedimentary basins. In Figure 3.16 low group wave velocities are observed in Marmara Sea, Antalya Bay, Isparta angle and also in Adana-Cilicia Basin. Aegean Sea, The Rhodope-Strandja massif and the Pontides along the Black Sea coast present higher group wave velocities.

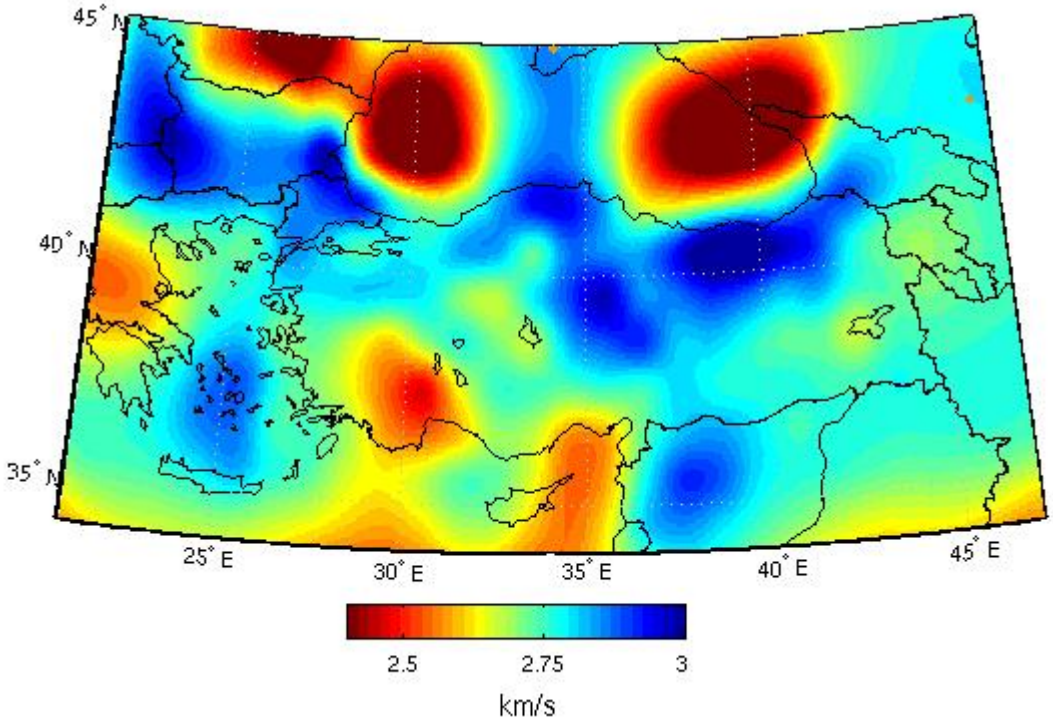

Figure 3.16. Rayleigh wave group velocity maps obtained from the Green's functions estimated by the cross correlations at 15 sec period.

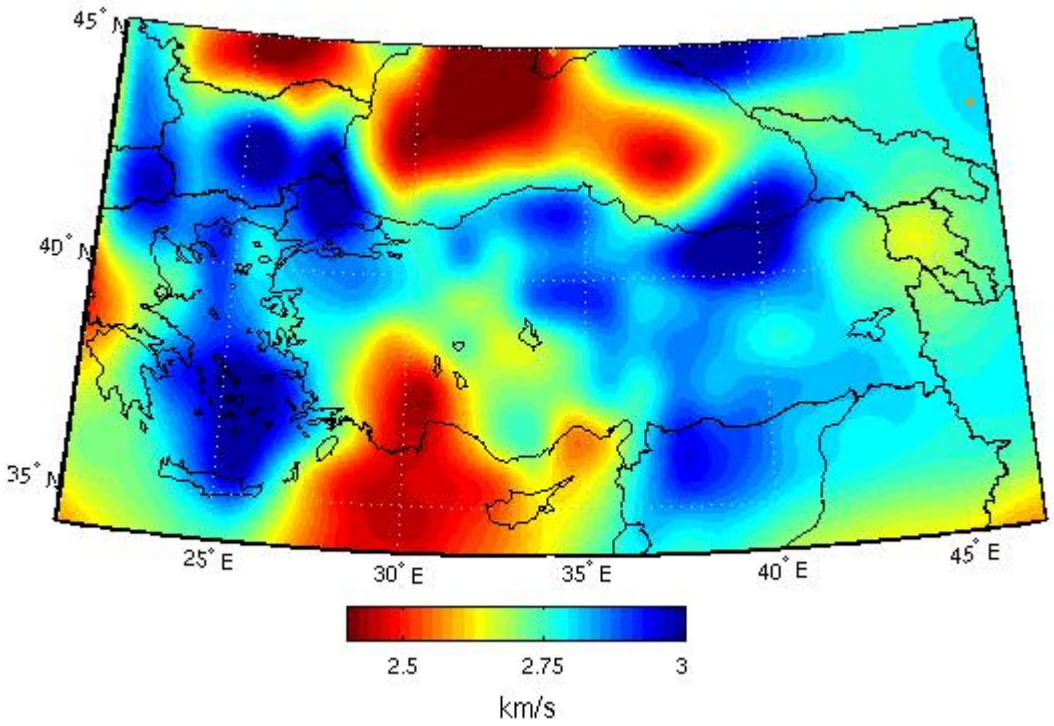

Figure 3.17. Rayleigh wave group velocity maps obtained from the Green's functions estimated by the cross correlations at 20 sec period.

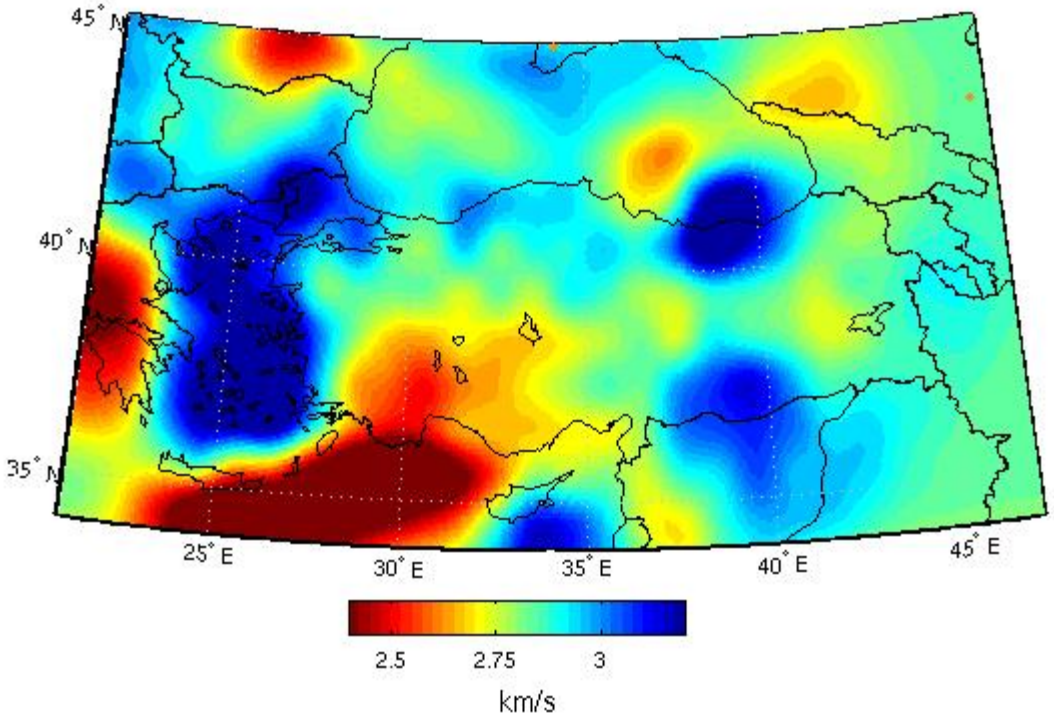

Figure 3.18. Rayleigh wave group velocity maps obtained from the Green's functions estimated by the cross correlations at 25 sec period.

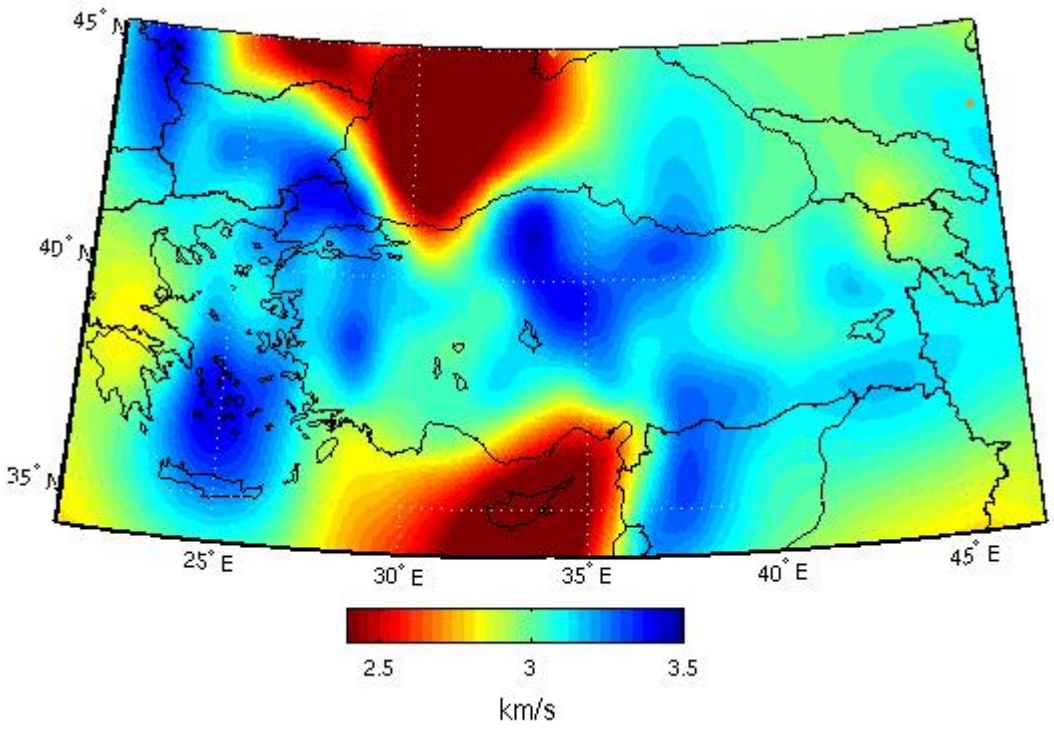

Figure 3.19. Love wave group velocity maps obtained from the Green's functions estimated by the cross correlations at 20 sec period.

Rayleigh wave group velocity maps for 20 sec period were calculated and presented at Figure 3.17. Low group wave velocities at this period range are observed in Antalya Bay with a continuation toward the Isparta angle and also in Adana-Cilicia Basin. Higher group wave velocities observed mainly at Aegean Sea, Pontides, Istanbul zone and Strandja massif.

Rayleigh wave group velocity maps for 25 sec period have similar variations with Rayleigh wave group velocity maps for 20 sec period. Figure 3.18 shows the Rayleigh wave group velocities at 25 sec period. Low group wave velocities at this period range are observed in the eastern Mediterranean and the Black sea. Group wave velocities at his period range are higher along the Pontides, Istanbul zone and Strandja massif. High group wave velocities are also observed in central Anatolia and at the north of the Hellenic Arc. Lower velocities are observed in Antalya Bay, Isparta angle and also in Adana-Cilicia Basin.

Figure 3.19 shows 20 sec group velocity map for Love waves. Although there are similarities between the results of Love and Rayleigh waves we will not make any interpretation for the Earth structure. The reliability of the maps will be discussed in 4th chapter with the results obtained from earthquake sources.

4. SURFACE WAVE TOMOGRAPHY FROM REGIONALWAVEFORMS

4.1. Introduction

Surface wave tomography has proven to be very useful in determining the structure of the crust and uppermost mantle on both regional and global scale (Dziewonski, 1984; Woodhouse and Dziewonski, 1984; Trampert and Woodhouse, 1995; van der Lee and Nolet, 1997; van Heijst and Woodhouse, 1999). Their large amplitudes with relatively low attenuation and long propagation paths provided significant contribution to our knowledge of the Earth's upper mantle and crustal structure. One dimensional earth models has been routinely obtained along great circle paths using the dispersive nature of surface waves while long period surface waves have been the main source of the observation for determining the tomographic image of the mantle (Oliver, 1962; Dziewonski, 1972; Knopoff, 1972).

During the last decade with the availability of high quality digital broadband seismic data we have seen a rapid progress in imaging the structure of crust and upper mantle with increasing resolutions. Studies at local and regional scales are now common for regions with good coverage of stations and earthquakes. Phase and group velocity maps obtained from dispersive surface waves correlate well with the main tectonic belts and geologic units providing better constrains on their geometry and relation to the regional tectonics (Levshin *et al.,* (1992, 1994); Ritzwoller *et al.,* 2002; Pasyanos, 2005).

In the last decade various researchers performed surface wave studies in Turkey and surrounding areas (Ritzwoller and Levshin, 1998; Pasyanos *et al*., 2001; Maggi and Priestly 2005; Pasyanos, 2005; Gök *et al*., 2007). Ritzwoller and Levshin (1998) were studied the dispersion characteristics of surface waves propagating across Eurasia. Pasyanos *et al*., (2001) performed a larger–scale study on surface wave group velocity dispersion including the Middle East, North Africa, southern Eurasia, and the Mediterranean. Maggi and Priestly (2005) used surface waveform tomography in order to clarify the upper-mantle shear wave velocity structure beneath the Turkish-Iranian plateau and surroundings. Pasyanos (2005) carried out a variable smoothing technique in order to

improve the resolution of previous surface wave works by enlarging the study area. Beside these studies which performed in a large scale in the region with other continents around Turkey and surroundings, Gök *et al*., (2007) performed a small scale surface wave study in order to understand the lithospheric structure of the continent-continent collision zone. However, all of these studies were performed using limited path coverage in a large scale study or it just comprises a limited part of Turkey. In this work we have used a denser coverage of stations and events in order to obtain the crustal structure of Turkey and its surroundings by acquiring a higher resolution in the whole area. For this aim, Love wave group velocity maps were obtained for periods 10-50 sec using local and regional earthquakes. Available data were used from broadband stations operated between years 1997 and 2009 in Turkey and surrounding regions. 285 earthquakes with magnitudes greater than 4.5 are selected for the analysis. Fundamental mode group velocities of Love and Rayleigh waves at 271 stations along 12500 paths are computed using Multiple Filter Analysis (Dziewonski *et al*., 1969). Approximately 25 per cent of the paths for Love waves provided reliable group velocity measurements. Group wave velocity maps were obtained and the results are interpreted in relation to the geologic and tectonic observations in the region. The group wave velocity maps also provide constrains on the determination of the shear wave velocities.

4.2. Data

A waveform database for the surface wave investigations has been formed from the permanent and temporary digital broadband stations operated in the region between the years of 1997 and 2009 (Figure 4.1). The main source of data is the National Network of Turkey operated by Kandilli Observatory and Earthquake Research Institute. The network has been continuously upgraded since 2004 and the number of broadband stations exceeded 100 in the year of 2008. The majority of the stations record signals at periods 100 sec or higher. However approximately 10 per cent of the instruments have lower recording range (<40 sec). Supplementary data from IRIS and ORFEUS depository were obtained for the permanent stations operated in the region.

Data from several portable deployments are also included in the study. A temporary network operated between the years 1999-2001 with 29 broadband stations during the

Eastern Turkey Seismic Experiment (ETSE) (Sandvol *et al*., 2003). The average station separation was approximately 50 km for the network. The western Anatolia Seismic Recording Experiment (WASRE) operated from November 2002 to October 2003 with 45 short period and five broadband stations (Zhu *et al*., 2006). In this study, only the broadband stations of WASRE have been used. We also include data from local networks which have been operating in the various regions of Turkey. The total number of stations exceeds 270 and distributed non-uniformly throughout the region. The station coverage is dense in the Marmara region and the eastern Anatolia while the central Anatolia, Black Sea and Eastern Mediterranean regions are poorly sampled by stations.

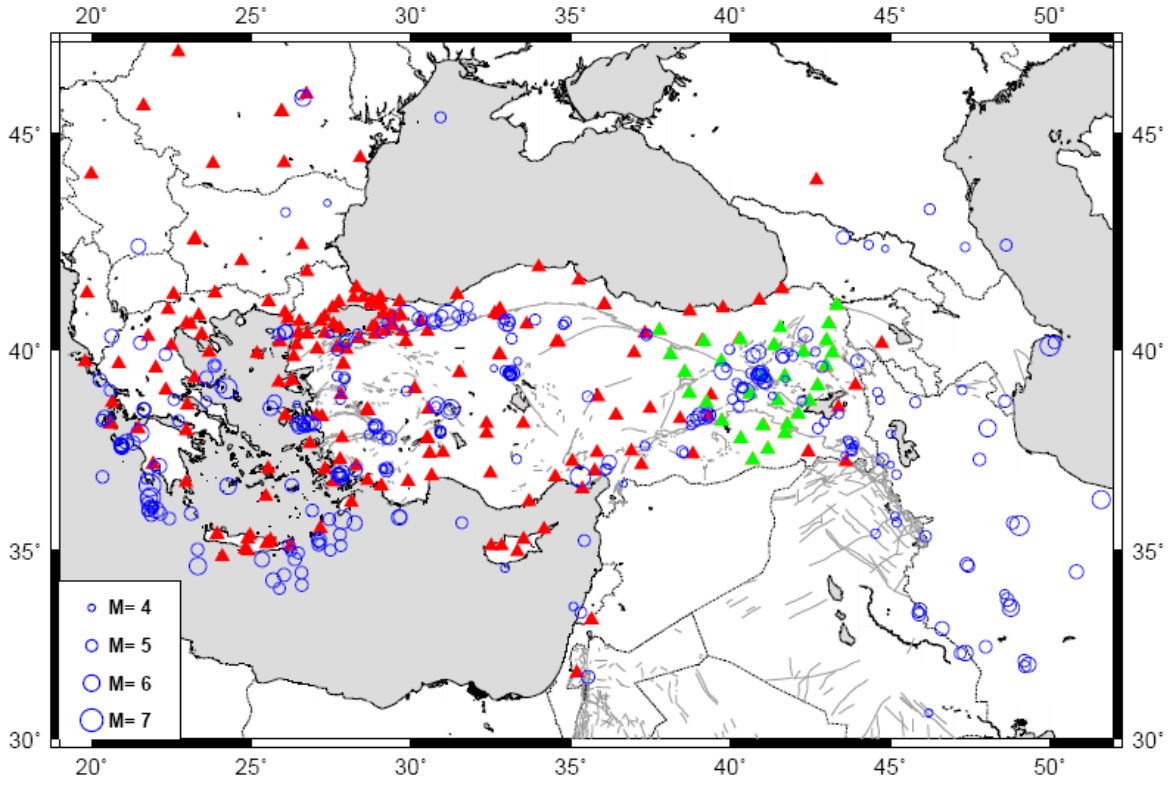

Figure 4.1. Distribution of earthquakes (circles), seismic stations (triangles). The earthquakes with magnitudes greater than 4.5 which occurred between the years 1997 and 2009 are selected. Red triangles show the stations recorded the presented earthquakes by different networks during 1997-2009. Green triangles show the stations recorded during the ETSE project in between 1999-2001.

We selected 285 earthquakes which occurred between the years 1997-2009 with magnitudes greater than 4.5 and the depth less than 30 km (Figure 4.1). Event distribution is also non-uniform. The majority of the earthquakes located along the active seismic zones, North Anatolian Fault, East Anatolian Fault and Aegean subduction zone. Fewer earthquakes are included from Caucausus and Iran. The earthquakes along North and East Anatolian Fault have mostly strike slip mechanisms while the events from the western Anatolia and Aegean have normal and reverse mechanisms. The range of the recording distance used for the surface wave analysis is greater than 600 km and less than 2200 km.

4.3. Surface Wave Dispersion Measurements

The surface wave dispersion curves are computed in several steps. The first step involves visual check of the waveform data to insure reasonable signal-to-noise ratios and eliminate problematic recordings. Radial and transverse components are computed by rotating NS and EW components into backazimuth directions. We obtained Love waves from the transverse components and Rayleigh waves from the vertical components. The waveforms with complicated surface wave patterns resulted from the multhipathing and higher mode contributions were discarded. The instrument response was removed from the selected waveforms and the waveforms were decimated to 20 sps.

We employed both Multiple Filter Analysis (MFA) (Dziewonski *et al*., 1969; Herrmann, 1973) and Reassigned Multiple Filter Analysis (RMFA) (Pederson *et al*., 2003) of the seismograms to estimate the surface wave group velocities. Reassigned Multiple Filter Analysis is an improved interpretation of MFA. Rather than attributing the energy in a point of the time-frequency domain to the center of the applied frequency and time windows, it is attributed to a location within the window that corresponds to the center of gravity of the energy. Objective of the method is to improve the precision of group wave velocity measurements with energy reassignment in time-frequency domain (Pederson *et al*., 2003) Reassigned MFA gives better constrained narrow dispersion curve than the classical MFA which shows smeared image of the group wave velocity dispersion curve especially at the higher periods.

In order to test the accuracy of group wave velocity estimates both synthetic and real waveforms were used. Figure 4.2 indicates RMFA and the group wave velocity dispersion curve of the recording AGIN station from one of the aftershocks (Mw=5.0) of 12 November 1999 Düzce (Mw=7.2) Earthquake. Figure 3.2.b shows RMFA of a synthetic waveform for an earth obtained by a simple grid search based on the dispersion curve in Figure 4.2.a. Discrete wavenumber summation method (Herrmann, 1973) were used to compute the synthetic waveform. The theoretical dispersion curve from the same model is also shown in Figure 4.2.b (Herrmann, 1973).

Group wave velocities were interactively picked from both MFA and RMFA. MFA provided better continuity at lower periods while RMFA provided increased resolution at greater periods. Two dispersion curves calculated from two reference models are used to guide the picks (Figure 4.3). The first reference earth model with thick crust is determined from a simple grid search as explained above while the second earth model corresponding thin crust is obtained from Akyol *et al*., (2006) assuming a Vp/Vs ratio of 1.75. The period ranges were selected where the curves are continuous and the amplitude of the signals are large. Using the picked group wave velocities we applied velocity filtering to the waveforms (Herrmann, 1973) and recalculated RMFA of the velocity filtered waveforms. Group wave velocity picks were improved. Assuming that the wave followed the great circle arc between the source and the receiver, the group velocity for a given period is estimated by dividing the epicentral distance by the group wave arrival time. Standard deviations of group wave velocities are estimated from 95 per cent of group wave velocities.

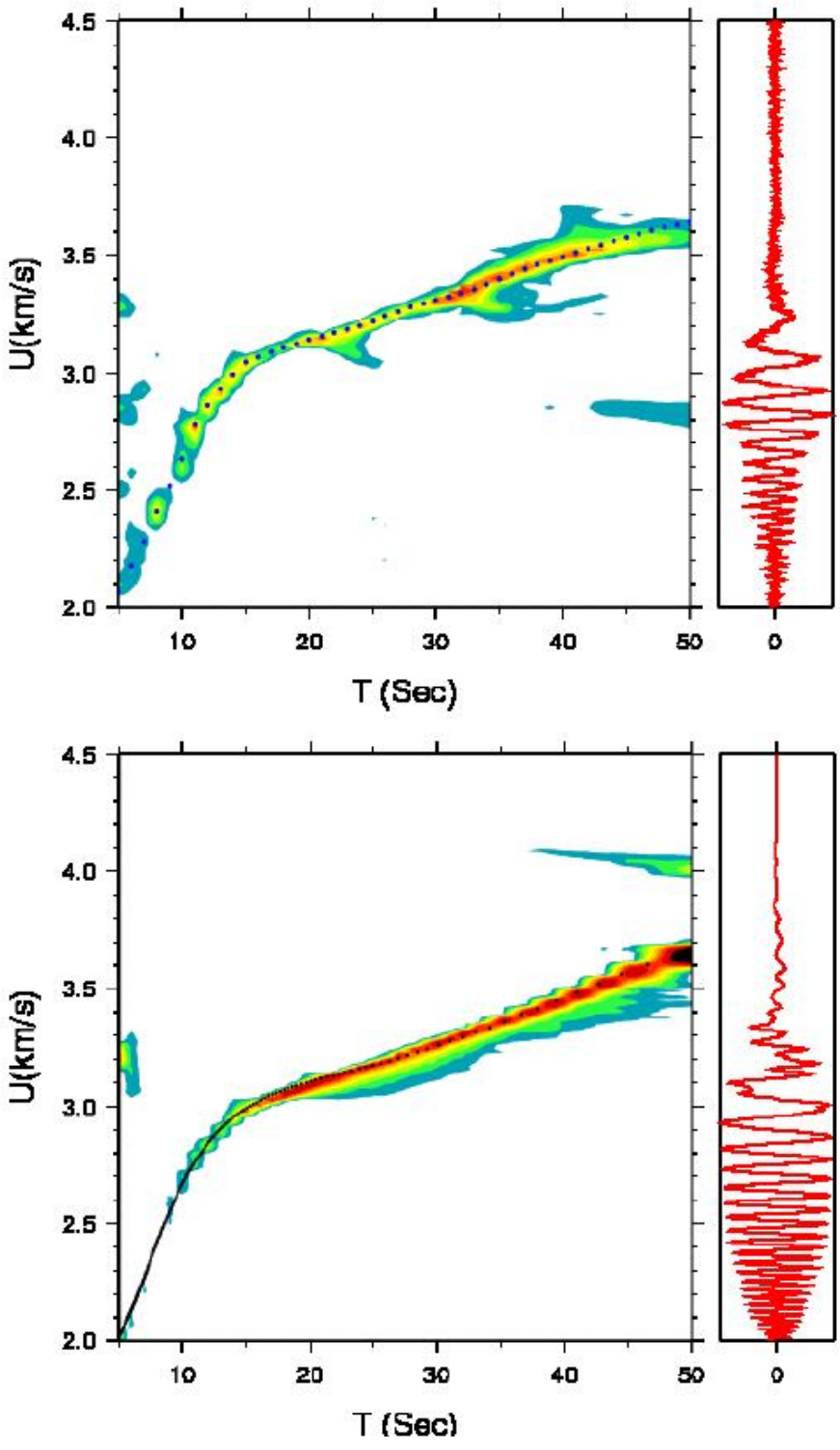

Figure 4.2. Analysis of waveforms using reassigned multiple filter technique. Top: RMFA for the transverse component of the aftershock of Düzce Earthquake recorded at AGIN station (Δ=960km). Bottom: RMFA for the transverse component of the synthetic waveform computed from the earth model shown in Figure 4.3. The black dots shown on the top figure shows the picks of group wave velocities and on the bottom shows computed group wave velocities from the earth model.

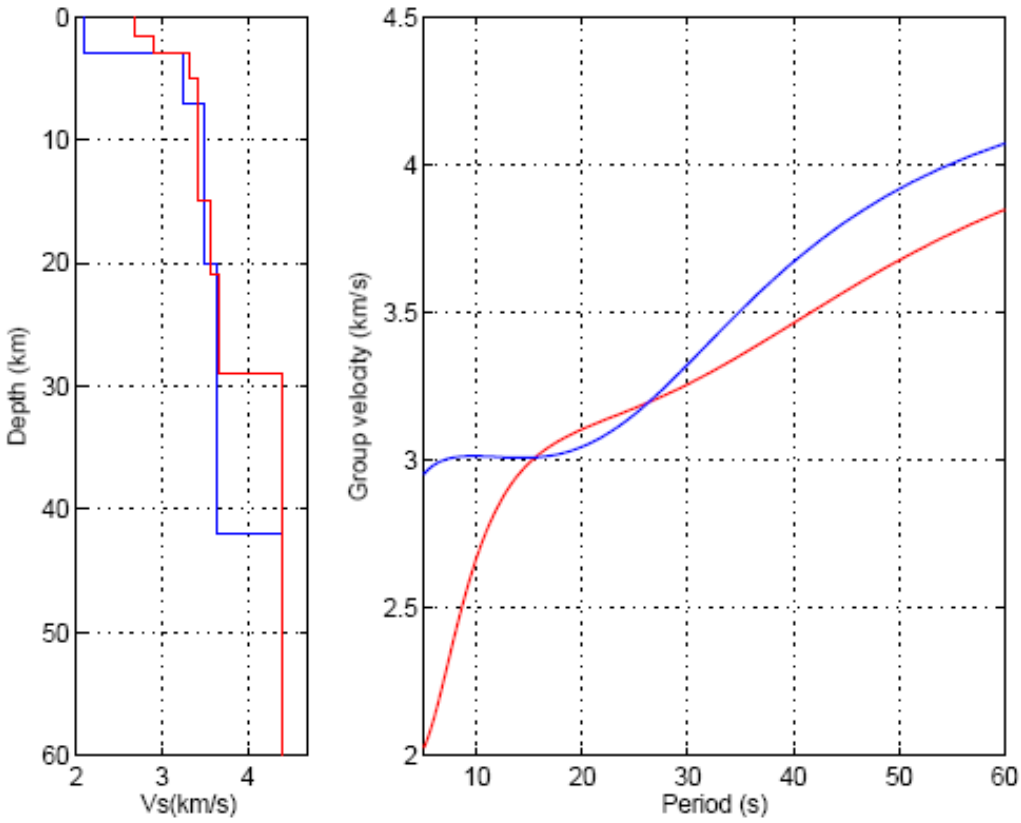

Figure 4.3. Dispersion curves calculated from two reference earth models.

4.3.1. Multiple Filter Analysis

The multiple filter technique is proposed by Dziewonski *et al*., (1969) for the determination of dispersive surface wave group velocities. The multiple filter technique has been used as an efficient way of resolving complex transient signals composed of several dominant periods that arrive to the recording station at the same time. A narrow band, Gaussian filter is used and group wave velocities can be obtained as the distance divided by the time of arrival to the station. Different filters resolve the transient signal that is composed of simultaneous arrival of several dominant periods. Group wave velocity curve can be drawn for amplitude ridges of filtered signal within the frequency range where the signal is well observed. Further detail on the theory of group wave velocity estimation by using multiple filter technique can be found at Dziewonski *et al*., (1969) and Bhattacharya, (1983).

Due to the Heisenberg inequality improved resolution in one domain causes the inverse effect in other domain. In order to obtain the optimum resolution both in time domain and frequency domain a Gaussian function was chosen as a window function. Other filters were experienced by different researchers in the latter applications (Herrmann, 1973; Canıtez, 1977).

4.3.2. Energy Reassignment Method

Different techniques were developed for the measurements of surface wave group velocity. However, the selection of the proper technique becomes significant when the wave trains of two or more modes overlap. More than that, most of the methods used to obtain the group wave velocity are based on the Fourier transforms and therefore introduce an important smearing in the time-frequency domain. Another relevant problem is the systematic errors introduces by the non-stationarity and strongly varying spectral amplitude of the seismic signal. For this reason, methods such as Wigner distribution, Choi-Williams distribution or Reassigned Multiple Filter Analysis have been proposed to overcome the shortcomings of earlier techniques.

The reassignment method is used for sharpening the time frequency representation by mapping the data to time-frequency coordinates that are closer to the true region of support of the analyzed signal. Energy reassignment was first arising from the idea of Kodera *et al*., (1976). Pedersen *et al*., (2003) applied the reassignment of energy in order to improve the surface wave group velocity measurements. According to their work, energy reassignment technique is based on the fact that the smearing and systematic errors are predictable effects when the time and frequency filters are known and rather than attributing the energy in a point of the time-frequency domain to the center of the applied frequency and time windows, the energy is attributed to a location within the window that corresponds to the center of gravity of the energy (Pedersen *et al*., 2003). Objective of the method was to improve the precision of group wave velocity measurements with energy reassignment in time-frequency domain.

The reassignment method introduced by Kodera *et al*., (1976) and used in the improvement of surface wave measurements by Pedersen *et al*., (2003) reassigns the

energy to the center of gravity. Further detail on the theory of energy reassignment method can be found at Kodera *et al*., (1976) and Pedersen *et al*., (2003).

4.3.3. Computation of the Dispersion Curves

In order to obtain the surface wave dispersion curves 12400 paths for both Love and Rayleigh waves have been computed for the analysis. After the revision and application of the selection criteria approximately one forth of the paths provided reliable dispersion measurements for Love waves. Since the number of dispersion measurements for Rayleigh waves were much lower than those of Love waves (about one third of Love waves) the analysis proceeded only using Love waves. Additional measurements are needed to compute reliable maps for Rayleigh waves. Figure 4.4 shows the number of Love wave measurements at different periods before and after discarding the paths with epicentral distances outside of the pre-selected range and eliminating improper group wave velocity curves.

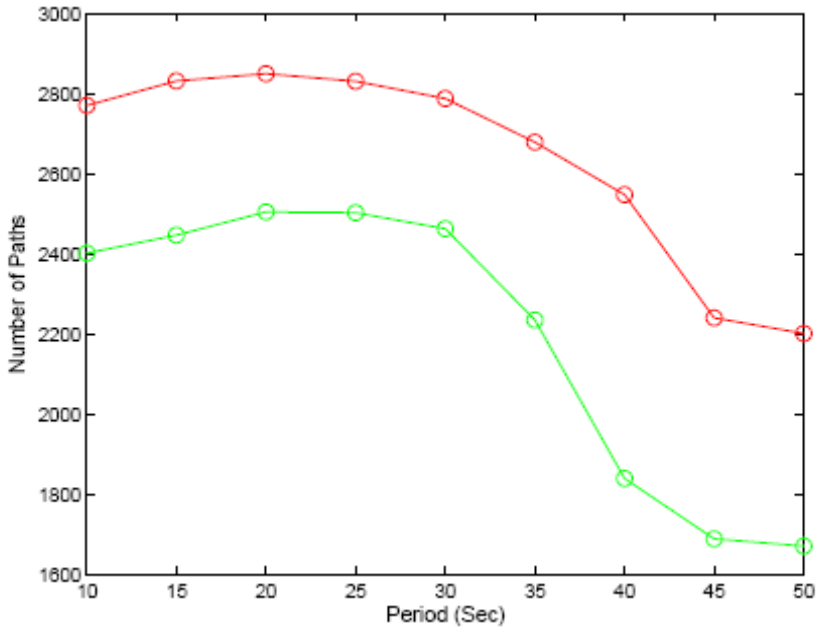

Figure 4.4. Number of Love wave group velocity measurements as a function of period before and after the paths eliminated.

Number of dispersion measurements for Rayleigh waves is found to be much lower than Love waves. This observation is not consistent with the observations worldwide. This differences are attributed to the facts that; first, the majority of the earthquakes used in this study has strike-slip (SS) mechanisms. It is well known that the earthquakes with strike-slip mechanisms generate Love waves more efficiently than Rayleigh waves and the amplitudes of Rayleigh waves attenuate faster at greater periods than Love waves (Tsai and Aki, 1971). Moreover the amplitude spectra of Rayleigh waves usually have spectral holes which can affect the continuity of dispersion curves (Tsai and Aki, 1971). When the magnitude threshold of the used earthquakes were reduced to Mw=4.5 the amplitudes become an important factor for a better signal to noise ratio. Second, the vertical component of surface waves is more affected by free surface topography than horizontal components. Turkey is surrounded by sea on three sides, high mountain ranges on the north and south (Figure 1.2). Such elevation differences may distort propagation paths and introduce scattering.

4.4. Group Velocity Maps

In order to compute the group velocity maps the same method that is applied and described in previous chapter was used. More detailed description of the variable smoothing technique is presented by Pasyanos (2005). The resolution of the data set is also a function of the path density, azimuthal distribution and average path length of rays. The path distribution depends on the nature of the data set and related to resolution when the azimuthally coverage is relatively uniform. A number of tests using both real and synthetic data are performed to select the optimum cell size and smoothing parameters for tomography. Figure 4.5 shows the ray hit-count and ray path coverage and Figure 4.6 checkerboard tests to determine the effect of path coverage on the solution. The results will only indicate if the path coverage is sufficient but will not give information on the irresolution (Vdovin *et al*., 1999). The initial checkerboard models contain alternating velocity values of 3.0 and 3.5 km/s for low and high velocity regions with four degree, two degree and one degree patterns. As a similar way that is performed in ambient noise correlation tomography, a grid size of two degrees were used at the beginning, then the image computed with one degree grid size and final image is estimated with 0.5 degree grid size. Both the magnitudes and the shape of the rectangular patterns were recovered in the

majority of Turkey for four degree, two degree and one degree patterns (Figure 4.6). The results are consistent with the path densities shown in Figure 4.5. The resolution degrades for four degree and one degree patterns outside of Turkey with poor ray coverage, especially in the Black Sea and the Mediterranean Sea. In the Arabian plateau the smearing of the patterns also indicates the insufficient ray coverage. Structures smaller than two degree, cannot be resolved in the areas with low ray coverage. Such areas are located along the Black Sea coast, Hellenic arc and Mediterranean coast. However the long wavelength features (>2.0 degree) can still be recovered in majority of the domain with the exception of the northern part of the Black Sea.

Group velocity maps of Love waves are computed in few steps. At first the smooth group wave velocity maps obtained at each period to identify and discard group wave velocity measurements with travel time residuals larger than 20 sec. Then the final group wave velocity maps computed in three steps as explained during the checkerboard test. The group wave velocity maps estimated with two degree grid interval and then the resulting maps used as the input model to compute maps with one degree grid spacing. Final images are calculated for 0.5 degree grid interval.

There are additional concerns other than path distribution, weighting of the data and spatial smoothing that may affect the estimated maps. These are 1) mislocations of the earthquakes, 2) distortions in 3-D wavefields due to lateral inhomogeneities 3) anisotropy (Vdovin *et al*., 1999). The earthquakes selected for the group wave velocity dispersion measurements are also relocated using the available data. The hypocentral errors of the earthquakes in Turkey are usually less than 5.0 km. However the estimated errors for the events outside of the network coverage may reach 10 km. These values will have negligible effects on the estimated travel times in the distance ranges used in this work.

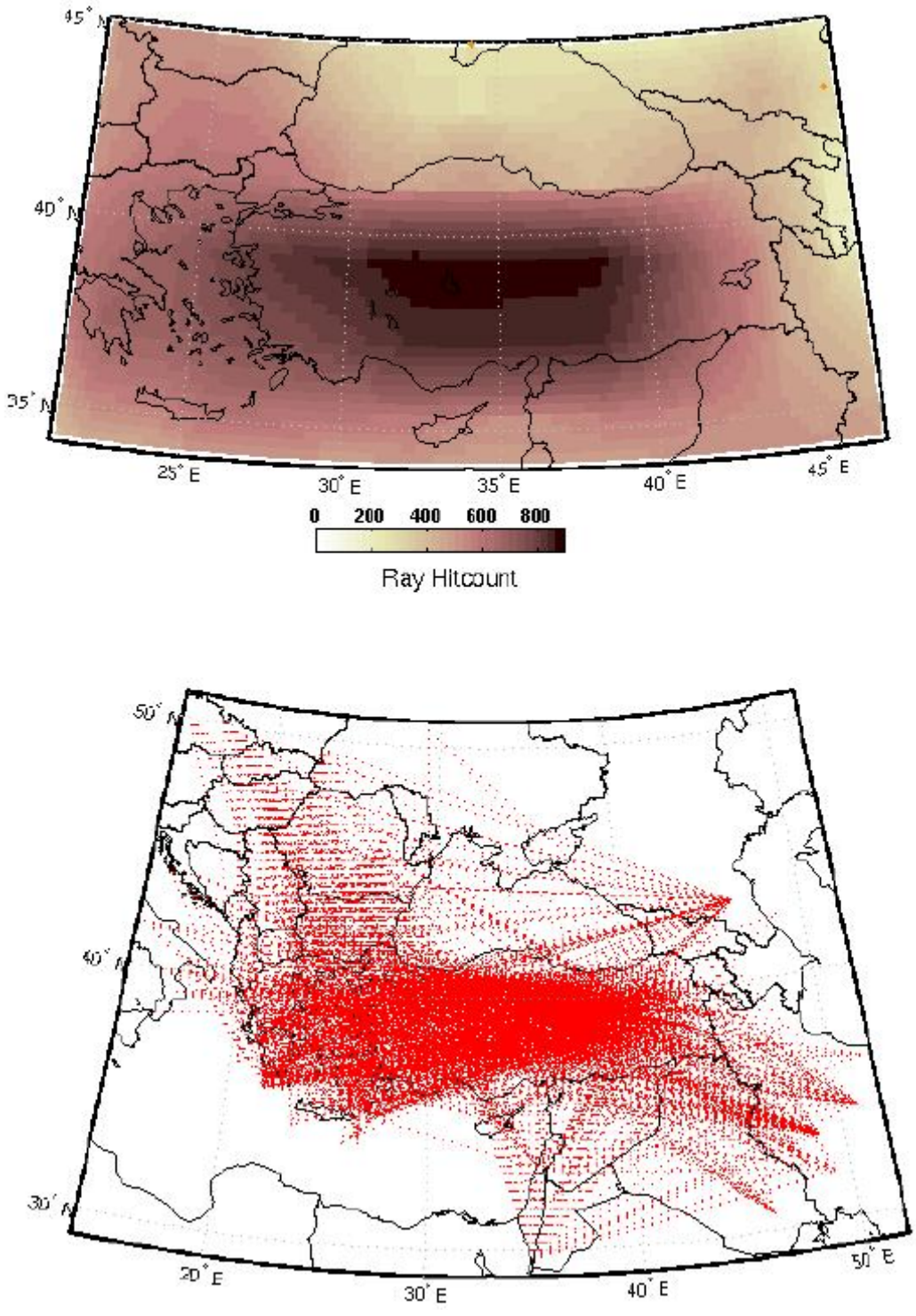

Figure 4.5. Ray hit-count (top) and ray paths (bottom) for 20 sec period Love wave group velocity measurements.

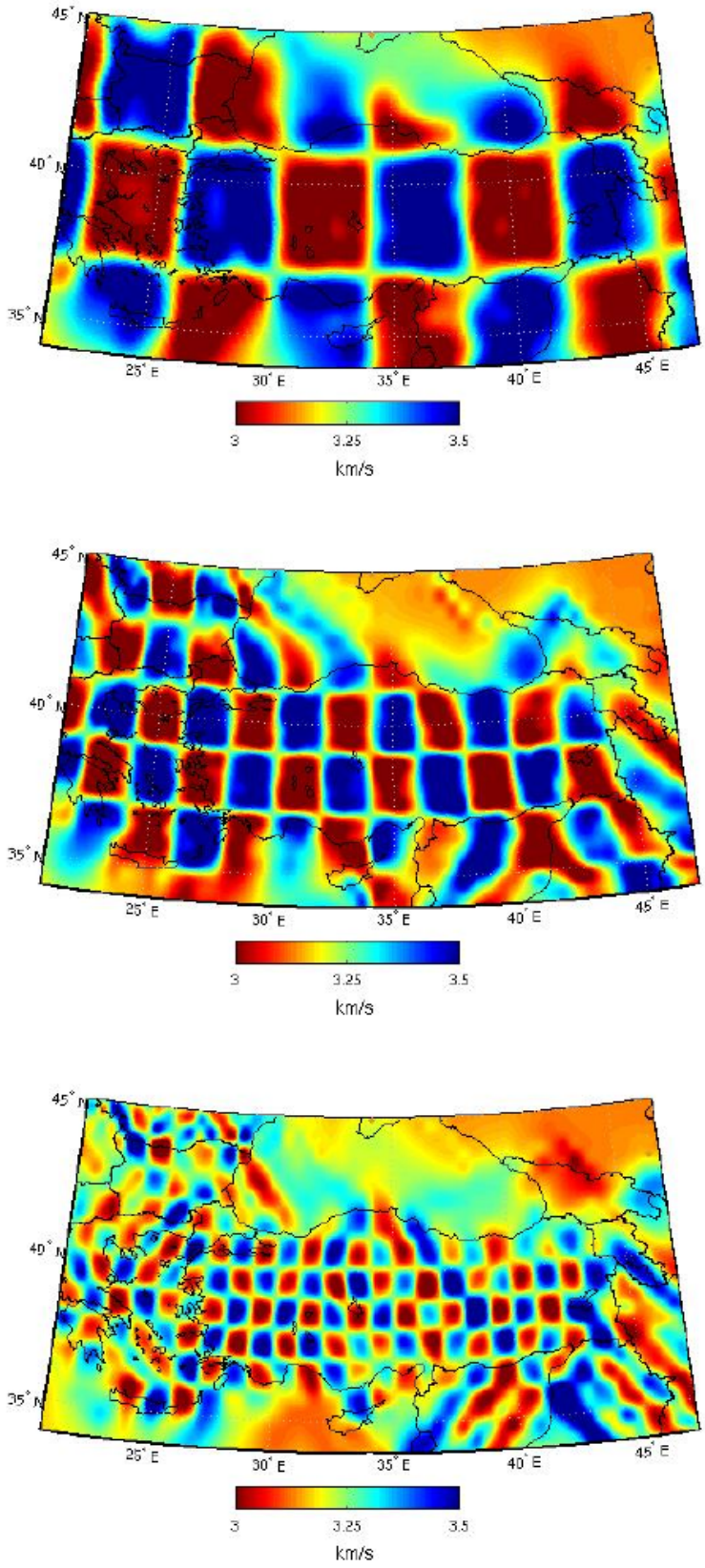

Figure 4.6. Checkerboard resolution tests using the path coverage of 20 sec Love waves. Three types of input patterns with four by four degree (top), two by two degree (middle) and one degree by one degree (bottom) are tested.

The assumptions made in the formulation of tomography problem provide significant simplifications. The effect of anisotropy and deviations from straight ray paths are totally ignored in this study. It is well known that ray-theory is a high frequency approximation which is not justified in the presence of large lateral heterogeneities. For the ray approximation to be valid, the first Fresnel zone must be smaller than the scale-length of the heterogeneity, which places limitations on the lateral resolution of seismic models based on ray-theory (Levshin *et al*., 2005). Such effects are not investigated in this study and may have varying degrees of importance when large lateral velocity contrasts exist.

Using the tomographic inversion method as described in the previous section, Love wave group wave velocity maps at 10, 15, 20, 30, 40 and 50 sec are computed. Group wave velocity maps are produced for several smoothing parameters, λ = 50, 100, 200. Smoothing parameter with a value of 200 was preferred in this study, which gives relatively smooth maps with small solution errors. The RMS travel time errors for the initial and final velocity maps at different periods are listed in Table 4.1. Histograms corresponding to travel time errors at each step for initial and final group wave velocity maps were also computed. Figure 4.7 illustrates the histograms for travel time errors at 20 sec period. The histograms show that the misfit for the data meets the criteria which eliminate travel time errors grater than 20 sec.

Table 4.1. Number of observations used for the tomographic images, values of the initial and final group wave travel-time residuals and standard deviations for different periods.

Period (sec)	Number of Observations	Initial error (Sec)	Standart Dev (Sec)	Final error (Sec)	Standart Dev (Sec)
10	2402	20.1	28.9	10.5	10.1
15	2447	12.1	20.1	5.7	8.0
20	2505	8.9	15.2	4.1	5.9
30	2463	7.3	10.2	3.4	4.6
40	1739	6.5	8.6	3.4	4.3
50	1670	4.8	6.0	3.2	4.0

Sensitivity kernels of Love waves were also computed in order to determine how the structure in a certain depth interval influences the group velocities. These functions are the partial derivatives of group wave velocity with respect to perturbation of shear wave velocity in the reference model through which they are computed. Figure 4.8 shows both the sensitivity kernels for two reference earth models at different periods. Slowly varying sensitivities of Love waves limits the depth resolution and mask deeper structures. The shallow structures dominate at lower periods and have significant influence at higher periods. Vdovin *et al*., (1999) indicated that the group wave velocity maps will have positive correlation with shear wave anomalies or boundary topography in the neighborhood of the positive maximum of the sensitivity kernel.

At 10 and 15 sec Love waves mainly sample the upper crust of 10 km thickness. Waves with 20 sec period are more sensitive up to a depth of 20 km and therefore contain information on both upper and lower of the crust. Intermediate periods (20-40 sec) sample the crust more uniformly and influenced by the upper mantle velocity for a crustal thickness of 28 km. At greater periods (>40 sec) the influence of upper mantle is apparent for crustal thickness less than 35 km when there is no significant masking from thick sedimentary basins.

Group wave velocities at 10 and 15 sec are sensitive to upper crust and influenced by local sedimentary basins and topographic features (Figure 4.9). Several inland and offshore basins exist in Turkey (*e.g.,* Thrace Basin, Clicia-Adana Basin, Tuz Gölü Basin, Sinop-Boyabat Basin, Marmara Sea, Black Sea, Aegean Sea and Mediterranean Sea Basins). Low group wave velocities are observed in the Marmara Sea, Thrace Basin, Saros Bay, Sinop Basin, Black Sea and Mediterranean Sea indicating the presence of thick sedimentary deposits. Low group wave velocities observed in the Eastern Anatolia take place at a region with widespread volcanic activity.

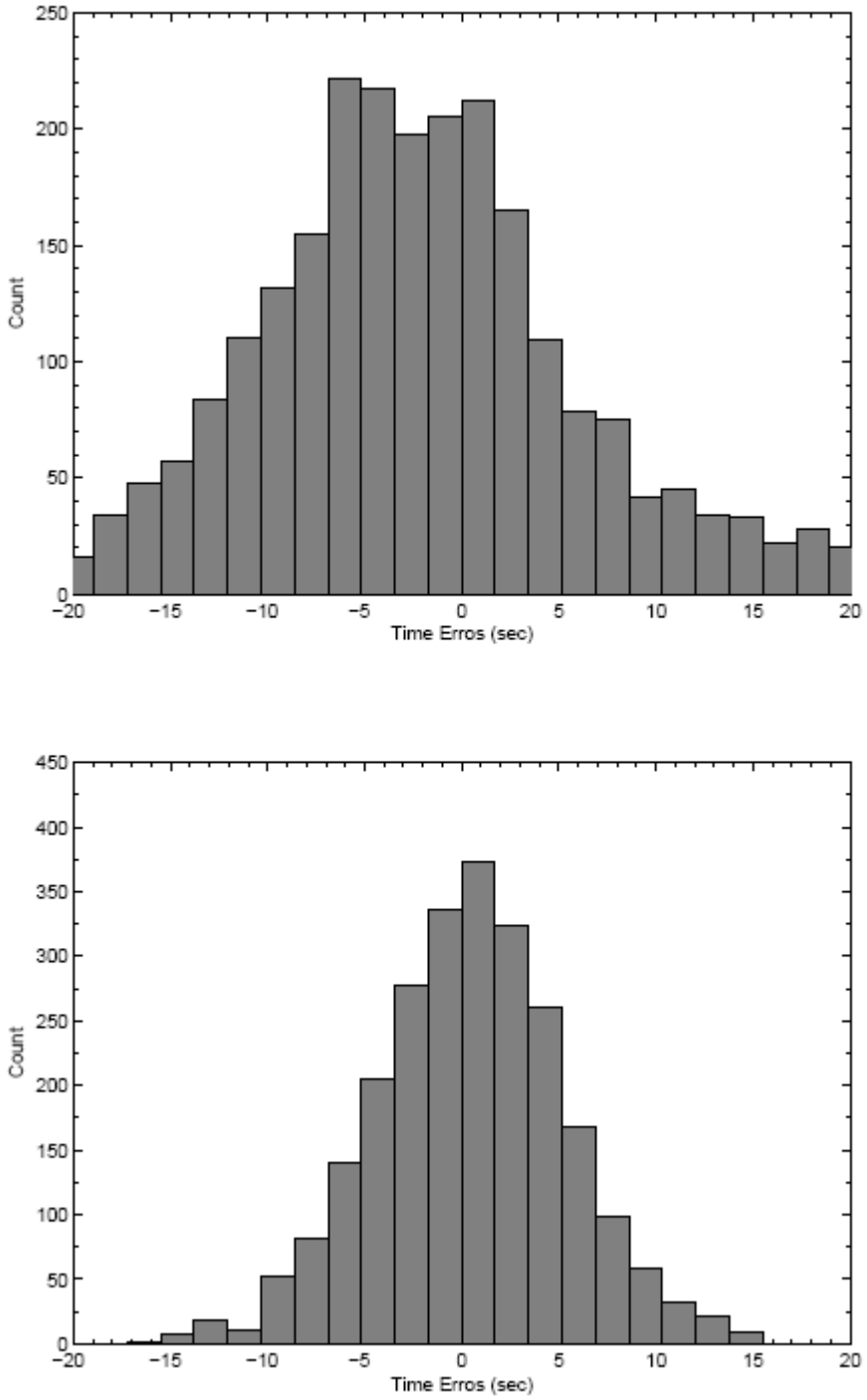

Figure 4.7. Histograms of travel time misfits for initial model (top) and final model (bottom) at 20 sec period.

As indicated by the sensitivity kernels the group wave velocities at 20-30 sec periods are influenced by a thickness of 20-25 km (Figure 4.10). As a result, anomalies associated with geological structures at crustal scale were observed. Group wave velocities are higher along the Pontides, İstanbul zone, Strandja massif on the north of the İzmit-Ankara and Ankara-Erzincan suture zone. High group wave velocities are observed in central Anatolia, Hellenic arc, Menderes massif. The collision belt in Bitlis suture is characterized by high group wave velocities. A large velocity contrast exists between the high velocities in the Bitlis massif and the low velocities in the EAAC. Lower velocities are observed in Antalya Bay, west of Cyprus, with a continuation towards the Isparta angle. A wedge shaped anomaly in the Isparta angle has been a prominent feature on the group wave velocity maps beginning from 10 sec period. The low group wave velocities observed in Black Sea can be associated with two deep basins. Low velocity anomaly observed in the western Black Sea basin extends to Moesian Basin. However, both the geometry and magnitude of these anomalies may have significant uncertainties due to poor ray coverage.

Group wave velocities at 40 and 50 sec are influenced by the lower crust and upper mantle structure (Figure 4.11). In this period range the wavelength of the anomalies on the maps are larger with smaller velocity perturbations. The central Anatolia and Taurides have uniform distribution of group wave velocities. High group wave velocities are observed in the Aegean region, Rodophe-Strandja massif, eastern Pontides and Bitlis suture zone while the low group wave velocities appears in the Eastern Anatolia and Antalya Basin- Isparta Angle.

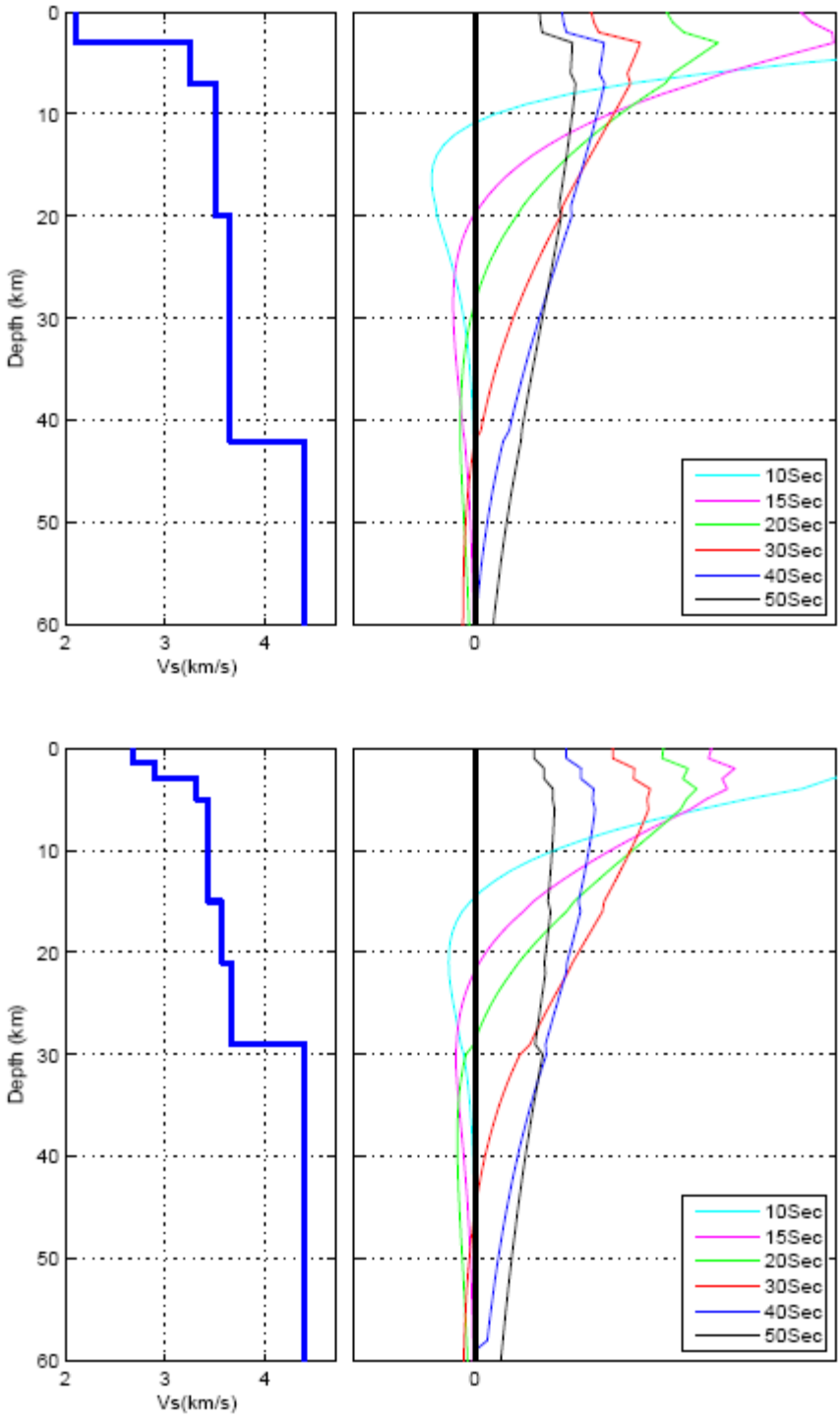

Figure 4.8. Shear wave sensitivity kernels of Love waves at periods ranging from 10 to 50 sec for a shear velocity-depth function using two reference earth models.

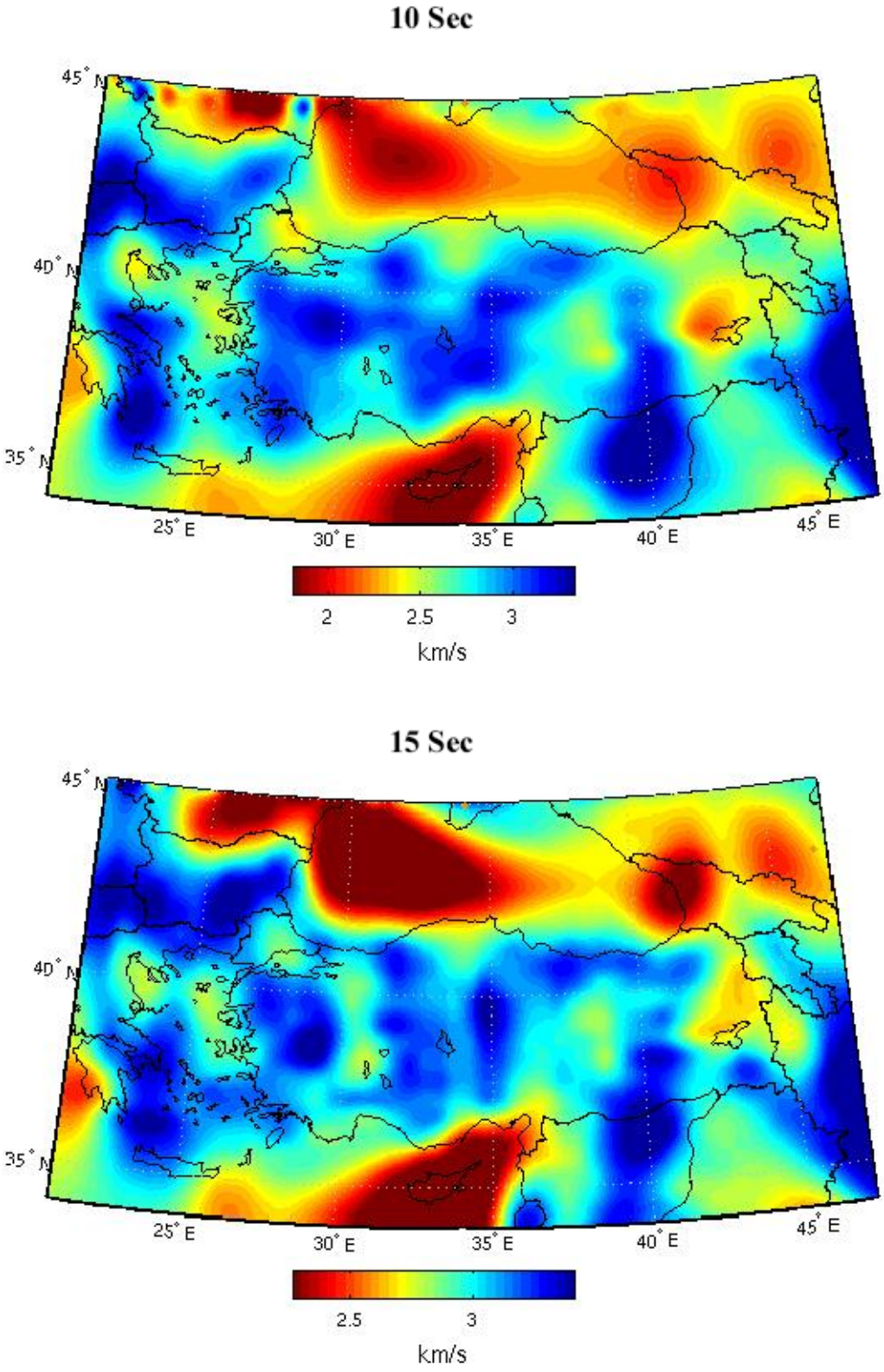

Figure 4.9. Estimated group velocity maps of Love waves at 10, 15 sec periods.

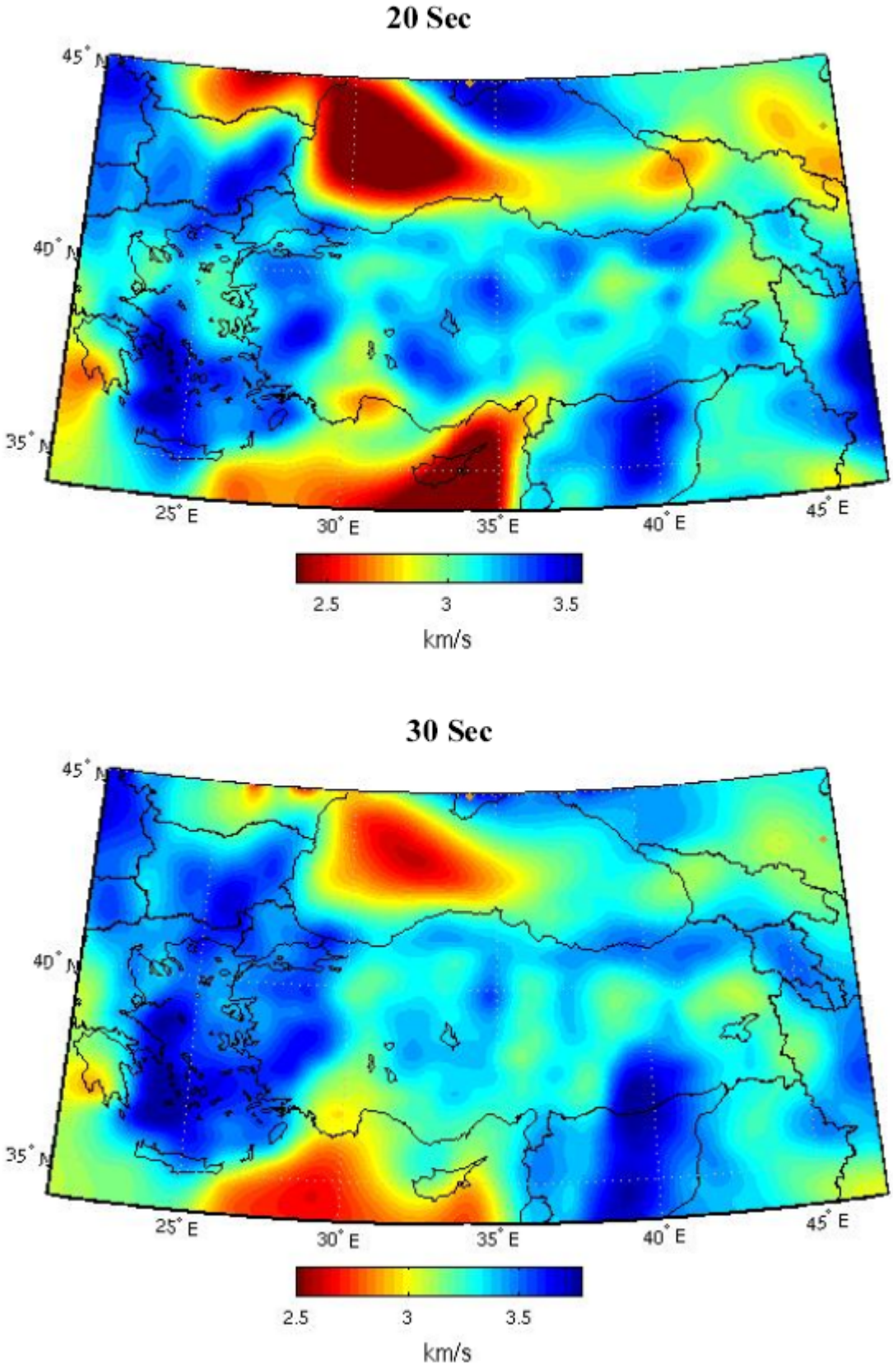

Figure 4.10. Estimated group velocity maps of Love waves at 20, 30 sec periods.

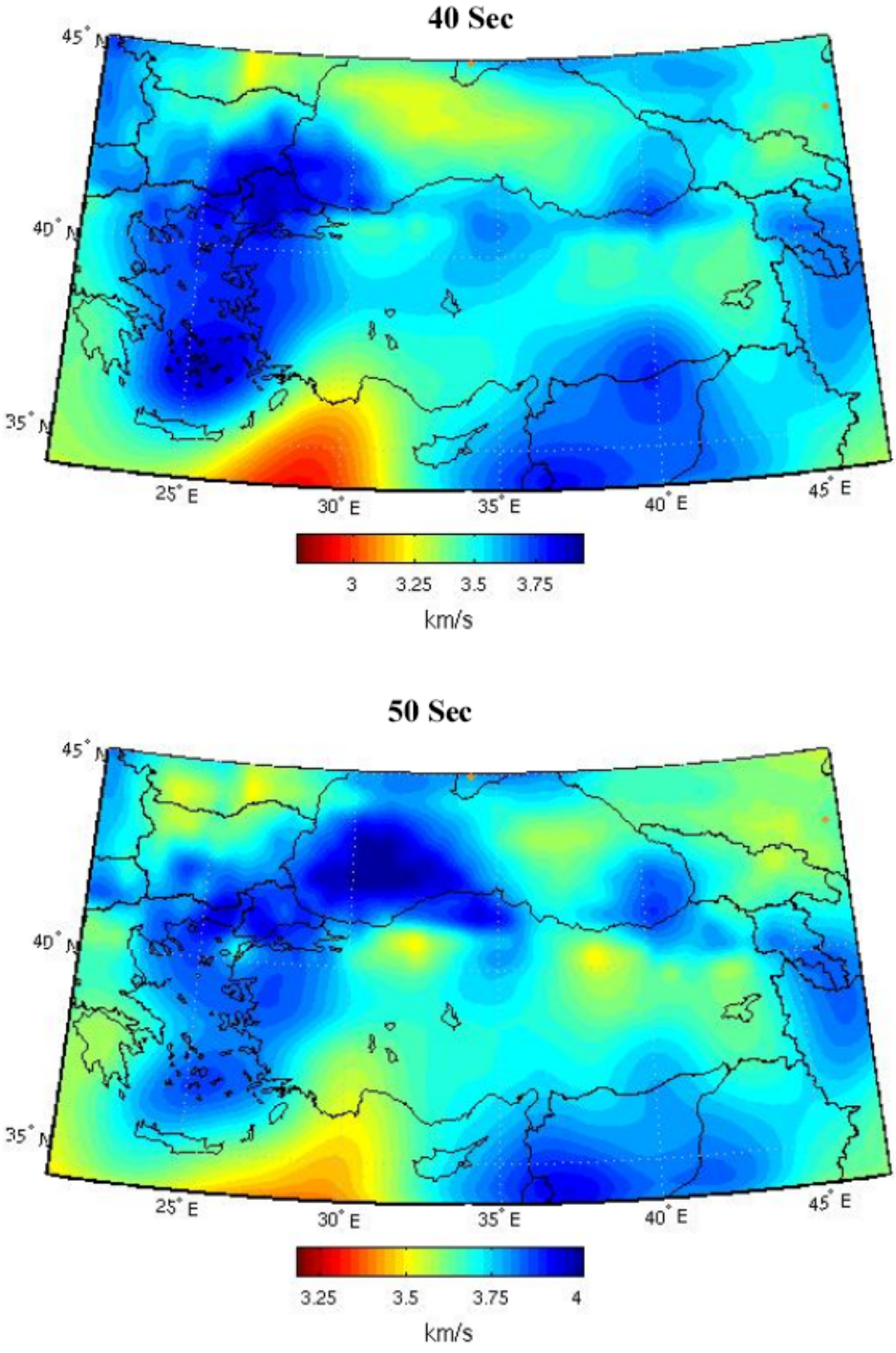

Figure 4.11. Estimated group velocity maps for Love waves at 40, 50 sec periods.

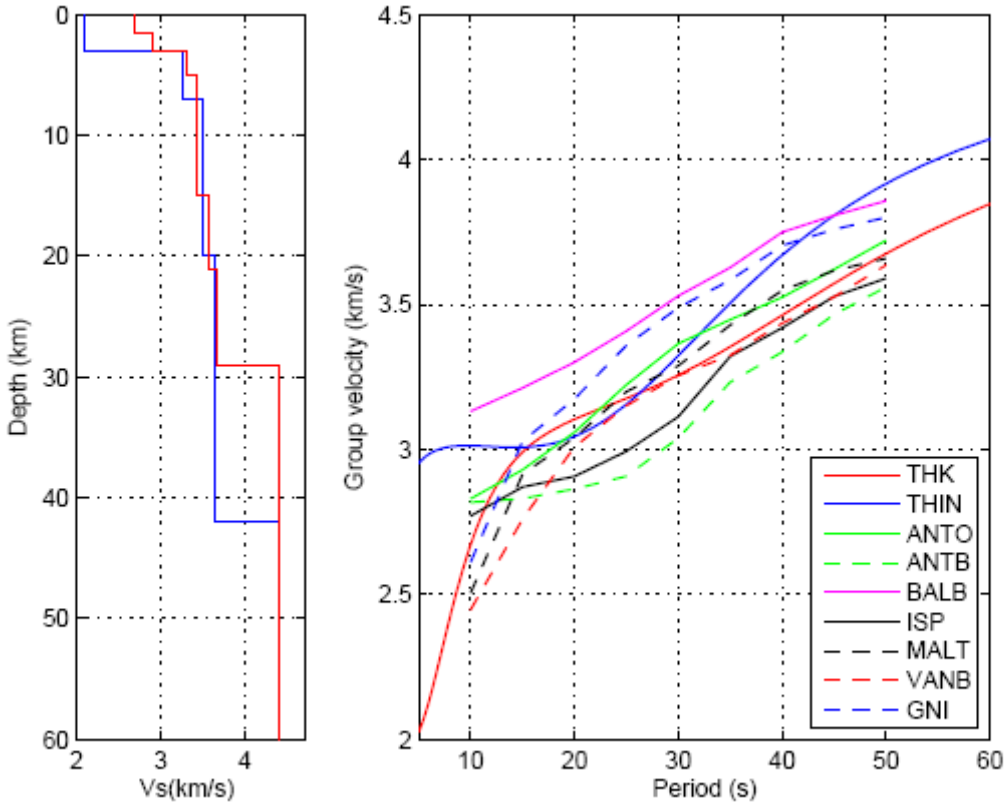

Figure 4.12. Local dispersion curves derived from the tomographic maps at five seismic stations shown in Figure 1.2.

Using the group wave velocity maps of Love waves at different periods obtained from tomography, local group wave velocity curves were constructed (Figure 4.12). Local group wave velocities are computed for the stations shown in Figure 1.2. Figure 4.12 shows that there is a good continuity of tomographic images of increasing periods. The lowest group wave velocity curve is obtained for the station located in Antalya Bay (ANTB) while the highest group wave velocity curve is obtained for the Western Anatolia (BALB).

25 sec

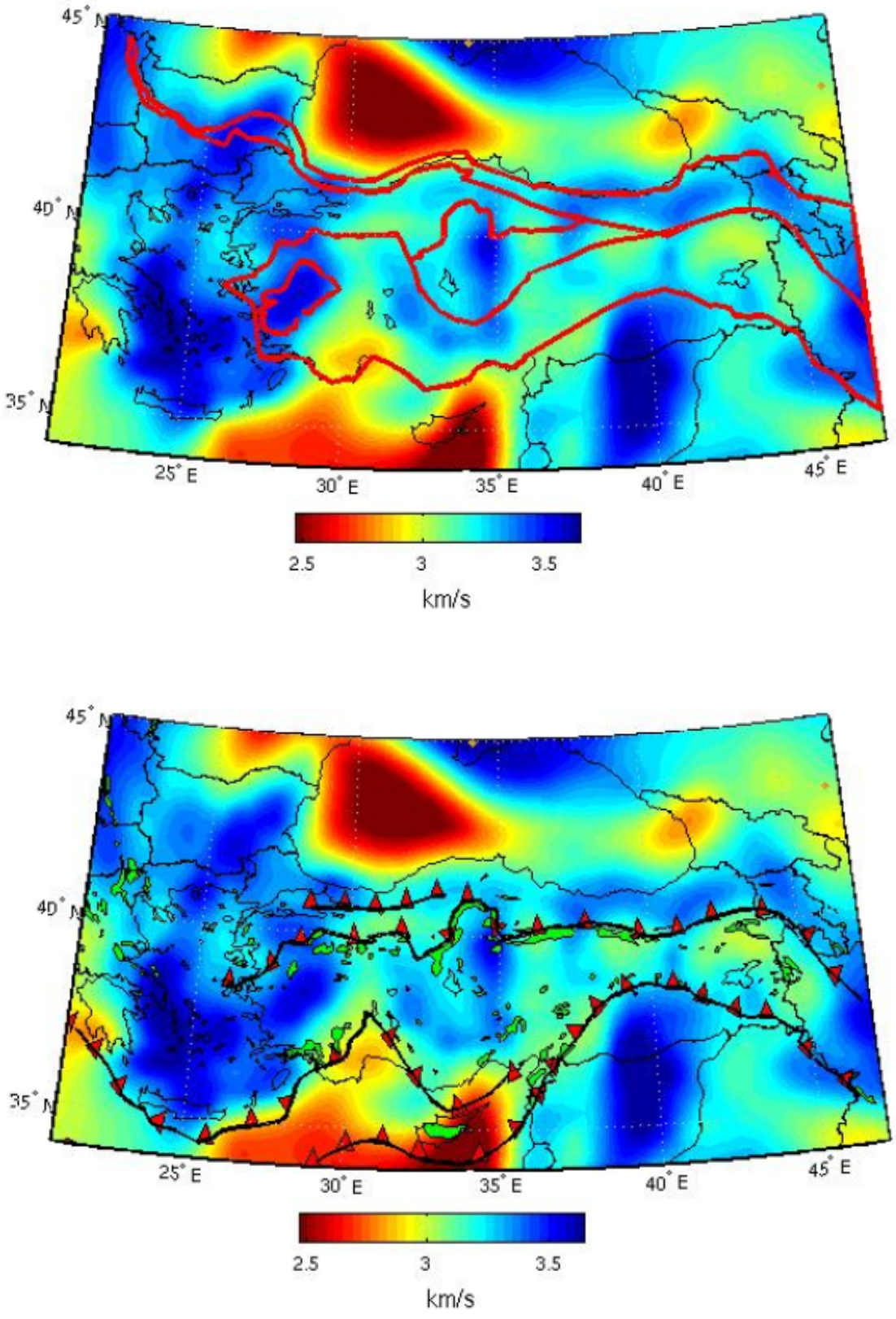

Figure 4.13. Estimated group velocity maps of Love waves at 25 sec period with major tectonic units (top), with major suture zones and ophiolites (bottom).

25 sec

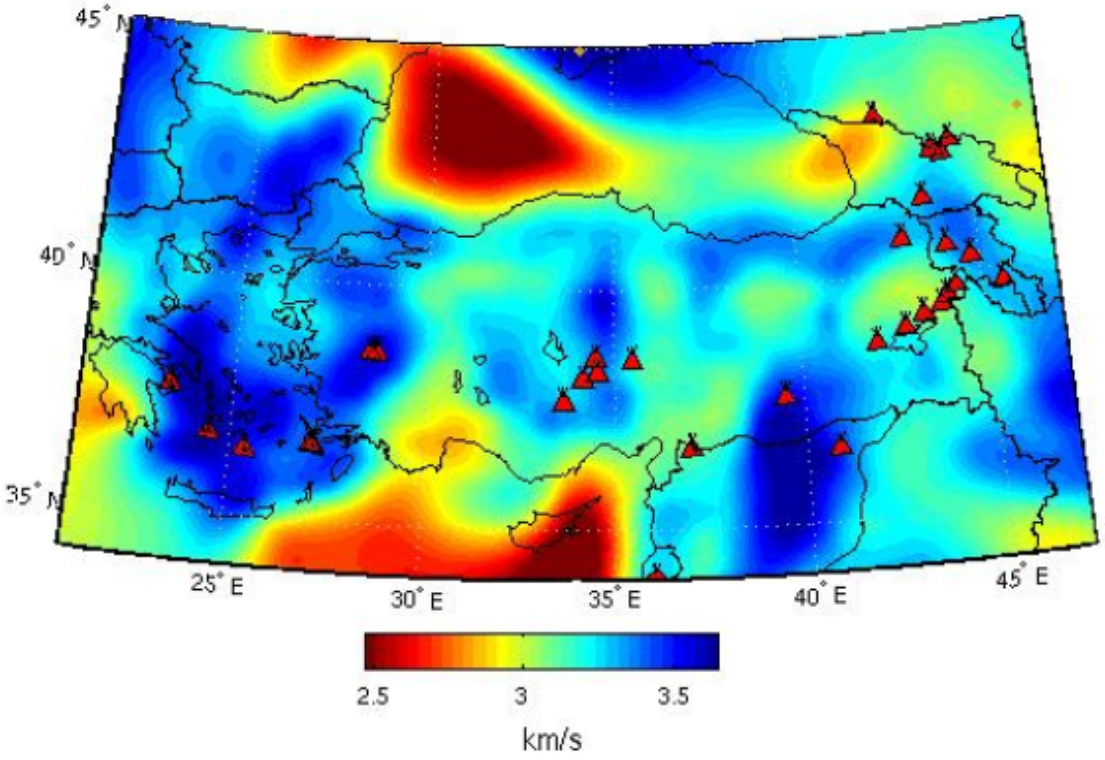

Figure 4.14. Estimated group velocity maps of Love waves at 25 sec period with volcanoes.

4.5. Discussions

In this part of the thesis Love wave group velocities in Turkey and the surrounding regions are measured from the local and regional earthquakes recorded at a large number of stations. Group velocity maps for Love waves are obtained between 10-50 sec periods using a tomographic inversion method. The maps indicate the presence of significantly different crustal compositions and structures resulting from different tectonic evolutions. Group wave velocity maps exhibit strong velocity perturbations and correlates well with the known tectonic structures. In general, the tomographic images at short periods (10-15 sec) displaying low velocities associate with the sedimentary basins, intermediate periods (20-30 sec) with regional geologic structures and greater periods (40-50 sec) total crustal structure and upper mantle.

Several inland and offshore sedimentary basins manifest themselves on the maps by low group wave velocities at 10-15 sec periods (Figure 4.9). The recent seismic reflection studies show that three sedimentary basins in the Marmara Sea exceeding six kilometers of thickness (Laigle *et al*., 2008). These basins are filled with low velocity sediments overlying high velocity basement of the Istanbul zone characterized by Paleozoic units. The low group wave velocities observed in the Marmara Sea is extending to Thrace Basin which is largest and thickest Tertiary sedimentary basin in Turkey with a sedimentary fill reaching to a depth of nine kilometers. The basin on the north was boarded by metamorphics and granites of the Strandja Massif which is characterized by high group wave velocities on the maps.

The Rodop – Strandja Massif on the north of the Aegean Sea appears with higher group wave velocities at all periods (Figure 4.9- Figure 4.11). This indicates high crustal velocities which are related to metamorphics and plutonic rocks. The high velocities along the Rodop- Strandja Massif have the continuity on the north of the Marmara region. The results of receiver function analysis indicate a crustal thickness of ~30 km on the north increasing to ~34 km on the south of the Marmara Sea (Zor *et al*., 2006).

Lower group wave velocities are also observed in Saros Bay, on the west of the Marmara Sea and elongating towards the North Aegean Through and Axion Basin (Figure 4.9). Karagianni *et al*., (2002) also observed low group wave velocities along these transtensional basins which are controlled by the North Anatolian Fault of strike slip character and the Aegean tectonics of extensional nature. The thickness of the sediments in these basins is expected to reach up to six kilometers (Karagianni *et al*., 2002).

High group wave velocities on the north of Hellenic Arc in the Aegean Sea appear at 10 sec period and consistently increase with the increasing periods. On the other hand, the Aegean Sea along the Anatolian coast exhibits low velocities on 10-15 sec maps and increase at the larger periods. Significant velocity contrast exists between low group wave velocities in the Aegean Sea and high group wave velocities of the Western Turkey which are associated with the metamorphic core complex in the region (e.g., Menderes Massif). However the low velocities in the North Aegean Trough and Saros Bay are persistent even at 20 sec period. This may be an indication crustal thickening from the southern Crete

towards the northern Aegean Sea. Sensitivity kernels in Figure 4.8 (bottom) shows the group wave velocities at 20 sec period will begin to be influenced by a thickness of greater than 20 km. Moho depths for the Aegean plate computed by Sodoudi *et al*., (2006) indicate that the southern part of the Aegean has a crustal thickness of 20-22 km while the northern Aegean Sea shows a relatively thicker crust (25-28 km). Such differences in the crustal thicknesses has been interpreted that the extension strongly influenced the southern Aegean while presently undergoing high crustal deformation in the northern Aegean Sea (Sodoudi *et al*., 2006).

One of the prominent features of the group wave velocity maps is the observation of a wedge shape low velocity anomaly in the Antalya Bay elongating towards the Isparta angle (IA). Low velocities start appearing at 10 sec map and continue to be present at greater periods with increasing wavelengths. The low velocity anomaly of IA is delimited by the high velocity Menderes massif in the west and Sultandağ-Beyşehir Massif in the east. In the center of the IA, a regional allochthonous unit, Antalya complex, represents a critical part of the evidence of a southerly Neotethyan Oceanic Basin (Robertson *et al*., 2000). Several carbonate platforms, sedimentary basins and ophiolits exist in the complex. The deep structure of Antalya Bay and the offshore extension of the Isparta angle are poorly known. Earthquake locations suggest the existence of a detached oceanic slab beneath Antalya Bay even though the timing and the geometry of the slab remains unclear (Engdahl *et al.,* 1998; Robertson, 2000). The crustal thickness obtained from receiver function analysis at ISP station which is located within Isparta angle is found as 42 km significantly thicker than ANTO station (36 km) (Zhu *et al*., 2006). This indicates significant crustal thickening as a result of subduction-related compression. Low group wave velocities observed in the IA at low periods (10-20 sec) are related to the regional allochthonous units while at greater periods (40-50 sec) as an indication of thicker crust.

Low group wave velocities at 10-15 sec appear in the Clicia-Adana Basin located between Turkey and the Northern Cyprus. The seismic reflection data shows that this basin contains up to three kilometer thick sediments (Aksu *et al*., 2005). The lower sections of the Cilicia – Adana Basin are not imaged by the seismic reflection data but expected to contain a thicker sedimentary sequence. The low group wave velocities observed on the 10-20 sec maps also supports the presence of a thicker sedimentary basin.

A prominent low velocity anomaly on the 10-30 sec group wave velocity maps appears in the Eastern Anatolia region surrounded by higher velocities of the eastern Pontides and the collision zone of Anatolian – Arabian plates. Keskin (2003) and Şengör (2003) indicated that the Eastern Anatolia region can be characterized by three tectonic units; the Pontides on the north, in the center the Eastern Anatolia Accretionary Complex (EAAC) and collision related volcanics and finally on the south Bitlis-Pötürge Massif.

The eastern Pontides characterized by higher group wave velocities are considered as a magmatic arc developed of Albian to Oligocene age. Its basement is represented by a metamorphic massive named the Pulur Complex (Topuz *et al*., 2004). The magmatic arc formed by a north-dipping subduction under the Eurasian continental margin (Yılmaz *et al*., 1997; Şengör, 2003). Along the suture zone separating the Pontids from Anatolian-Iranian platform ophiolites, mélanges and fore arc deposits are exposed. There is a gradual crustal thickening along the Pontids starting at 32 km in the western Pontids and reaching to 44 km in the eastern Pontids (Bassin *et al*., 2000). Crustal thickening and initiation of volcanic activity started as a result of subduction related compression and consumption.

The volcanism started earlier in the north and migrated to the south as a result of the slab steepening under Eastern Anatolia region. The EAAC is produced by the consumption of the Neo-Tethyan Ocean and a widespread volcanic activity from upper Miocene to Quaternary was observed in the region with the complete elimination of the Neo-Tethyan Ocean floor as a result of collision between Arabia and Eurasia during Early Miocene (Yılmaz *et al*., 1987). Several tectonic models have been proposed to explain the subduction and post-collisional evolution of the region. Based on the crustal thickness (Zor *et al*., 2003), low Pn velocities (Al-Lazki *et al*., 2003) and high Sn attenuation (Gök *et al*., 2003), Keskin (2003) and Şengör (2003) proposed the absence of the subducting Arabian Plate beneath the Anatolian Plateau. They proposed that the lithospheric mantle is either thinned or totally removed in the region. Keskin (2003) also proposed that the interaction of hot asthenosphere with the EAAC that contains retained water decreases the melting temperatures at a giving depth, generating extensive melting in the crust. Such interaction can account for the variability of lava chemistry and magma-crust interaction as well as low velocity zones in the crust at shallow depths. The low group wave velocities are also observed on the tomographic images presented by Gök *et al.,* (2007). There is a good

correlation between the 30-40 sec maps of this study and the depth slices of 31-37 km of Gök *et al.,* (2007). Gök *et al*., (2007) computed the crustal thickness as 44 km in Anatolian Block, 48 km in the Anatolian Plateau and 36 km in the Arabian Plate.

The Kırşehir Massif is located in the central Anatolia do not appear as a uniform velocity block on 10-20 sec group wave velocity maps. Higher group wave velocities are observed in the core of the massif and relatively lower velocities in the area of the Tuz Gölü Basin. However at greater periods (40-50 sec) the group wave velocities have a more uniform distribution. This may indicate that the heterogeneities are confined to the upper crust in the massif. The Kırsehir Massif is regarded either as the methamorphized northern margin of the Anatolide-Tauride terrane or a distinct terrane separated from Anatolide-Taurides by the Inner Tauride suture. The massi contains oceanic remnants derived from the Neotethys Ocean which separate them from the Sakarya continent. It is considered to represent variably tectonized and subducted oceanic lithosphere and continental carbonate platform that were subsequently ejected from an accretionary-subduction complex on the collision with the Sakarya micro-continent (Floyd *et al*., 2000). The present seismicity of Turkey indicates that internal deformation of the central Anatolia appears to be less than eastern and western Anatolia. Therefore it is not surprising to expect a more rigid and homogeneous lower crust in the region.

Two distinct group wave velocity anomalies appear in the Black Sea starting at 10 sec period. Although additional ray coverage is necessary to increase the reliability of the maps the features with larger wavelengths (>2 degree) can still be associated with the known geologic features. The Black Sea is composed of two deep basins. The western Black Sea basin has a maximum thickness of 20 km (Spadini *et al.,* 1996). We do not clearly observe the effect of crustal thinning on the group wave velocity maps. The low velocity basins mask the deeper structures which can be observed from the slowly varying sensitivities of Love waves.

Figure 4.13 and Figure 4.14 shows the tomographic image at 25 sec with major tectonic units, suture zones along with the ophiolits and volcanism. The suture zones with ophiolits indicate the boundaries along which the closure and the destruction of Neotethyan Ocean took place. This appears on the group wave velocity maps with significant velocity

contrasts. The İzmir-Ankara and Ankara-Eskişehir suture zone separate the Pontids from the Sakarya continent in the west and Anatolia-Arabian plate in the east. Intra Pontid suture zone separates the Sakarya continent from the western Pontides and characterized by a velocity contrast.

Although one of the objectives of this study was to make comparative analysis between correlation based and earthquakes source tomography we only had limited success. Unfortunately the number of paths for Rayleigh waves obtained from earthquake sources was insufficient while the cross correlations provided sufficient paths for good resolution. On the other hand the cross correlation for Love waves did not provide sufficient path coverage while the path coverage from earthquakes was very good.

Figure 4.15 shows 20 sec group velocity maps for Love waves obtained from earthquake sources and correlations. The tomographic images were computed with 1^{o} grid interval. The major differences take place in the areas of low ray coverage. Additional data both on the earthquakes sources and cross correlation will be necessary for a better analysis. However joint inversion of both data sets will further improve the resolution and increase path coverage.

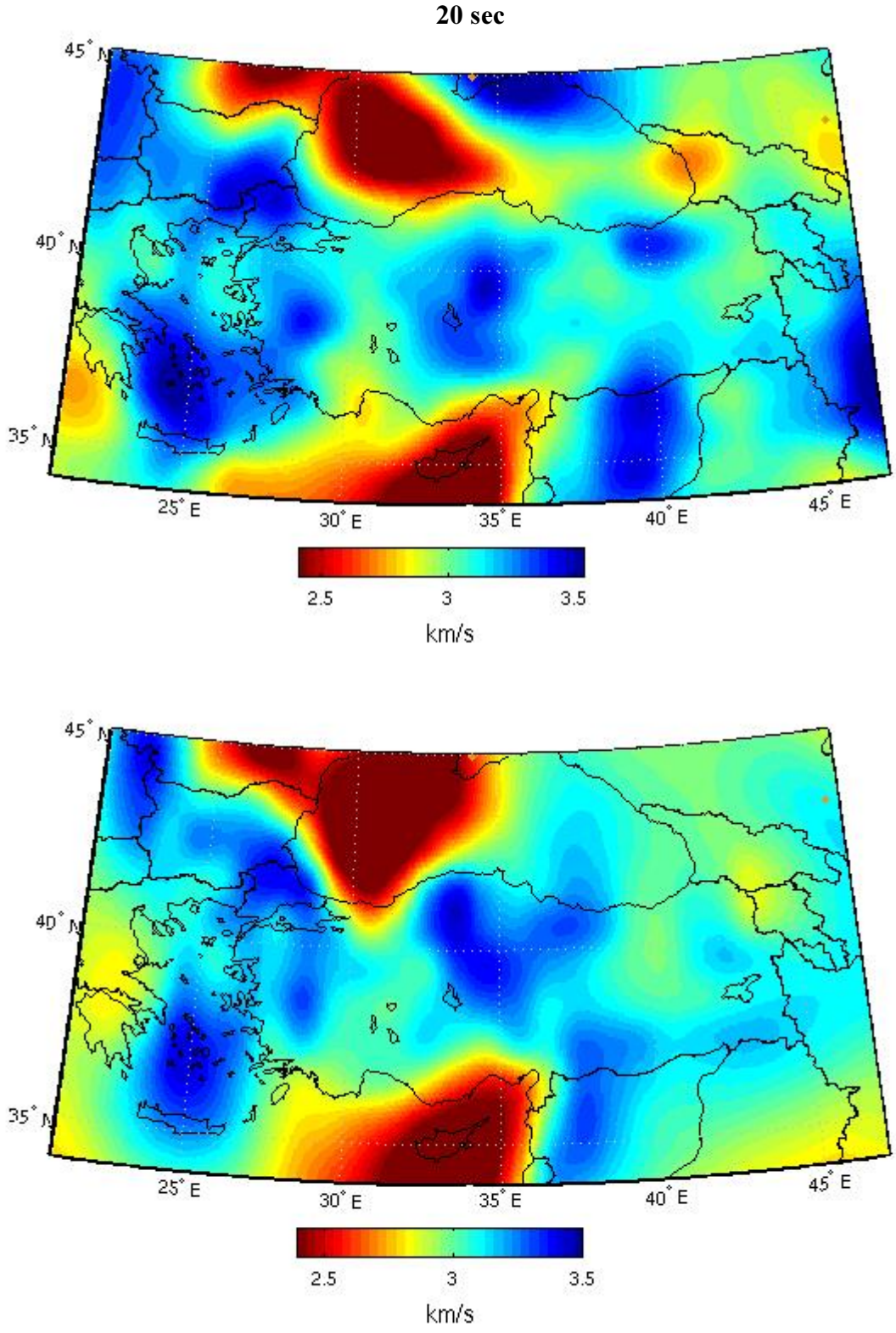

Figure 4.15. Estimated group velocity maps of Love waves from earthquakes (top) and correlations (bottom) at 20 sec period for one by one degree grid size.

5. CONCLUSIONS

In this study a comprehensive noise analysis is performed for the permanent and temporary broadband stations in Turkey and surrounding areas. Temporal and spatial variations of seismic noise for each component of each broadband station are computed. Crustal structure of Turkey and surroundings is investigated by the group wave velocity maps of the surface waves for the selected period ranges from ambient seismic noise correlations and earthquakes.

Seismic noise analysis is presented with a realistic model based on the power spectral density methods. The seismic noise analysis exhibits variations on noise levels for diurnal, seasonal, geographic and installation types. Diurnal variations of seismic noise mainly occur at higher frequencies (> 1.0 Hz). Seismic noise levels are generally higher at day time hours than night time hours due to the increase of cultural noise. Seasonal variations occur as a result of microseisms at single frequency peak (~14 sec) and double frequency peak (~7.0 sec). These microseisms at single frequency peak and double frequency peak originate by the conversion of ocean wave energy into seismic energy and by the superposition of ocean waves, respectively. Seasonal noise levels vary especially at these period ranges and have higher values during winter than the noise levels of other seasons (spring, fall and summer). Spatial variation of seismic noise is computed at the selected period ranges (1.0 sec, 4.0 sec and 15 sec). At 1.0 sec period range seismic noise is mainly higher along the coastal stations than continental stations. Seismic noise level at this period range is mainly sensitive to the cultural noise. But at longer periods (4.0 sec and 15 sec) significant perturbations are not observed. Seismic noise variations according to the installation types are also investigated. Spectral densities of seismic noise for broadband seismic stations with different installation types and seismometers are compared. Seismic stations with 30 sec, 120 sec and 360 sec bandwidths are compared and the results exhibit significant variations at higher periods. Installation properties of stations play an essential role in the quality of the records. Broadband stations installed at deep boreholes have lower noise levels at all period ranges.

Application of the seismic noise correlation technique for extracting the Green's function is performed. Data recorded during 2006 - 2009 by using 156 broadband stations in the region has been collected and 24 hour long data segments are formed for each station. Raw seismic data have been re-sampled to one sample per second. Cross-correlations are computed for each station pair. Approximately 12000 paths computed for both Rayleigh and Love waves but after the revision and selection, approximately one forth of the paths for Rayleigh waves and lesser amount for Love waves provided reliable data. Since the number of paths for Love waves was much lower than those of Rayleigh waves only 20 sec period was selected to present group wave velocity maps of Love waves. Group velocity maps of Rayleigh waves were computed for three different periods (15, 20 and 25 sec).

In the last part of this work, group velocities of Love waves in Turkey and the surrounding regions are computed from the local and regional earthquakes. Available data are used from broadband stations operated between years 1997 and 2009 in Turkey and surrounding regions. 285 earthquakes with magnitudes greater than 4.5 are selected for the analysis. Fundamental mode group velocities of Love and Rayleigh waves at 271 stations along 12500 paths are computed. By using the tomographic inversion method, group velocity maps of Love waves at 10, 15, 20, 30, 40 and 50 sec are computed.

The group wave velocity maps indicate the presence of significantly different crustal compositions and structures resulting from different tectonic evolutions. Obtained maps exhibit strong velocity perturbations and correlates well with the known tectonic structures. In general, the tomographic images at short periods (10-15 sec) displaying low velocities associate with the sedimentary basins, intermediate periods (20-30 sec) with regional geologic structures and greater periods (40-50) total crustal structure and upper mantle. Low group wave velocities are observed in the Marmara Sea, Thrace Basin, Saros Bay, Sinop Basin, Black Sea and Mediterranean Sea indicating the presence of thick sedimentary deposits. Low group wave velocities observed in the Eastern Anatolia take place at a region with widespread volcanic activity. One of the prominent features of the group wave velocity maps is the observation of a wedge shape low velocity anomaly in the Antalya Bay elongating towards the Isparta angle. Low velocities start appearing at 10 sec map and continue to be present at greater periods with increasing wavelengths.

Tomographic image at 25 sec shows major tectonic units, suture zones along with the ophiolits and volcanism. The suture zones with ophiolits indicate the boundaries along which the closure and the destruction of Neotethyan Ocean took place. This appears on the group wave velocity maps with significant velocity contrasts. The İzmir-Ankara and Ankara-Eskişehir suture zone separate the Pontids from the Sakarya continent in the west and Anatolia-Arabian plate in the east. Intra Pontid suture zone separates the Sakarya continent from the western Pontides and characterized by a velocity contrast. The suture zone along the Anatolian-Arabian plates is well characterized by a high velocity anomaly. A good correlation between the suture zone and the wedge shaped anomaly in the Antalya basin-Isparta angle. Along the Hellenic arc in the south Aegean high velocities appears on the back arc with significant crustal thinning.

The vital point in introducing the ambient seismic noise correlation technique was its applicability in places where earthquakes do not occur. In regions where the station coverage is sufficient and earthquake occurrence is limited ambient seismic noise correlation can be used fruitfully. However, in places such as Turkey, which can be accepted as a natural laboratory due to the occurrence of earthquakes group wave velocity maps can be obtained with good resolutions. However as indicated in this study the earthquakes at regional distances may not provide sufficient ray path coverage for Rayleigh wave tomography. On the contrary correlation based tomography may provide sufficient data and higher resolution images. Two different approaches complement each other to obtain higher resolution images. At shorter distances correlations provide accurate measurements of group velocities along the paths while at greater distances poor S/N degrades the estimation of Green's functions. The estimation of the Green's functions will improve as more data becomes available.

Future work will concentrate on the joint inversion of both types of data and provide better estimation of group velocity maps. The group velocity maps will also be used to determine the velocity structure with the joint inversion of receiver functions and Pn velocities.

APPENDIX A: LIST OF BROADBAND STATIONS

Table A.1. List of broadband stations.

	STATION	LATITUDE (N$^{\circ}$)	LOGITUDE (E$^{\circ}$)	INSTRUMENT TYPE	NETWORK
1	AAK	42.639	74.494	STS1	IRIS
2	ADVT	40.4332	29.7383	CMG-3ESP	KOERI
3	AFSR	39.4468	33.0707	CMG-3ESP	KOERI
4	AGG	39.0211	22.336	CMG-3ESP	HT
5	AGIN	38.9391	38.7130	STS1	ETSE
6	AGRB	39.5755	42.992	CMG-3T	KOERI
7	AHLT	38.7481	42.4770	STS1	ETSE
8	AKH	38.9149	27.8081	STS2	WASRE
9	ALN	40.8957	26.0497	CMG-3ESP	HT
10	ALT	39.0552	30.1103	CMG-3T	KOERI
11	ALTB	41.0880	28.7400	CMG-3T	TUBITAK
12	ANTB	36.8998	30.6538	CMG-6T	KOERI
13	ANTO	39.8689	32.7936	KS3-6000	IRIS
14	AOS	39.1654	23.8639	CMG-3ESP	HT
15	APE	37.0689	25.5306	STS2	GEOFON
16	APEZ	34.977	24.886	STS2	GEOFON
17	AQU	42.3539	13.4019	STS2	MEDNET
18	ARG	36.220	28.130	LE-3D/20	HL
19	ARMT	40.5683	28.866	CMG-3ESP	KOERI
20	ARU	56.430	58.563	STS1	IRIS
21	ATH	37.97	23.72	LE-3D/20	NOA
22	AYD	37.8407	27.8374	STS2	WASRE
23	BALB	39.64	27.88	CMG-3T	KOERI
24	BAYT	40.3935	40.141	CMG-3ESPCD	KOERI
25	BCA	41.445	41.6223	CMG-3ESP	KOERI
26	BCK	37.461	30.5877	CMG-3T	KOERI
27	BFO	48.3311	8.3303	STS1	IRIS
28	BGKT	41.181	28.773	CMG-3ESP	KOERI
29	BLCB	38.3853	27.042	CMG-3T	KOERI
30	BNGB	38.9913	40.6792	CMG-3ESPCD	KOERI
31	BNGL	38.9195	40.5966	STS1	ETSE
32	BNI	45.0522	6.6786	STS2	MEDNET
33	BNN	38.8522	35.8472	CMG-3T	KOERI
34	BODT	37.0622	27.3103	CMG-3ESP	KOERI
35	BOZ	38.3002	28.0495	STS2	WASRE
36	BOZX	40.534	28.782	CMG-40T	TUBITAK
37	BTLS	41.96	34.0035	CMG-3T	KOERI

	STATION	LATITUDE (N°)	LOGITUDE (E°)	INSTRUMENT TYPE	NETWORK
38	BUC1	44.3479	26.0281	KS2000	RO
39	BUYB	40.8523	29.1175	CMG-3T	TUBITAK
40	BYBT	40.2353	40.2655	STS1	ETSE
41	BYKN	38.1665	41.7823	STS1	ETSE
42	BZK	41.9600	34.0035	CMG-3T	KOERI
43	BZS	45.6167	21.6167	STS2	RO
44	CANB	40.0168	27.0624	CMG-3T	TUBITAK
45	CANT	40.6062	33.6197	CMG-3T	KOERI
46	CART	37.587	-1.001	STS2	GEOFON
47	CAVI	40.2018	29.8378	CMG-3ESP	KOERI
48	CEL	38.2603	15.8939	STS2	MEDNET
49	CEYT	37.0107	35.7478	CMG-3ESP	KOERI
50	CHOS	38.3868	26.0550	CMG-3ESP	HT
51	CII	41.723	14.305	STS2	MEDNET
52	CLDR	39.1432	43.917	CMG-3ESP	KOERI
53	CLTB	37.5786	13.2156	STS2	MEDNET
54	CMCY	39.9205	43.1968	STS1	ETSE
55	CMHB	40.0120	27.9700	CMG-3T	TUBITAK
56	CORM	40.1785	34.6302	CMG-3ESP	KOERI
57	CRLT	41.1372	27.7378	CMG-3ESP	KOERI
58	CSS	34.9622	33.3306	STS2	GEOFON
59	CTKS	41.2373	28.5072	CMG-3ESP	KOERI
60	CTYL	41.4759	28.2897	CMG-3T	KOERI
61	CUC	39.9938	15.8155	STS2	MEDNET
62	CUKT	37.2473	43.6077	CMG-3ESP	KOERI
63	DALT	36.7692	28.6372	CMG-3T	KOERI
64	DARE	38.5712	37.4832	CMG-6T	KOERI
65	DAT	36.7308	27.5768	CMG-3ESP	KOERI
66	DEU	38.3710	27.2078	STS2	WASRE
67	DGRL	41.0568	43.3268	STS1	ETSE
68	DGSU	39.1311	42.7297	STS1	ETSE
69	DIKM	41.6495	35.2578	CMG-3T	KOERI
70	DIVS	44.0981	19.9917	STS1	MEDNET
71	DRGR	46.7917	22.7111	KS2000	RO
72	DPC	50.3583	16.4111	STS2	CZ
73	DSB	53.245	-6.376	STS2	GEOFON
74	DYBR	37.8230	40.3186	STS1	ETSE
75	ECH	48.216	7.158	STS1	GEOSCOPE
76	EDC	40.3468	27.8633	CMG-3T	KOERI
77	EDRB	41.847	26.7437	CMG-3T	KOERI
78	EIL	29.6699	34.9512	STS2	GEOFON
79	ELL	36.7483	29.9085	CMG-3T	KOERI
80	ENEZ	40.7362	26.1532	CMG-3T	KOERI
81	EREN	35.5292	34.1742	CMG-3T	KOERI
82	ERGN	38.2587	39.7287	STS1	ETSE

	STATION	LATITUDE (N°)	LOGITUDE (E°)	INSTRUMENT TYPE	NETWORK
83	ERIK	40.6708	26.5132	CMG-3ESP	KOERI
84	ERZN	39.5867	39.722	CMG-3ESP	KOERI
85	ESK	55.317	-3.205	STS1	IRIS
86	ESPY	40.9167	38.7273	CMG-ESP	KOERI
87	EVR	38.92	21.81	LE-3D/20	NOA
88	EZN	39.8267	26.3258	CMG-3ESP	KOERI
89	EZRM	40.1035	41.3637	CMG-3T	ETSE
90	FETY	36.6353	29.0835	CMG-3ESP	KOERI
91	FNA	40.7817	21.3836	CMG-3ESP	HT
92	FODE	35.3800	24.9580	STS2	GEOFON
93	FURI	8.903	38.688	STS1	IRIS
94	GADA	40.1908	25.8987	CMG-3T	KOERI
95	GAZ	37.1722	37.2113	CMG-3T	KOERI
96	GBZX	40.7865	29.4502	CMG-40T	TUBITAK
97	GELI	40.398	26.4742	CMG-3ESP	KOERI
98	GEMT	40.435	29.189	CMG-3T	KOERI
99	GLHS	37.156	29.4983	CMG-6T	KOERI
100	GNI	40.1495	44.7414	STS1	IRIS
101	GONE	40.0466	27.686	CMG-3ESP	KOERI
102	GRG	40.9558	22.4029	CMG-3ESP	HT
103	GULT	40.4323	30.515	CMG-3ESP	KOERI
104	GVD	34.8390	24.0870	STS2	GEOFON
105	HAMR	39.6136	42.9927	STS1	ETSE
106	HDMB	36.964	32.486	CMG-40T	KOERI
107	HINS	39.3489	41.6972	STS1	ETSE
108	HLG	54.185	7.884	STS2	GEOFON
109	HORT	40.5978	23.0995	CMG-3ESP	HT
110	HRPT	38.7043	39.2453	STS1	ETSE
111	HRSN	39.9453	42.2874	STS1	ETSE
112	HRTX	40.8217	29.668	CMG-3ESP	KOERI
113	IAS	47.1933	27.5617	CMG-40T	RO
114	IBBN	52.307	7.757	STS2	GEOFON
115	IDI	35.288	24.890	STS2	MEDNET
116	IGT	39.5315	20.3299	CMG-3ESP	HT
117	IKL	36.2387	33.6852	CMG-3T	KOERI
118	ILIC	39.4531	38.5686	STS1	ETSE
119	IMRL	39.8787	38.1183	STS1	ETSE
120	ISK	41.0615	29.0592	CMG-3T	KOERI
121	ISP	37.8227	30.5222	STS1	KOERI
122	ITM	37.1800	21.9300	LE-3D/20	HL
123	JAN	39.66	20.85	LE-3D/20	NOA
124	JER	31.772	35.197	STS2	GEOFON
125	JMB	42.491	26.530	CMG-40T	BS
126	KARA	37.2607	35.0547	CMG-3ESP	KOERI
127	KARN	35.4019	23.9174	STS2	GEOFON

	STATION	LATITUDE (N°)	LOGITUDE (E°)	INSTRUMENT TYPE	NETWORK
128	KARP	35.55	27.16	LE-3D/20	NOA
129	KARS	40.6277	43.0788	CMG-3T	KOERI
130	KBS	78.9256	11.9417	STS1	GEOFON
131	KCTX	40.2655	28.3565	CMG-3ESP	KOERI
132	KDZE	41.3132	31.443	CMG-3T	KOERI
133	KEK	39.71	19.80	LE-3D/20	HL
134	KEV	69.755	27.007	STS1	IRIS
135	KHC	49.1309	13.5702	STS2	CZ
136	KIEV	50.6944	29.2083	STS1	IRIS
137	KIV	43.956	42.689	STS1	IRIS
138	KLCB	40.6330	29.3980	CMG-3T	TUBITAK
139	KLYT	41.253	29.042	CMG-3T	KOERI
140	KMBO	-1.274	36.804	STS1	GEOFON
141	KMRB	40.418	27.069	CMG-3T	TUBITAK
142	KMRS	37.5053	36.9	CMG-3T	KOERI
143	KONO	59.649	9.598	STS1	IRIS
144	KONT	37.9453	32.3605	CMG-3T	KOERI
145	KOTK	40.2227	43.0094	STS1	ETSE
146	KOZT	37.4805	35.8268	CMG-3T	KOERI
147	KRBG	40.3932	27.2977	CMG-3ESP	KOERI
148	KRIS	35.1780	25.5030	STS2	GEOFON
149	KRLV	39.3746	40.9881	STS1	ETSE
150	KRTS	36.5732	35.375	CMG-3ESP	KOERI
151	KSDI	33.192	35.659	STS2	GEOFON
152	KTLN	37.9533	41.7052	STS1	ETSE
153	KTUT	40.987	39.7667	CMG-3T	KOERI
154	KUL	38.5401	28.6339	STS2	WASRE
155	KULA	38.5145	28.6607	CMG-3T	KOERI
156	KURK	50.7153	78.6201	STS1	IRIS
157	KVT	41.0807	36.0463	CMG-3T	KOERI
158	KWP	49.631	22.708	STS2	GEOFON
159	KYPR	37.5589	41.1692	STS1	ETSE
160	KZN	40.31	21.77	LE-3D/20	NOA
161	LADK	38.1999	32.3648	CMG-3T	KOERI
162	LAP	40.3727	26.7602	CMG-3ESP	KOERI
163	LAST	35.1611	25.4786	STS2	GEOFON
164	LEF	35.1118	32.506	CMG-3T	KOERI
165	LFK	35.2832	33.5337	CMG-3ESP	KOERI
166	LIA	39.90	25.18	CMG-40T	NOA
167	LIT	40.1033	22.4892	CMG-3ESP	HT
168	LKD	38.7074	20.6505	CMG-3ESP	HT
169	LKR	38.65	23.00	CMG-40T	NOA
170	LOD	39.8893	32.764	CMG-3T	KOERI
171	MAHO	39.896	4.267	STS2	GEOFON
172	MALT	38.313	38.427	STS2	KOERI

	STATION	LATITUDE (N°)	LOGITUDE (E°)	INSTRUMENT TYPE	NETWORK
173	MATE	40.6491	16.7044	STS2	GEOFON
174	MDNY	40.369	28.884	CMG-3ESP	KOERI
175	MDUB	40.4711	31.1976	CMG-3T	KOERI
176	MELI	35.290	-2.938	STS2	GEOFON
177	MERS	36.8677	34.5222	CMG-3T	KOERI
178	MFTX	40.7867	27.2978	CMG-40T	KOERI
179	MHV	54.958	37.767	STS2	GEOFON
180	MLR	45.4912	25.9456	STS2	RO
181	MLSB	37.2953	27.7765	CMG-40T	KOERI
182	MORC	49.776	17.547	STS2	GEOFON
183	MRDN	37.2897	40.7000	STS1	ETSE
184	MRNI	33.1178	35.3920	STS2	GEOFON
185	MRMX	40.6058	27.5837	CMG-3T	KOERI
186	MSDY	40.4616	37.7765	STS1	ETSE
187	MTE	40.403	-7.537	STS2	GEOFON
188	MUSH	38.7571	41.4831	STS1	ETSE
189	NEO	39.31	23.22	LE-3D/20	NOA
190	NEVB	39.954	27.263	CMG-3T	TUBITAK
191	NPS	35.26	25.61	LE-3D/20	NOA
192	NVR	41.35	23.86	CMG-40T	NOA
193	OBN	55.114	36.569	STS1	IRIS
194	OUR	40.3325	23.9791	CMG-3ESP	HT
195	PAIG	39.9363	23.6768	CMG-3ESP	HT
196	PDG	42.4297	19.2608	STS2	MEDNET
197	PLD	42.147	24.749	CMG-40T	BS
198	PLG	40.37	23.45	LE-3D/20	NOA
199	PRK	39.23	26.27	LE-3D/20	NOA
200	PRU	49.9883	14.5417	STS2	CZ
201	PSZ	47.919	19.894	STS2	HU
202	PTK	38.8923	39.3923	CMG-3T	KOERI
203	PUL	59.767	30.316	STS2	GEOFON
204	PZAR	41.178	40.8988	CMG-ESP	KOERI
205	RAYN	23.5225	45.5032	STS2	IRIS
206	RDO	41.15	25.54	LE-3D/20	HL
207	RGN	54.546	13.364	STS2	GEOFON
208	RKY	40.6875	27.1777	CMG-3ESP	KOERI
209	RLS	38.06	21.47	LE-3D/20	NOA
210	RSDY	40.3972	37.3273	CMG-3T	KOERI
211	RTC	33.9881	-6.8569	STS1	MEDNET
212	RUE	52.480	13.780	STS2	GEOFON
213	SANT	36.371	25.459	STS2	GEOFON
214	SARI	38.4072	36.4182	CMG-3T	KOERI
215	SELV	37.238	-3.728	STS2	GEOFON
216	SFJ	66.997	-50.615	STS1	GEOFON
217	SFS	36.466	-6.206	STS2	GEOFON

	STATION	LATITUDE (N°)	LOGITUDE (E°)	INSTRUMENT TYPE	NETWORK
218	SFUC	36.637	-6.175	STS2	GEOFON
219	SHUT	38.553	30.551	CMG-3T	KOERI
220	SIGR	39.2114	25.8553	CMG-3ESP	HT
221	SILN	38.1352	41.0410	STS1	ETSE
222	SILT	41.153	29.643	CMG-3ESP	KOERI
223	SIRN	40.2016	39.1199	STS1	ETSE
224	SIRT	37.501	42.4392	CMG-3T	KOERI
225	SIVA	33.017	24.8100	STS2	GEOFON
226	SKD	35.412	23.928	STS2	GEOFON
227	SLVT	41.23	28.21	CMG-3ESP	KOERI
228	SMG	37.71	26.84	LE-3D/20	NOA
229	SOH	40.8206	23.3556	CMG-3ESP	HT
230	SPNC	40.686	30.3083	CMG-3ESP	KOERI
231	SRS	41.1087	23.5950	CMG-3ESP	HT
232	SSB	45.2790	4.5420	STS1	MEDNET
233	STU	48.770	9.193	STS2	GEOFON
234	SULT	38.1988	33.5157	CMG-3T	KOERI
235	SUMG	72.576	-38.454	STS2	GEOFON
236	SUTC	37.4765	30.9997	CMG-3ESP	KOERI
237	SUW	54.013	23.181	STS2	GEOFON
238	SVRC	38.3775	39.306	CMG-3T	KOERI
239	SVRH	39.44694	31.52301	CMG-3T	KOERI
240	SVSK	39.9175	36.9925	CMG-40T	KOERI
241	TAM	22.791	5.527	STS1	GEOSCOPE
242	THE	40.6319	22.9628	CMG-3ESP	HT
243	TIP	39.1794	16.7583	STS2	MEDNET
244	TIR	41.3472	19.8631	STS2	MEDNET
245	TIRR	44.4581	28.4128	STS2	RO
246	TKR	40.9947	27.5372	CMG-3ESP	KOERI
247	TRI	45.7089	13.7642	STS1	MEDNET
248	TRNX	40.5060	27.7771	CMG-40T	TUBITAK
249	TROY	40.1096	26.4185	CMG-3T	TUBITAK
250	TRTE	58.379	24.721	STS2	GEOFON
251	TUE	46.4722	9.3473	STS2	MEDNET
252	URFA	37.441	38.8213	CMG-3ESP	KOERI
253	UZML	39.7134	39.7156	STS1	ETSE
254	VAM	35.41	24.20	LE-3D/20	NOA
255	VANB	38.595	43.3888	CMG-3T	KOERI
256	VLC	44.1594	10.3864	STS2	MEDNET
257	VLI	36.72	22.95	LE-3D/20	NOA
258	VLS	38.18	20.59	LE-3D/20	NOA
259	VRI	45.8657	26.7277	CMG-3ESP	RO
260	VRTB	39.1603	41.456	CMG-3ESPCD	KOERI
261	VSL	39.4960	9.3780	STS1	MEDNET
262	VSU	58.4620	26.7347	STS2	GEOFON

	STATION	LATITUDE (N$^{\circ}$)	LOGITUDE (E$^{\circ}$)	INSTRUMENT TYPE	NETWORK
263	VTS	42.5916	23.2083	STS1	MEDNET
264	WDD	35.8373	14.5242	STS2	MEDNET
265	WLF	49.665	6.152	STS2	GEOFON
266	XOR	39.3660	23.1918	CMG-3ESP	HT
267	YER	37.1362	28.2858	CMG-3T	KOERI
268	YLVX	40.5667	29.3728	CMG-40T	KOERI
269	ZKR	35.1147	26.2170	STS2	GEOFON

APPENDIX B: LIST OF EARTHQUAKES

Table B.1. List of earthquakes.

	DATE (yr.mn.dy)	ORIGIN TIME (hr:mn:sc.ms)	LATITUDE (N°)	LONGITUDE (E°)	DEPTH (KM)	MAGNITUDE
1	1997.02.28	12:57:18.64	38.08	48.05	10	6.1
2	1998.06.27	13:55:52.08	36.88	35.31	33	6.6
3	1999.11.07	16:54:41.73	40.69	30.73	10	5.0
4	1999.11.11	14:41:25.61	40.74	30.27	22	5.7
5	1999.11.12	16:57:19.55	40.76	31.16	10	7.2
6	1999.11.16	17:51:18.10	40.72	31.61	10	5.1
7	1999.11.17	08:15:26.20	40.81	31.47	9	5.0
8	1999.11.19	19:59:07.96	40.81	30.97	6	5.0
9	1999.11.22	20:23:02.59	35.00	27.48	33	5.0
10	1999.12.03	17:06:54.70	40.36	42.35	19	5.7
11	2000.02.14	06:56:34.35	41.02	31.76	10	5.0
12	2000.02.26	08:18:37.69	37.30	44.76	33	5.2
13	2000.03.10	22:01:45.97	34.36	26.03	10	5.3
14	2000.04.02	11:41:25.20	37.64	37.32	9	4.5
15	2000.04.05	04:36:58.80	34.22	25.69	38	5.6
16	2000.04.21	12:23:10.51	37.84	29.33	33	5.5
17	2000.05.07	23:10:54.19	38.16	38.78	5	4.5
18	2000.05.12	03:01:44.47	37.05	36.08	10	4.8
19	2000.05.24	05:40:37.74	36.04	22.01	33	5.9
20	2000.06.06	02:41:47.70	40.65	33	13	6.1
21	2000.06.08	21:27:58.65	40.72	32.94	36	4.5
22	2000.06.09	03:14:19.58	40.69	32.92	10	4.6
23	2000.06.13	01:43:14.43	35.15	27.12	10	5.4
24	2000.06.15	16:10:18.26	35.16	27.17	10	4.8
25	2000.07.25	19:33:56.07	37.13	21.99	10	4.7
26	2000.08.17	11:49:50.38	40.72	33.89	33	4.8
27	2000.08.22	03:35:37.76	39.62	23.88	10	4.6
28	2000.08.23	13:41:28.14	40.68	30.72	15	5.8
29	2000.09.08	05:46:47.01	39.36	27.7	10	4.7
30	2000.09.11	16:54:56.52	35.71	45.21	74	4.6
31	2000.10.04	02:33:57.01	37.92	29.05	8	4.7
32	2000.10.06	06:20:25.22	36.93	45.2	77	4.5
33	2000.11.13	05:55:07.21	35.43	44.54	33	4.5
34	2000.11.17	00:28:00.13	38.24	42.94	33	4.6
35	2000.12.02	15:35:22.67	42.43	47.35	33	4.6
36	2000.12.09	08:37:06.29	42.48	44.33	33	4.6
37	2000.12.15	16:44:43.44	38.54	31.21	10	5.0
38	2000.12.24	11:30:47.50	38.62	40.26	10	4.8
39	2001.01.07	06:49:00.63	40.17	50.14	33	5.2

	DATE (yr.mn.dy)	ORIGIN TIME (hr:mn:sc.ms)	LATITUDE (N°)	LONGITUDE (E°)	DEPTH (KM)	MAGNITUDE
40	2001.01.17	12:09:53.95	37.06	36.13	10	4.9
41	2001.03.10	11:20:58.53	34.98	26.25	33	4.8
42	2001.03.22	14:02:25.32	40.66	33.09	33	4.5
43	2001.03.23	05:24:11.94	32.95	46.62	33	5.5
44	2001.04.03	17:36:34.22	32.47	47.99	33	5.2
45	2001.05.01	06:00:56.00	35.79	27.44	8	5.2
46	2001.05.24	03:18:09.75	39.30	27.92	15	4.5
47	2001.05.29	04:43:57.94	35.41	27.78	20	5.2
48	2001.05.29	13:14:30.35	39.80	41.65	33	4.8
49	2001.05.29	14:15:54.94	39.85	41.96	33	4.7
50	2001.06.05	15:33:29.77	42.47	48.63	60	5.0
51	2001.06.10	13:11:04.23	38.58	25.61	33	5.6
52	2001.06.12	01:46:49.94	39.02	47.26	33	4.5
53	2001.06.22	11:54:50.96	39.31	27.91	10	5.0
54	2001.06.23	06:52:45.00	35.69	28.24	58	5.7
55	2001.06.25	13:28:46.51	37.24	36.21	5	5.5
56	2001.07.10	21:42:03.80	39.85	41.63	33	5.4
57	2001.07.26	00:21:36.92	39.06	24.24	10	6.6
58	2001.07.30	15:24:56.74	39.09	24.04	10	5.0
59	2001.08.26	00:41:13.17	40.95	31.57	7	5.4
60	2001.09.01	22:38:16.83	32.73	47.68	14	5.0
61	2001.09.16	02:00:47.39	37.24	21.87	10	5.5
62	2001.10.31	12:33:52.81	37.25	36.14	10	5.2
63	2001.11.26	05:03:21.01	34.82	24.28	33	5.3
64	2001.12.07	19:44:50.06	39.38	23.81	10	5.0
65	2002.02.03	07:11:28.20	38.55	31.23	8	6.5
66	2002.02.03	09:26:42.90	38.65	30.8	8	5.9
67	2002.04.24	10:51:50.93	42.44	21.47	10	5.7
68	2002.04.24	19:48:07.12	34.64	47.4	33	5.4
69	2002.05.21	20:53:29.70	36.63	24.27	97	5.9
70	2002.06.18	03:19:24.25	33.33	45.91	33	5.3
71	2002.06.22	02:58:21.30	35.63	49.05	10	6.5
72	2002.09.02	01:00:03.27	35.70	48.84	10	5.2
73	2002.09.25	22:28:11.92	32.00	49.33	10	5.6
74	2002.10.12	05:58:50.11	34.77	26.37	10	5.4
75	2002.12.02	04:58:55.30	37.79	21.13	10	5.7
76	2002.12.24	17:03:02.94	34.59	47.45	33	5.2
77	2003.01.27	05:26:21.40	39.48	39.77	10	6.1
78	2003.04.10	00:40:15.80	38.21	26.83	17	5.8
79	2003.04.17	22:34:24.59	38.16	27	10	5.2
80	2003.04.29	01:51:20.20	36.83	21.72	67	5.1
81	2003.05.01	00:27:04.60	38.97	40.47	11	6.4
82	2003.06.09	07:06:39.33	39.89	22.31	17	5.2
83	2003.06.09	17:44:2.90	40.19	27.94	17	5.1
84	2003.07.06	19:10:27.60	40.42	26.06	17	5.7
85	2003.07.06	20:10:15.10	40.44	26.08	16	5.3
86	2003.07.13	01:48:20.90	38.33	38.99	10	5.6

	DATE (yr.mn.dy)	ORIGIN TIME (hr:mn:sc.ms)	LATITUDE (N°)	LONGITUDE (E°)	DEPTH (KM)	MAGNITUDE
87	2003.07.23	04:56:02.80	38.14	28.88	5	5.4
88	2003.07.26	01:00:57.60	38.11	28.89	10	5.0
89	2003.07.26	08:36:48.40	38.12	28.91	10	5.6
90	2003.10.17	12:57:07.72	35.94	22.16	33	5.3
91	2003.11.16	07:22:49.70	38.27	20.34	8	5.2
92	2003.12.11	16:28:17.35	31.95	49.21	33	5.0
93	2004.02.07	21:17:23.40	36.02	26.91	25	5.2
94	2004.02.11	08:15:03.83	31.67	35.55	26	5.3
95	2004.03.01	00:35:58.05	37.14	22.12	9	5.6
96	2004.03.17	05:21:00.80	34.59	23.33	24	6.1
97	2004.03.25	19:30:47.00	39.86	40.71	18	5.6
98	2004.03.28	03:51:09.60	39.94	40.88	10	5.6
99	2004.04.07	01:32:30.47	40.67	20.38	68	5.0
100	2004.06.15	12:02:38.20	40.37	25.87	21	5.2
101	2004.07.01	22:30:06.60	39.73	43.98	5	5.4
102	2004.08.03	13:11:31.30	36.95	27.7	12	5.2
103	2004.08.04	03:01:06.80	36.92	27.74	15	5.6
104	2004.08.04	04:19:47.10	36.91	27.76	13	5.2
105	2004.08.04	14:18:50.16	36.83	27.83	10	5.3
106	2004.08.11	15:48:23.10	38.36	39.21	7	5.7
107	2004.10.16	10:04:37.60	33.45	45.94	39	5.3
108	2004.10.27	20:34:36.81	45.79	26.62	95	5.9
109	2004.11.04	06:22:39.40	35.94	23.11	74	5.4
110	2004.11.23	02:26:16.35	40.32	20.63	15	5.5
111	2004.12.20	23:02:12.81	37.04	28.27	5	5.4
112	2005.01.10	23:48:49.50	36.98	27.85	20	5.5
113	2005.01.11	04:35:56.60	36.96	27.76	14	5.1
114	2005.01.23	22:36:05.20	35.84	29.63	13	5.8
115	2005.01.25	11:39:20.91	33.39	45.87	45	5.0
116	2005.01.25	15:24:27.59	37.56	43.78	19	4.8
117	2005.01.25	16:44:14.30	38.04	43.15	34	4.6
118	2005.01.29	18:52:26.50	38.17	26.71	17	4.5
119	2005.01.30	16:23:48.10	35.85	29.66	22	5.3
120	2005.02.04	00:19:55.40	37.78	43.69	9	4.6
121	2005.03.12	07:36:12.18	39.44	40.98	11	5.6
122	2005.03.14	01:55:55.60	39.35	40.89	5	5.8
123	2005.03.14	04:58:06.57	39.43	40.96	10	4.6
124	2005.03.23	21:44:53.02	39.43	40.92	10	5.7
125	2005.03.23	23:43:41.33	39.39	40.79	5	4.7
126	2005.04.29	22:28:09.55	40.66	34.85	31	4.8
127	2005.05.12	08:59:58.60	40.38	37.4	10	4.6
128	2005.05.12	09:25:38.40	40.35	37.37	10	4.9
129	2005.05.14	23:46:45.30	35.70	31.59	69	5.1
130	2005.05.15	10:54:26.20	38.63	30.78	22	4.5
131	2005.05.29	08:55:35.80	38.26	22.73	104	5.0
132	2005.06.05	03:44:59.12	37.52	43.82	10	4.7
133	2005.06.06	07:41:28.70	39.22	41.08	10	5.6

	DATE (yr.mn.dy)	ORIGIN TIME (hr:mn:sc.ms)	LATITUDE (N°)	LONGITUDE (E°)	DEPTH (KM)	MAGNITUDE
134	2005.07.30	21:45:00.00	39.44	33.09	5	5.3
135	2005.07.31	00:45:12.40	39.41	33.12	10	4.5
136	2005.07.31	23:41:33.20	39.39	33.11	10	4.8
137	2005.08.01	00:45:06.00	39.39	33.11	7	4.6
138	2005.08.04	10:45:28.50	34.93	26.47	7	5.0
139	2005.08.06	09:09:26.50	39.36	33.11	10	4.6
140	2005.08.09	01:28:4.00	40.55	33.04	15	4.7
141	2005.08.10	08:58:17.60	39.32	41.12	20	4.5
142	2005.09.02	07:42:25.64	34.01	25.88	15	5.1
143	2005.09.26	18:57:04.00	37.30	47.8	14	5.2
144	2005.10.17	05:45:16.00	38.13	26.5	8	5.7
145	2005.10.17	09:46:53.90	38.20	26.5	10	5.8
146	2005.10.19	10:11:31.00	38.15	26.68	17	4.6
147	2005.10.20	21:40:02.50	38.18	26.72	15	5.9
148	2005.10.29	14:48:41.00	38.10	26.64	14	4.5
149	2005.10.31	05:26:38.00	38.16	26.58	8	4.8
150	2005.11.25	09:30:56.90	35.02	23.32	32	5.2
151	2005.11.26	15:56:55.00	38.27	38.84	9	5.3
152	2005.12.10	00:09:50.23	39.39	40.95	10	5.4
153	2005.12.24	03:56:06.50	38.79	27.79	14	4.6
154	2005.12.26	23:15:50.00	32.10	49.2	18	5.2
155	2006.01.08	11:34:55.64	36.31	23.21	66	6.7
156	2006.02.06	04:08:00.80	42.51	43.45	18	5.3
157	2006.02.06	04:08:03.07	42.65	43.53	17	5.3
158	2006.02.08	04:07:40.80	40.71	30.36	8	4.6
159	2006.03.29	22:05:15.19	35.25	35.43	27	5.0
160	2006.03.30	19:36:17.26	33.56	48.75	10	5.2
161	2006.03.31	01:17:00.96	33.50	48.78	7	6.1
162	2006.03.31	11:54:02.28	33.72	48.67	10	5.3
163	2006.04.03	00:49:42.80	37.59	20.95	20	5.0
164	2006.04.04	22:05:05.08	37.64	20.96	16	5.5
165	2006.04.11	00:02:41.50	37.64	20.92	18	5.5
166	2006.04.11	17:29:28.40	37.68	20.91	18	5.5
167	2006.04.12	16:52:01.20	37.61	20.95	19	5.7
168	2006.04.19	15:16:24.60	37.66	20.93	19	5.4
169	2006.05.21	03:48:32.40	38.08	42.74	9	4.9
170	2006.05.25	23:14:36.90	36.87	20.34	35	5.2
171	2006.06.03	14:40:24.30	39.19	40.2	7	4.5
172	2006.06.05	04:23:29.20	37.93	28.69	10	4.5
173	2006.06.21	15:54:44.60	39.01	20.59	10	5.0
174	2006.07.02	19:39:36.60	39.41	40.87	3	4.9
175	2006.08.13	10:35:12.70	34.42	26.57	32	5.2
176	2006.08.22	09:23:21.20	35.24	27.12	31	5.1
177	2006.10.20	18:15:23.70	40.22	27.99	11	5.2
178	2006.10.22	17:16:44.40	38.97	44.61	14	4.5
179	2006.10.24	14:00:21.67	40.42	29.11	9	5.0
180	2006.11.01	21:19:45.00	39.43	40.65	5	4.8

	DATE (yr.mn.dy)	ORIGIN TIME (hr:mn:sc.ms)	LATITUDE (N°)	LONGITUDE (E°)	DEPTH (KM)	MAGNITUDE
181	2006.11.23	04:37:33.00	39.95	42.66	5	4.6
182	2006.12.19	19:15:37.00	40.39	28.32	11	4.6
183	2006.12.21	18:30:52.90	39.32	23.6	23	5.4
184	2007.01.21	07:38:57.00	39.59	42.86	3	5.1
185	2007.01.23	21:22:00.81	38.13	28.82	26	4.6
186	2007.01.26	08:20:34.30	38.80	40.07	8	4.7
187	2007.02.03	13:43:23.08	35.81	22.43	59	5.2
188	2007.02.09	02:22:55.00	38.43	39.03	2	5.4
189	2007.02.21	11:05:26.60	38.41	39.31	12	5.7
190	2007.02.28	23:27:45.80	38.40	39.25	8	4.7
191	2007.03.08	12:35:37.60	39.09	40.38	5	4.8
192	2007.03.09	23:24:53.30	39.07	40.37	5	4.7
193	2007.03.25	13:57:58.20	38.34	20.42	15	5.7
194	2007.03.30	16:56:52.40	38.02	30.91	6	4.7
195	2007.03.30	19:23:54.70	37.97	30.93	5	4.9
196	2007.04.10	03:17:56.35	38.55	21.64	2	5.4
197	2007.04.10	10:41:00.24	38.55	21.64	0	5.3
198	2007.04.10	22:00:34.24	38.01	30.92	5	4.9
199	2007.05.05	21:11:36.00	38.76	42.24	7	4.5
200	2007.05.18	23:27:42.70	37.31	33.31	6	4.5
201	2007.05.21	16:39:08.67	35.12	27.81	10	5.0
202	2007.06.05	11:50:20.50	38.54	21.65	0	5.3
203	2007.06.18	14:29:48.29	34.44	50.83	5	5.5
204	2007.06.29	18:09:11.22	39.27	20.26	10	5.4
205	2007.07.11	06:51:14.32	38.75	48.6	25	5.2
206	2007.07.17	18:23:21.97	40.16	21.53	22	5.4
207	2007.08.25	22:05:46.20	39.23	41.06	10	5.4
208	2007.08.31	20:52:43.43	36.65	26.27	25	5.4
209	2007.09.23	00:54:29.60	35.27	27.12	24	5.6
210	2007.10.27	05:29:39.00	37.72	21.3	16	5.5
211	2007.10.29	09:23:14.00	37.03	29.23	5	5.3
212	2007.11.09	01:43:04.20	38.73	25.72	9	5.5
213	2007.11.16	09:08:23.10	37.09	29.24	5	5.0
214	2007.12.20	09:48:30.02	39.42	33.16	10	5.7
215	2008.01.31	00:01:20.43	40.27	33.15	5	4.9
216	2008.02.14	10:09:23.42	36.65	21.83	29	6.9
217	2008.02.14	12:08:55.79	36.35	21.86	28	6.5
218	2008.02.15	10:36:19.76	33.38	35.32	10	5.0
219	2008.02.19	23:15:40.00	36.19	21.77	22	5.3
220	2008.02.20	18:27:08.26	36.33	21.79	22	6.1
221	2008.02.26	10:46:07.33	35.91	21.87	5	5.4
222	2008.02.26	16:10:40.00	36.09	21.89	37	5.0
223	2008.02.29	03:12:29.00	40.60	34.77	5	4.5
224	2008.03.12	18:53:32.27	40.66	29.2	10	4.2
225	2008.03.14	05:09:31.70	38.78	44.69	10	4.4
226	2008.03.14	07:10:21.60	36.01	21.76	5	5.1
227	2008.03.15	10:15:37.90	39.48	32.96	10	4.5

	DATE (yr.mn.dy)	ORIGIN TIME (hr:mn:sc.ms)	LATITUDE (N°)	LONGITUDE (E°)	DEPTH (KM)	MAGNITUDE
228	2008.03.15	11:52:12.00	39.04	27.83	12	4.2
229	2008.03.20	09:32:02.20	35.87	45.15	16	4.4
230	2008.03.23	20:11:11.92	36.15	21.86	35	5.0
231	2008.03.28	00:16:19.90	34.76	25.34	45	5.6
232	2008.03.29	02:12:29.00	40.60	34.76	5	4.4
233	2008.04.01	12:35:48.50	30.70	46.21	8	4.2
234	2008.04.15	01:21:51.50	37.17	45.02	4	4.0
235	2008.04.25	04:48:54.00	37.82	29.25	5	5.0
236	2008.05.01	00:15:27.40	33.86	48.59	16	4.5
237	2008.05.01	16:51:09.80	39.41	33.13	10	5.0
238	2008.05.03	03:20:53.70	36.69	36.66	10	4.0
239	2008.05.07	08:00:21.40	45.36	30.92	10	4.9
240	2008.05.08	12:26:22.62	36.11	21.95	10	4.9
241	2008.05.12	10:11:55.40	43.23	26.07	10	4.5
242	2008.06.06	00:12:52.90	34.54	32.95	10	4.4
243	2008.06.08	03:06:50.40	37.40	43.58	10	4.0
244	2008.06.08	12:25:29.71	37.96	21.52	16	6.4
245	2008.06.09	22:21:56.00	42.39	44.85	10	4.0
246	2008.06.12	00:20:45.60	35.11	26.19	29	5.1
247	2008.06.12	15:41:03.40	33.53	35.09	10	4.3
248	2008.06.21	03:58:35.00	38.88	41.32	7	4.1
249	2008.06.21	05:57:16.20	36.10	21.93	17	5.2
250	2008.06.27	10:50:05.00	39.93	41.84	5	4.1
251	2008.07.02	19:42:33.00	37.61	43.86	5	4.1
252	2008.07.03	17:37:03.00	37.09	29.12	7	4.3
253	2008.07.10	07:49:53.00	39.99	27.7	13	4.2
254	2008.07.11	14:11:49.00	37.05	29.15	3	4.1
255	2008.07.12	05:54:03.00	39.29	41.73	5	4.0
256	2008.07.15	03:26:31.00	35.78	27.85	19	6.4
257	2008.07.15	09:19:48.00	40.37	27.45	6	4.1
258	2008.07.20	10:15:24.00	38.67	26.43	5	4.0
259	2008.07.26	22:16:50.00	38.44	43.4	11	4.6
260	2008.07.31	05:02:10.00	39.72	33.34	3	4.2
261	2008.08.03	00:39:16.86	39.61	23.85	10	5.3
262	2008.08.04	19:38:25.30	34.10	26.58	30	5.3
263	2008.08.19	09:50:04.00	37.67	43.88	5	4.1
264	2008.08.27	21:52:38.11	32.31	47.35	10	5.8
265	2008.09.02	20:00:50.82	38.72	45.79	3	5.0
266	2008.09.03	02:22:47.00	37.50	38.5	6	5.0
267	2008.09.03	22:43:13.00	32.30	47.2	8	5.1
268	2008.09.04	22:54:32.00	37.47	38.54	10	4.3
269	2008.09.06	19:48:03.12	45.85	26.55	24	4.5
270	2008.09.17	12:08:12.00	40.01	39.97	5	4.8
271	2008.09.23	08:04:09.00	39.55	39.85	5	4.1
272	2008.09.23	09:09:42.00	39.46	33.05	4	4.5
273	2008.09.30	07:30:00.00	38.99	29.86	5	4.4
274	2008.10.03	12:41:47.00	37.94	45.02	9	4.3

	DATE (yr.mn.dy)	ORIGIN TIME (hr:mn:sc.ms)	LATITUDE (N°)	LONGITUDE (E°)	DEPTH (KM)	MAGNITUDE
275	2008.10.07	23:54:14.00	39.55	32.6	5	4.0
276	2008.10.10	06:36:59.00	39.46	33.05	7	4.5
277	2008.10.11	09:06:09.80	43.30	46.24	10	4.9
278	2008.10.14	02:06:38.70	38.74	23.58	35	5.2
279	2008.11.05	07:36:49.00	43.44	27.38	13	4.0
280	2008.11.12	11:57:34.00	40.78	31.92	7	4.0
281	2008.11.12	14:03:15.00	38.86	35.53	3	4.9
282	2008.12.01	10:18:38.19	35.36	46.1	10	5.0
283	2008.12.13	08:27:23.43	38.79	22.58	38	5.1

REFERENCES

Agnew, D. C. and J. Berger, 1978, "Vertical Seismic Noise at Very Low Frequencies", *Journal of Geophysical Research,* Vol. 83, pp. 5420-5424.

Aksu, A.E., T. J. Calon, J. Hall, S. Mansfield and D. Yaşar, 2005, "The Cilicia–Adana Basin Complex, Eastern Mediterranean: Neogene Evolution of an Active Fore-Arc Basin in an Obliquely Convergent Margin", *Marine Geology*, Vol. 221, pp.121–159.

Akyol, N., L. Zhu, B. J. Mitchell, H. Sözbilir, and K. Kekovalı, 2006, "Crustal Structure and Local Seismicity in Western Anatolia", *Geophysical Journal International,* Vol. 166, No. 3, pp. 1259-1269.

Al-Lazki A., D. Seber, E. Sandvol, N. Turkelli, R. Mohamad and M. Barazangi, 2003, "Tomographic Pn Velocity and Anisotropy Structure Beneath the Anatolian Plateau (Eastern Turkey) and the Surrounding Regions", *Geophysical Research Lett*ers, Vol. 30, No. 24.

Bassin, C., G. Laske and G. Masters, 2000, "The Current Limits of Resolution for Surface Wave Tomography in North America", *EOS Trans AGU*, 81, F897.

Bhattacharya, S. N., 1983, "Higher Order Accuracy in Multiple Filter Technique", *Bulletin of the Seismological Society of America,* Vol. 73, No. 5, pp. 1395-1406.

Bensen, G.,D., M. H. Ritzwoller, M. P. Barmin, A. L. Levshin, F. Lin, M. P. Moschetti, N. M. Shapiro and Y. Yang, 2007, "Processing Seismic Ambient Noise Data to Obtain Reliable Broadband Surface Wave Dispersion Measurements", *Geophysical Journal International*, Vol. 169, pp. 1239-1260.

Bernard, P., 1938, L'agitation Microseismique au Japon, *Ann. Phys.* Globe France outré-mer 5-29, pp. 135-136.

Bernard, P., 1941a, *Etude sur l'agitation Microseismique,* Presses Universitaires de France.

Bernard, P., 1941b, Etude sur l'agitation Microseismique et ses Variations. *Annales de l'Institut de Physique du Globe de Paris* 19, 77.

Bertelli T., 1872, "Osservazioni sui Piccolo movimenti dei Pendoli in Relazione ad Alcuni Fenomeni Meteorologiche", *Bullettino Meteorologico dell'Osservatorio dell Collegio Romano*, Roma, Italy.

Bonnefoy-Claudet, S., F. Cotton and P. Bard, 2006, "The Nature of Noise Wavefield and its Applications for Site Effects Studies: A literature Review", *Earth Science Review*, 79, pp. 205-227.

Brune, J. N., and J. Oliver, 1959, "The Seismic Noise of the Earth's Surface", *Bulletin of the Seismological Society of America,* Vol. 49, No. 4, pp. 349-353.

Campillo, M., 2006, "Phase and Correlation in 'Random' Seismic Fields and the Reconstruction of the Green Function", *Pure and Applied Geophysics*, Vol. 163.

Campillo, M. and A. Paul, 2003, "Long Range Correlations in the Diffuse Seismic Coda", *Science*, 299, pp. 547-549.

Canıtez, N., 1977, "Optimum Filter for Surface-Wave Group-Velocity Determination", *Bulletin of the Seismological Society of America,* Vol. 67, No. 1, pp. 79-85.

Curtis A., J. Trampert, R. Snieder, and B. Dost, 1998, "Eurasian Fundamental Mode Surface Wave Phase Velocities and Their Relationship with Tectonic Structures", *Journal of Geophysical Research*, 103, pp. 26919-26947.

Derode, A., E. Larose, M. Tanter, J. de Rosny, A. Tourin, M. Campillo, M. Fink, 2003, "Recovering the Green's Function From Field-Field Correlations in an Open Scattering Medium", *The Journal of the Acoustical Society of America,* Vol. 113 pp. 2973-2976.

DiLuccio F. and M. E. Pasyanos, 2007, "Crustal and Upper Mantle Structure in the Eastern Mediterranean from the Analysis of Surface Wave Dispersion Curves", *Geophysical Journal International,* Vol. 169, pp. 1139–1152.

Dziewonski, A. M., S. Bloch and M. Landisman, 1969, "A Technique for the Analysis of Transient Seismic Signals", *Bulletin of the Seismological Society of America,* Vol. 59, No.1, pp. 427-444.

Dziewonski, A. M., J. Mills, S. Bloch, 1972, "Residual Dispersion Measurement – A New Method of Surface-Wave Analysis", *Bulletin of the Seismological Society of America,* Vol. 62, No.1, pp. 129-140.

Dziewonski, A. M., 1984, "Mapping the Lower Mantle Determination of Lateral Heterogeneity in P-velocity up to Degree and Order 6, *Journal of Geophysical Research,* 89, pp. 5929-5952.

Engdahl, E. R., R. van der Hilst and R. Buland, 1998, "Global Teleseismic Earthquake Relocation with Improved Travel Times and Procedures for Depth Determination", *Bulletin of the Seismological Society of America,* Vol. 88, pp. 722-743.

Ekström, G., 2001, "Time Domain Analysis of Earth's Long-Period Background Seismic Radiation", *Journal of Geophysical Research,* Vol. 106, pp. 26483-26494.

Floyd, P. A., M. C. Göncüoğlu, J. A. Winchester, J. A. and M. K. Yalınız, 2000, "Geochemical Character and Tectonic Environment of Neotethyan Ophiolitic Fragments and Metabasits in the Central Anatolian Crystalline Complex, Turkey", in E. Bozkurt, J. A. Winchester, J. D. A. Piper, (eds.) *Tectonics and Magmatism in Turkey and the Surrounding Area,* 173, pp. 183-202, Geological Society, London.

Friedrich, A., F. Kruger, K. Klinge, 1998, "Ocean-Generated Microseismic Noise Located with the Graffenberg Array", *Journal of Seismology*, Vol. 2, pp. 47-64.

Glover, C., A. H. F. Robertson, 1998, "Neogen Intersection of the Aegean and Cyprus Arcs: Extensional and Strike-Slip Faulting in the Isparta Angle, SW Turkey." *Tectonophysics,* Vol. 298, pp. 103-132.

Gouedard, P., L. Stehly, F. Brenguier, M. Campillo, C. de Verdiere, E. Larose, L. Margerin, P. Roux, F. J. Sanchez-Sesma, N. M. Shapiro, R. L. Weaver, 2008, "Cross-correlation of Random fields: Mathemaical Approach and Applications", *Geophysical Prospecting,* 56, pp. 375-393.

Gök, R., E. Sandvol, N. Turkelli, D. Seber, M. Barazangi, 2003, "Sn Attenuation in the Anatolian and Iranian Plateaus and Surrounding Regions", *Geophysical Research Letters*, Vol. 30, No. 24.

Gök, R., M. Pasyanos, E. Zor, 2007, "Lithospheric Structure of the Continent–Continent Collision Zone: Eastern Turkey", *Geophysical Journal International,* Vol. 169, pp. 1079–1088.

Göncüoğlu, M.C., N. Turhan, K. Şentürk, A. Özcan, Ş. Uysal, M. K. Yalınız, 2000, "A Geotraverse Across Northwestern Turkey: Tectonic Units of the Central Sakarya Region and Their Tectonic Evolution." in E. Bozkurt, J. A. Winchester, J. D. A. Piper, (eds.) *Tectonics and Magmatism in Turkey and the Surrounding Area,* 173, pp. 139-161, Geological Society, London.

Gutenberg, B., 1911, *Die Seismiche Bodenruhe*. Ph.D. Dissertation, University of Gottigen, Germany.

Gutenberg, B., 1931, "Microseisms in North America", *Bulletin of the Seismological Society of America,* Vol. 21, pp.1-24

Gutenberg, B., 1958, "Microseisms", *Advances in Geophysics*, Vol. 5, pp. 53-92.

Haubrich, R. A., W. H. Munk, F. E. Snodgras, 1963, Comparative Spectra of Microseisms and swell, *Bulletin of the Seismological Society of America,* Vol. 53, pp. 27-37.

Herrmann, R. B., 1973, “Some Aspects of Band-Pass Filtering of Surface Waves”, *Bulletin of the Seismological Society of America,* Vol. 63, No. 2, pp. 663-671

Holcomb, L. G., 1989, *A Direct Method for Calculating Instrument Noise Levels in Side-by-Side Seismometer Evaluations*, U.S. Geological Survey Open file Report, pp. 89-214.

Karagianni, E. E., D. G. Pabagiotopoulos, G. F. Panza, P. Suhadolc, C. B. Papazachos, A. Kirtazi, D. Hatzfeld, K. Makropoulos, K. Priestley, A. Vuan, 2002, “Rayleigh Wave Group Velocity Tomography in the Aegean Area”, *Tectonophysics,* Vol. 358, pp. 187– 209.

Karagianni, E. E., C. B. Papazachos, D. G. Panagiotopoulos, P. Suhadolc, A. Vuan, G. F. Panza, 2005, “Shear velocity structure in the Aegean area obtained by inversion of Rayleigh waves”, *Geophysical Journal International*, Vol. 160, pp. 127–143.

Kay, S. M., 1988, *Modern Spectral Estimation: Theory and Application,* Prentice Hall, New Jersey.

Keskin, M. 2003, “Magma Generation by Slab Steepening and Break off beneath a Subduction–Accretion Complex: An Alternative Model for Collision-Related Volcanism in Eastern Anatolia, Turkey”, *Geophysical Research Letters*, 30, 8046.

Koçyiğit, A., E. Ünay, G. Saraç, 2000, “Episodic Graben Formation and Extensional Neotectonic Regime in West Central Anatolia and the Isparta Angle: A Case Study in the Akşehir-Afyon Graben, Turkey. *Geological Society of London,* 173, pp. 405-421.

Knopoff, L., 1972, “Observation and Inversion of Surface Wave Dispersion”, *Tectonophysics*, Vol. 13, pp. 497-519.

Kodera, K., C. de Valledary, R. Gendrin, 1976, "A New Method for the Numerical Analysis of Non-Stationary Signals", *Physics of the Earth and Planetary Interior,* Vol. 12, pp. 142-150.

Köseoğlu A., 2001, *Spectral Characteristics of Noise in Broadband and Semi-Broadband Stations*, M.Sc. Thesis, Boğaziçi University

Laigle, M., A. Becel, B. de Voogd, A. Him, T. Taymaz, S. Özalaybey, 2008, A First Deep Seismic Survey in the Sea of Marmara: Deep Basins and Whole Crust Architecture and Evolution, *Earth and Planetary Science Letters,* Vol. 270, pp. 168-179.

Larose, E., A. Derode, M. Campillo, M. Fink, 2004, "Imaging From One-Bit Correlations of Wideband Diffuse Wave Fields", *Journal of Applied Physics*, Vol. 95, No. 12, pp. 8393-8399.

Lay T. and T. C. Wallace, 1995, *Modern Global Seismology*, Academic Press, Inc.

Levshin, A.L., L. Ratnikova, J. Berger, 1992, "Peculiarities of Surface Wave Propagation Across Central Eurasia", *Bulletin of the Seismological Society of America,* Vol. 82, pp. 2464-2493.

Levshin, A.L., M. H. Ritzwoller and L. Ratnikova, 1994, "The Nature and Cause of Polarization Anomalies of Surface Waves Crossing Northern and Central Eurasia", *Geophysical Journal International*, Vol. 117, pp. 577-590.

Levshin, A. L., M. P. Barmin, M. H. Ritzwoller, J. Trampert, 2005, Minor-Arc and Major-Arc Global Surface Wave Diffraction Tomography, *Physics of the Earth and Planetary Interior,* Vol. 149, pp. 205-223.

Li, T. M. C., 1981, "*Lajitas Quiet Site Noise Study"*, *Teledyne-Geotech Technical Report* 81-10, Garlad, Texas.

Li, H., F. Bernardi, A. Michelini, 2010, "Surface Wave Dispersion Measurements from Ambient Seismic Noise Analysis in Italy", *Geophysical Journal International,* doi: 10.1111/j.1365-246X.2009.04476.x.

Lin, F. C., M. H. Ritzwoller, J. Townend, M. Savage, S. Bannister, 2007, "Ambient Noise Rayleigh Wave Tomography of New Zealand", *Geophysical Journal International,* Vol. 72, pp. 649-666.

Lobkis, O. I. and R. L. Weaver, 2001, "On the Emergence of the Green's Function in the Correlations of a Diffuse Field", *The Journal of the Accoustical Society of America,* Vol. 110, pp. 3011-3017.

Longuet-Higgins, M. S. 1950, "A Theory of the Origin of Microseisms", *Phil. Trans. Roy. Soc.,* 243, pp. 1-35.

Maggi, A. and K. Priestley, 2005, "Surface Waveform Tomography of the Turkish-Iranian Plateau", *Geophysical Journal International*, Vol. 160, pp. 1068-1080.

Marple, S. L., 1987, *Digital Spectral Analysis*, Prentice Hall, New Jersey.

McNamara D. and R. P. Buland, 2004, "Ambient Noise Levels in the Continental United States", *Bulletin of the Seismological Society of America,* Vol. 94, pp. 1517-1527.

McNamara D. and R. I. Boaz, 2005, "Seismic Noise Analysis System: A Stand-Alone Software Package", *Preprint for a USGS Open File Report*, ver2.0.

Mindevalli, O. Y. and B. J. Mitchell, 1989, "Crustal Structure and Possible Anisotropy in Turkey from Seismic Surface Wave Dispersion", *Geophysical Journal International,* Vol. 98, pp. 93-106.

Mooney, W., G. Laske. and T. Master, 1998, "CRUST 5.1: a Global Crustal Model at 5x5", *Journal of Geophysical Research*, Vol. 102, pp.727-747.

Moschetti, M. P., M. H. Ritzwoller, N. M. Shapiro, 2007, "Surface Wave Tomography of the Western United States from Ambient Seismic Noise: Rayleigh Wave Group Velocity Maps", *Geochemistry Geophysics Geosystems*, Vol. 8, doi:10.1029/2007GC001655.

Nikishin, A.M., M. V. Korotaev, A. V. Ershov, M.F. Brunet, 2003. The Black Sea Basin: Tectonic History and Neogene-Quaternary Rapid Subsidence Modeling, *Sedimentary Geology* 156, pp. 149-168.

Okay, A.I., 1989, "Tectonic Units and Sutures in the Pontides, Northern Turkey", in A. M. C. Şengör, (eds.), *Tectonic Evolution of the Tethyan Region*, 259, pp. 109-115, Kluwer Academic Publications, Dordrecht.

Okay, A.I., A. M. C. Şengör, N. Görür, 1994, "Kinematic History of the Opening of the Black Sea and its Effect on the Surrounding Regions", *Geology*, 22, pp. 267-270.

Okay, A.I. and O. Tüysüz, 1999, "Tethyan Sutures of Northern Turkey", in B. Durand, L. Jolivet, F. Horváth and M. Séranne, (eds.), *The Mediterranean Basins: Tertiary Extension Within the Alpine orogen*, 156, pp. 475-515, *Geological Society*, London.

Oliver, J., 1962, "A Summary of Observed Surface Wave Dispersion", *Bulletin of the Seismological Society of America*, Vol. 52, pp. 81-86.

Paul, A., M. Campillo, L. Margerin, E. Larose, A. Derode, 2005, Empirical Synthesis of Time Asymmetrical Green's Function from the Correlation of Coda Waves, *Journal of Geophysical Research*, Vol. 110, B08302.

Pasyanos, M., E., W. R. Walter, S. E. Hazler, 2001, "A Surface Wave Dispersion Study of the Middle East and North Africa for Monitoring the Comprehensive Nuclear-Test-Ban Treaty", *Pure and Applied Geophysics,* Vol. 158, pp. 1445-1474.

Pasyanos, M., E., 2005, “A Variable Resolution Surface Wave Dispersion Study of Eurasia, North Africa, and Surrounding Regions”, *Journal of Geophysical Research*, Vol. 110, B12301, doi:10.1029/2005JB003749.

Pedersen H. A., J. I. Mars, and P. O. Amblard, 2003, “Improving the Surface Wave Group Velocity Measurements by Energy Reassignment”, *Geophysics*, 68, pp. 679-684.

Pedersen H.A., Krüger F., and SVEKALAPKO Seismic Tomography Working Group, 2007, “Influence of the Seismic Noise Characteristic on Noise Correlations in the Baltic Shield”, *Geophysical Journal International,* Vol. 168, pp. 197-210.

Peterson, 1993, “Observation and Modeling of Seismic Background Noise”, *U.S. Geol. Surv. Tech. Rept*., 93-322, pp. 1-95.

Peterson, J. and N. Orsini, 1976, “Seismic Research Observatories: Upgrading the Worldwide Seismic Data Network”, EOS, AGU, 57, pp. 548-556.

Ramirez, J. E., 1940, “An Experimental Investigation of the Nature and Origin of Microseisms at St. Louis, Missouri”, *Bulletin of the Seismological Society of America,* Vol. 30, pp. 35-84.

Rickett, J. and J. Claerbout. “Calculation of the Acoustic Solar Impulse Response by Multi-Dimensional Spectral Factorization”, *Solar Physics,* 92, pp. 203-210.

Ritzwoller, M. H. and A. L. Levshin, 1998, “Eurasian Surface Wave Tomography : Group Velocities”, *Journal of Geophysical Research*, Vol. 103, B3, pp. 4839-4878.

Ritzwoller, M. H., N. M. Shapiro, M. P. Barmin, A. L. Levshin, 2002, “Global Surface Wave Diffraction Tomography”, *Journal of Geophysical Research*, Vol. 107, B12, 2335, doi: 10.1029/2002JB001777

Robertson, A. H. F., 2000, “Mesozoic-Tertiary Tectonic-Sedimentary Evolution of a South Tethyan Oceanic Basin and its Margin in Southern Turkey.” in Bozkurt, E.,

Winchester, J. A. and Piper, J. D. A. (eds.) *Tectonics and Magmatism in Turkey and the Surrounding Area.,* 173, pp. 97-138, Geological Society, London.

Robertson, A. H. F. and E. A. Pickett, 2000, "Palaeozoic- Early Tertiary Tethyan Evolution of Passive Margin Units in the Karaburun Peninsula (Western Turkey) and Chios Island (Greece)", in Bozkurt, E., Winchester, J. A. and Piper, J. D. A. (eds.) *Tectonics and Magmatism in Turkey and the Surrounding Area.,* 173, pp. 43-82, Geological Society, London.

Robinson, A.G., 1997, *Regional and Petroleum Geology of the Black Sea and Surrounding Region*, America Association of Petroleum Geologists, Memoir, 68, Tulsa, OK, 385.

Roux, P., Song, H. C., Kuperman, W.A., 2003, "Time-Reversal Using Ambient Noise as a Probe Source", *The Journal of the Acoustical Society of America,* Vol. 113, pp. 2218.

Roux, P., and M. Fink, 2003, "Green's Function Estimation Using Secondary Sources in a Shallow Water Environment", *The Journal of the Acoustical Society of America,* Vol. 113, pp. 1406-1416.

Roux, P., K. G. Sabra, W. A. Kupermaan, A. Roux, 2005, "Ambient Noise Cross Correlation in Free Space: Theoretical Approach", *The Journal of the Acoustical Society of America,* Vol. 117, pp. 79-84.

Sandvol, E., N. Turkelli, M. Barazangi, 2003, "The Eastern Turkey Seismic Experiment: The Study of a Young Continent-Continent Collision", *Geophysical Research Letters,* Vol. 30, No. 24, 8038.

Saunders, P., Priestly K., Taymaz T., 1998, "Variations in the Crustal Structure Beneath Western Turkey.", *Geophysical Journal International,* Vol. 134, pp. 373-389.

Seo, K., 1997, *Comparison of Measured Microtremors with Damage Distribution*, JICA, Research and Development Project on Earthquake Disaster Prevention.

Seymen, İ., 1984, "Geological Evolution of the Metamorphic Rocks of the Kırşehir Massif", *Proceedings of the Ketin Symposium Geological Society,* pp. 133-148, Ankara, Turkey.

Shapiro, N. M. and M. Campillo, 2004, "Emergence of Broadband Rayleigh Waves from Correlations of the Ambient Seismic Noise", *Geophysical Research Letters*, 31, L07614.

Shapiro, N. M., M. Campillo, L. Stehly, M. H. Ritzwoller, 2005, "High-Resolution Surface-Wave Tomography from Ambient Seismic Noise", *Science*, 307, pp. 1615–1618

Sheriff R. E., 1991, *Encyclopedic Dictionary of Exploration Geophysics*, SEG, pp. 204.

Snieder, R., 2004, "Extracting the Green's Function from the Correlation of Coda Waves: A derivation Based on Stationary Phase", *Physical Review*, 69.

Sodoudi, F., R. Kind, D. Hatzfeld, K. Priestley, W. Hanka, K. Wylegalla, G. Stavrakakis, A. Vafidis, H. P. Harjes, M. Bohnhoff, 2006, "Lithospheric Structure of the Aegean Obtained from P and S Receiver Functions." *Journal of Geophysical Research*, Vol. 111, B12307, doi:10.1029/2005JB003932.

Spadini, G., A. Robinson and S. Cloetingh, 1996, "Western Versus Eastern Black Sea Tectonic Evolution: Pre-rift Lithospheric Controls on Basin Formation", *Tectonophysics,* 266, pp. 139-154.

Stampfli G.M., 2000, "Tethyan Oceans", *From: Bozkurt E., Winchester, J. A. and Piper, J. D.A., (eds) Tectonic and Magmatism in Turkey and the Surrounding Area. Geological Society*, London, Special Publications, Vol.173, pp. 1-23.

Stehly L., Campillo N. M., Shapiro N.M., 2006, "A Study of the Seismic Noise from its Long-Range Correlation Properties", *Journal of Geophysical Research*, Vol. 111, B10306, doi:10.1029/2005JB004237.

Stoica, P., and R. L. Moses, 1997, Introduction to Spectral Analysis, Prentice Hall, New Jersey.

Stutzmann, E., Roult, G., Astiz L., 2000, "GEOSCOPE Station Noise Levels", *Bulletin of the Seismological Society of America,* Vol. 90, No. 3, pp. 690–701.

Şengör, A. M. C. and Y. Yılmaz, 1981, "Tethyan Evolution of Turkey, a Plate Tectonic Approach", *Tectonophysics*, 75, pp. 181-241.

Şengör, A. M. C., Y. Yılmaz, İ. Ketin, 1982, "Remnants of a pre-Late Jurassic Ocean in Northern Turkey, Fragments of Permo-Triassic Paleo-Tethys? : Reply." The *Geological Society of America Bulletin*, Vol. 93, pp. 932-936.

Şengör, A. M. C. 2003, "The Repeated Rediscovery of Melanges and its Implications for the Possibility and the Role of Objective Evidence in the Scientific Enterprise" *Geological Society of America,* Special Paper 373, pp. 385-445.

Tatar O., J. D. Piper, H. Gürsoy, 2000, "Paleomagnetic study of the Erciyes Sector of the Ecemiş Fault Zone: Neotectonic Deformation in the Southeastern Part of the Anatolian Block." in Bozkurt, E., Winchester, J. A. and Piper, J. D. A. (eds.) *Tectonics and Magmatism in Turkey and the Surrounding Area.,* 173, pp. 423-440, Geological Society, London.

Topuz, G., R. Altherr, A. Kalt, M. Satır, O. Werner, W. H. Schwardz, 2004, "Alumins Granulites from the Pulur Complex, NE Turkey: a Case of Partial Melting, Efficient Melt Extraction and Crystallization", *Lithos*, Vol. 72, pp. 183-207.

Trampert, J. and J. H. Woodhouse, 1995, "Global Phase Velocity maps of Love and Rayleigh Waves Between 40 and 150 seconds", *Geophysical Journal International*, Vol. 122, pp. 675-690.

Tsai Y. B. and K. Aki, 1971, “Amplitude Spectra of Surface Waves from Small Earthquakes and Underground Nuclear Explosions”, *Journal of Geophysical Research*, Vol. 76, pp. 3940-3952.

Van der Lee S. and G. Nolet, 1997, “Seismic Image of the Subducted Trailing Fragments of the Farallon Plate”, *Nature,* Vol. 386, pp. 266-269.

Van Heijst, H.J. and J. Woodhouse, 1999, “Global High-Resolution Phase Velocity Distributions of Overtone and Fundamental Mode Surface Waves Determined by Mode Branch Stripping”, *Geophysical Journal International,* Vol.137, pp. 601-620.

Vdovin, O., J. A. Rial, A. L. Levshin, M. H. Ritzwoller, 1999, “Group Velocity Tomography of South America and the Surrounding Oceans”, *Geophysical Journal International,* Vol.136, pp. 324-340.

Wapenaar, K., 2004, “Retrieving the Elastodynamic Green’s Function of an Arbitrary Inhomogeneous Medium by Cross Correlation”, *Physical Review Letters,* Vol. 93, 254301.

Wapenaar, K., 2004, “Green’s Function Retrieval by Cross-Correlation in Case of One-Sided Illumination”, *Geophysical Research Letters*, Vol. 33, doi.10.1029/2006GL027747.

Weaver, R. L., Lobkis, O. I., 2001, “Ultrasonics Without a Source: Thermal Fluctuation Correlations at MHz Frequencies”, *Physical Review Letters,* Vol. 87, 134301.

Withers, M. M., R. C. Aster, C. J. Young and E. P., Chael, 1996, “High Frequency Analysis of Seismic Background Noise Environment at Three Sites in the United States”, *Bulletin of the Seismological Society of America,* Vol. 86, pp. 1507-1515.

Woodhouse J. H., and A. M. Dziewonski, 1984, “Mapping the Upper Mantle: Three-Dimensional Modeling of Earth Structure by Inversion of Seismic Waveforms”, *Journal of Geophysical Research*, Vol. 89, pp. 5953-5986.

Yang, Y., M. H. Ritzwoller, A. L. Levshin, N. M. Shapiro, 2007, "Ambient Noise Rayleigh Wave Tomography Across Europe", *Geophysical Journal International,* Vol.168, pp. 259-274.

Yang, Y., and M. H. Ritzwoller, 2008, "The Characteristics of Ambient Seismic Noise as a Source for Surface Wave Tomography." *Geochemistry Geophysics Geosystems*, 9(2), Q02008, 18 pages, doi:10.1029/2007GC001814.

Yao H., X. Campman, M. V. de Hoop, R. van der Hilst, 2009, Estimation of Surface Wave Green's Functions from Correlation of Direct Waves, Coda Waves, and Ambient Noise in SE Tibet, *Phys. Earth Planet. Interior,* 177, pp. 1-11.

Yelkenci, S., 2006, *The Crustal Structure of the Central Anatolia by Using Receiver Function Analysis,* M.Sc. Thesis, Boğaziçi University.

Yılmaz, Y., 1993, "New Evidence and Model on the Evolution of the Southeast Anatolian Orogen", *Geological Society of America Bulletin*, Vol. 105, pp. 251–271.

Yılmaz, Y., E. Yiğitbaş, M. Yıldırım, 1987, "Güneydoğu Anadolu'da Triyas Sonu Tektonizması ve Bunun Jeolojik Anlamı", Türkiye 7. Petrol Kongresi Bildiriler Kitabı, pp. 65-77, Ankara.

Yılmaz, Y., O. Tüysüz, E. Yiğitbaş, Ş. C. Genç, A. M. C. Şengör, 1997, Geology and Tectonics of the Pontides", in A. G. Robinson (eds.) *Regional and Petroleum Geology of the Black Sea and Surrounding Region,* AAPG Memoir, 68, pp. 183-226.

Yılmaz, Y., Y. Güner, F. Şaroğlu, 1998, "Geology of the Quaternary Volcanic Centers of the East Anatolia", *Journal of Volcanology and Geothermal Research,* Vol. 85, pp. 173-210.

Zhu, L., B. J. Mitchell, N. Akyol, I. Cemen, K. Kekovali, 2006, "Crustal Thickness Variations in the Aegean Region and Implications for the Extension of Continental

Crust", *Journal of Geophysical Research*, Vol. 111, B01301. doi:10.1029/2005JB003770.

Zor, E., E. Sandvol, C. Gurbuz, N. Turkelli, D. Seber, M. Barazangi, 2003, "The Crustal Structure of the East Anatolian Plateau (Turkey) from Receiver Functions.", *Geophysical Research Letters*, 30 (24).

Zor, E., S. Özalaybey, C. Gürbüz, 2006, "The Crustal Structure of the Eastern Marmara Region (Turkey) by Teleseismic Receiver Functions". *Geophysical Journal International*, 1365- 246X, p.10.1111.

Zor, E., 2008, "Tomographic Evidence of Slab Detachment Beneath Eastern Turkey and the Caucasus", *Geophysical Journal International,* Vol.175, pp.1273-1282.